Experimental and Numerical Simulation of Stress Distribution in Landfills

by

Narges Karimi Tabar
B.Eng, Civil Engineering, Carleton University, 2012

A thesis submitted to The Faculty of Graduate and Post Doctoral Affairs
in partial fulfillment of the requirements for the degree of
Master of Applied Science
in
Civil Engineering

The Ottawa-Carleton Institute for Civil Engineering (OCICE)
Carleton University
Ottawa, Ontario

Abstract

This thesis conceptually illustrates stress distribution within landfills by hypothesising the concept of a “hard inclusion”. It was demonstrated, via laboratory experiments and numerical modelling, that the concept of a “hard inclusion” may be partially responsible for elevated stresses measured by Total Earth Pressure Cells (TEPCs) installed within waste in landfills during previous studies as well as horizontal pipe collection/recirculation systems. The high failure rate in horizontal collection systems in engineered landfills and horizontal gas and leachate collection and leachate recirculation systems in bioreactor landfills may be partially attributed to high contrasts in moduli between the bedding material surrounding the pipe collection/recirculation systems and the waste. Similar contrasts in moduli can explain elevated stress measurements obtained by TEPCs to date. Findings of numerical simulations conducted using GeoStudio software validated the results obtained from the experimental work. More stress is concentrated on TEPC/pipe surrounded by a stiff medium such as sand and more stress is distributed around the TEPC/pipe when they are surrounded by a less stiff medium. It is important to understand the stress distribution in landfills to help landfill designers in the design of collection/recirculation systems.

Acknowledgements

I would like to express my deepest gratitude and respect to Dr. Paul Van Geel and Dr. Mohammad Tofigh Rayhani, my supervisors, for their continuous help and support in all stages of this thesis work. I have been extremely fortunate to have Dr. Van Geel who always made the time and effort to respond to my queries with his constructive comments, and Dr. Rayhani for his tireless efforts, encouraging and helping me in all steps.

Thank you to our main sponsors, Waste Management of Canada (WM) and Ontario Centres of Excellence (OCE) and Natural Sciences and Engineering Research Council (NSERC) for their contributions for the success of this research. Thank you to our industry partners and consulting firms, Hoskin Scientific, RST Instruments, Golder Associates, WESA, WSP and GeoShack for their interest and support.

Thank you to Carleton University civil lab personals, Stanely Conely, Jason Arnott, Pierre Trudel and Kenneth Akhiwu for their valuable technical assistance during the experimental work and Benjamin Griffin who helped me a lot during experimental set-up.

I would like to extend my appreciation to my friends in Department of Civil and Environmental Engineering, Dina Megalla, James Doyle and Katie Murray for their continues support. I would also like to acknowledge Mehdi Mostajeran, Mana Zargari, Sahar Saeednooran and Pedram Falsafi for their friendship and support.

A great thank you to my parents, Hadi Karimi Tabar and Maryam Tavassoli Amin, and my lovely sister, Zahra, for their continuous encouragement, support and help. Last but not least, many thanks go to my love, Mohammad Reza Pasandideh for his unconditional company and help to complete this thesis.

Table of Contents

List of Tables

List of Figures

List of Abbreviations

EPC	Earth Pressure Cell
GPS	Global Position System
HDPE	High Density Polyethylene
LVDT	Linear Variable Differential Transformer
MSW	Municipal Solid Waste
NRRL	New River Regional Landfill
OCE	Ontario Centres of Excellence
PPMF	Prescale Pressure Measurement Film
RTK	Real-Time Kinematic
TEPC	Total Earth Pressure Cell
TESC	Total Earth Stress Cell
TSC	Total Stress Cell
U.S. EPA	United States Environmental Protection Agency
WM	Waste Management

List of Appendices

1.0 Introduction and Background

Solid waste management strategies are developing rapidly as more waste is being generated due to population growth. Solid waste is managed using different strategies worldwide based on the conceptual design, available technology, economical and social aspects, legislation and geographical situation (Reinhart et al., 2001). An integrated approach to waste management of Municipal Solid Waste (MSW), including recycling, incineration, composting and landfilling has been promoted among major waste management strategies (Reinhart et al., 2001). In Canada, despite increases in recycling, landfilling is still the most preferred strategy to dispose non-recoverable materials. Although several environmental impacts could be created as a result of inappropriate management and improper landfill operations, landfilling is considered to be a reliable and a cost effective approach to manage MSW if adequate land is available (Karthikeyan and Joseph, 2007).

Conventionally, engineered landfills are designed as containment systems which typically limit infiltration and minimize water content. Considering a low-infiltration approach, leachate production is minimized and the potential risk of groundwater contamination is reduced. Limited moisture in conventional landfills limits the waste biodegradation and stabilization and extends the contaminating lifespan of the landfill (Benson et al., 2007). An alternative approach to conventional landfills designed for containment is to encourage waste stabilization in order to recover landfill air space and to reduce the contaminating lifespan of the landfill. A bioreactor landfill is a controlled system that supports the degradation of waste at a much faster rate than typically

observed in a conventional landfill (WM. 2004; Sharma and Reddy 2004; Benson et al., 2007; Townsend et al., 2008). Bioreactor landfills also increase the rate of gas production by enhancing the microbiological processes (Karthikeyan and Joseph, 2007; Townsend et al., 2008).

To develop an environmentally friendly landfill, the essential elements including liner system, leachate collection and recirculation systems and gas control system are required to be designed for proper operation to fulfill the objectives of a bioreactor landfill. The elements of a bioreactor landfill need to be designed properly to avoid environmental and economical risks.

Liners are conventionally used as barriers to prevent the migration of pollutants into natural resources. Liners are aimed to limit the contamination of groundwater by limiting the infiltration of leachate into the subsurface soil. Regulatory agencies provide suggestions or stipulations regarding soil liner performance for the designers. According to the regulations, the maximum head on the liner system should not be more than 0.3m. One of the key parameters in the design of soil liners is the coefficient of permeability of the liner, which is strongly affected by environmental factors such as freeze/thaw cycles that cause the formation of channels in the compacted soil and thus, permit pollutant movement into the aquifer. Also, extremely high temperatures and humidity can contribute to desiccation cracks, leading to the movement of contaminant substances into the groundwater (Karthikeyan and Joseph, 2007). Liners typically consist of a compacted clay liner overlaid by a geomembrane. Most landfills are placed over a natural or constructed low permeable clay layer to prevent potential seepage of the leaked leachate

to the environment (Ontario Ministry of Environment, 1998). The thickness of a soil liner can vary through the range of 600 to 900mm; however, 1.5m thickness liners are not uncommon. The geomembrane must be installed directly and uniformly in contact with a clayey liner or a proper foundation. The geomembrane requires protection against puncturing and load-induced damages at time of installation and all other times (Ontario Ministry of Environment, 1998). A landfill with limited leachate migration into subsurface environment reduces the potential long term environmental risk (Karthikeyan and Joseph, 2007; Reinhart et al., 2001).

The leachate collection system, alternatively named as drainage system, is positioned above the liner system. Since bioreactor landfills might generate a higher volume of leachate, the design of the leachate collection system in bioreactor landfills must ensure the accommodation of the higher volume to avoid possible failure of either the leachate collection system or the liner (Karthikeyan and Joseph, 2007; Townsend et al., 2008; Pohland, 1975). Failure can be avoided either by requiring a larger size collection pipe and/or extra pumping capacity (Townsend et al., 2008). In case the leachate collection system fails due to any problem like clogging, the landfill needs to have a pumping system on standby that will be used to flush out the leachate collection system (Pohland, 1975).

Techniques used for leachate treatment include the recirculation of leachate through the landfill, biological treatment, chemical flocculation, filtering and reverse osmosis. These processes rapidly stabilize the organic components of municipal solid waste leachate. During leachate generation, the acid phase forms fatty acids, amino acids.

Therefore, leachate during this phase is considered to have high concentrations of volatile fatty acids and low pH. Low pH inhibits the process of the methane bacteria to biodegrade the waste forming methane gas. Hence, the recirculation of leachate is favorable to enhance methane generation (Bramryd and Binder, 2001). The need for proper selection of leachate recirculation system can be defined under some important parameters such as budget limitation, legislation, and ease of operation (Karthikeyan and Joseph, 2007). Leachate collection and distribution system is illustrated in Figure 1-1.

For bioreactor landfills, a more robust gas collection system may be required to handle the additional gas produced during a shorter period of time compared to a conventional landfill. The landfill gas collection system, shown in Figure 1-1, needs to be operating during the early stages of landfill operations to prevent emissions of greenhouse gases into the atmosphere (Karthikeyan and Joseph, 2007). To collect the produced gas, different methods of horizontal trenches, vertical wells, near surface collectors, and hybrid systems can be used (Pacey et al., 2000).

A multilayered final cover system acts as a barrier to impede precipitation infiltrating into the waste. Since rainfall infiltration provides additional moisture to accelerate biodegradation, final cover should be constructed after the waste has been sufficiently stabilized (Reinhart et al., 2001).

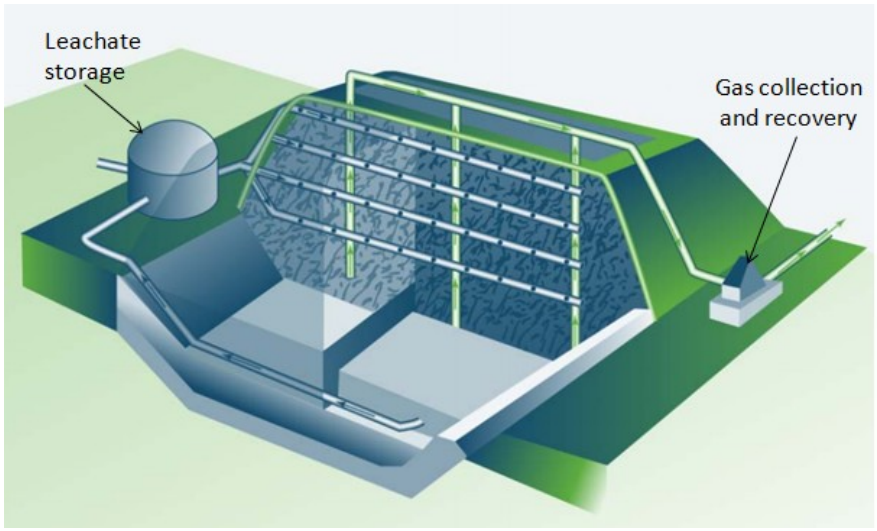

Figure 1-1: Gas collection and leachate collection and recirculation systems (ITRC, 2006)

Monitoring is vital in both conventional and bioreactor landfills. Balance in liquid volume, liquid head on linear, leachate characteristics, landfill gas volumes and quality, landfill settlement are common monitoring parameters (Townsend et al., 2008). Proper monitoring of biological, chemical, and hydrologic processes happening within a bioreactor landfill during operation results in desirable operation. Upon waste stabilization and landfill closure, the need for monitoring and maintenance programs are minimized (Pacey et al., 2000).

Despite the advantages that bioreactor landfills offer, there are some concerns associated with bioreactor landfills such as leachate seeps, landfill slope instability, high temperatures and potential explosions, and odours (Karthikeyan and Joseph, 2007; Townsend et al., 2008). Increased greenhouse gas emissions during operations is also a concern with bioreactor landfills which requires effective collection of the landfill gas.

Waste settlement in bioreactor landfills is larger and occurs at a faster rate compared to conventional landfills. Settlement in conventional landfills have been found to be about 8% of the height of the landfill whereas settlement in bioreactor landfills can be as high as 20-25% of its height (Benson et al., 2007; Reinhart and Townsend, 1998). Settlement in MSW landfills is not always beneficial as differential settlement can cause problems including crack formations in the liner and cover systems and large stresses can be induced on leachate collection and recirculation systems and gas collection systems as a result of rapid settlement in landfills. This causes the collection/recirculation systems to experience high failure rate.

1.1 Problem Description

In order to better understand the impacts of cold climates and operational parameters on waste stabilization in landfills operating in northern climates, a research group at Carleton University instrumented a landfill in Ste. Sophie, Quebec. Twelve instrument bundles in two vertical profiles were placed within the waste as the landfill was filled. Each instrument bundle consisted of a total earth pressure cell (TEPC), oxygen sensor, moisture and electrical conductivity sensor, a settlement sensor and lower four bundles included a vibrating wire piezometer to record any leachate mounding. The objective of the TEPC is to record the overburden pressures at the instrument bundle locations with a goal of confirming overburden pressure and linking this to settlement. However, the data collected by the TEPC to date, appear to overestimate the overburden pressures estimated based on a depth of waste multiplied by the unit weight of the waste. Application of TEPCs in landfill environments has been reported in other landfill studies (e.g. Timmons

et al., 2011) and inaccuracies in stress measurements obtained by TEPCs have been observed.

Contrasts in moduli may explain inaccuracies of the stress measurements obtained using TEPCs placed in landfills (Timmons et al., 2011; Vingerhoeds, 2011). As an example, results obtained by TEPCs installed in a landfill in Sainte-Sophie tended to over-estimate the expected stresses within the waste. The higher value of stress sensed by the TEPC is likely because of the greater modulus of the instrument bundle and surrounding sand than that of the surrounding waste. The greater modulus of the instrument bundle and surrounding sand will cause the stresses to be concentrated on the instrument bundle as the surrounding waste settles leading to higher than expected stress measurement by the TEPC.

Similar contrasts in moduli between the bedding material surrounding a pipe collection system and the waste may contribute to the failure of the pipes in the collection systems. The gas collection and leachate recirculation systems may experience high failure rates due to non-uniformity of waste stress distribution. Pipes may be exposed to higher than expected stress due to the heterogeneous nature of the waste and the contrasts in moduli between the bedding material and the waste. Given the high failure rate in collection systems, research is required to better understand the processes that can lead to elevated stresses in collection pipes and help landfill designers in the design of collection systems.

1.2 Overview of Thesis

This MASc thesis includes 6 chapters. Chapter 1 provides a background on landfills followed by problem and research description. Chapter 2 presents a brief review on Total Earth Pressure Cells, bioreactor landfills, studies where TEPCs have been employed within bioreactor landfills as well as studies of buried pipes.

Laboratory experiments were conducted to assess the elevated stresses that potentially occur as a result of differences in moduli of the materials. Experiments were conducted to test a hard medium within a soft bedding material. Steel plate and HDPE pipe served as the stiffer media and woodchips were used to represent the lower modulus of the waste. Chapter 3 describes the performed laboratory experiments including a brief introduction to the employed instruments and experimental set-up procedures. The results obtained from the laboratory experiments are described in Chapter 4.

Simulations were conducted using a finite element program to simulate the laboratory experiments and illustrate why increased pressures may be experienced due to contrasts in moduli. Simulation details including dimensions, boundary conditions, mesh sizing and data inputs are described in Chapter 5. Conclusions from this research and suggested future work are provided in Chapter 6, followed by references and appendices.

1.3 Research Description

A hypothesis is proposed to explain the elevated/overestimated, in-situ stress measurements recorded by TEPCs placed in solid waste. The same phenomenon may

explain the high failure rate of horizontal gas collection and leachate recirculation systems. High failure rate in horizontal collection and recirculation systems in bioreactor landfills may be explained by the "passive arching" phenomenon (Terzaghi, 1943) that is also known as "hard inclusion" as a result of differences in stiffness of materials.

It is postulated that the instrument bundles and surrounding sand bedding material have a higher modulus than the surrounding waste and as the waste settles and stabilizes, the instrument bundles and surrounding sand act as a "hard inclusion" leading to elevated stresses which are recorded by the TEPC within the instrument bundles. Similarly, it is anticipated that gas collection and leachate recirculation pipes placed in gravel trenches are exposed to elevated stresses due to the concept of a "hard inclusion".

The objective of this thesis is to confirm the hypothesis that the concept of a "hard inclusion" is responsible for the elevated stresses recorded by the TEPCs and to demonstrate that gas collection and leachate recirculation pipes surrounded by gravel may also experience elevated stresses due to this concept. The concept of a "hard inclusion" was implemented in the lab and simulated using GeoStudio.

To reap the benefits of the bioreactor technology, better understanding of the waste stress distribution within waste around horizontal gas collection and/or leachate recirculation pipes is required in order to reduce the failure rate of these systems. This research helps landfill designers in the design of recirculation and collection systems to reduce failure rates which will lead to more effective gas collection and leachate

recirculation systems. More effective gas collection will reduce greenhouse gas emissions and increase energy generation via the landfill gas.

2.0 Literature Review

A succinct review of the use of TEPCs including their design, operation, calibration and factors affecting their performance as well as a brief overview of bioreactor landfills with fundamental advantages and concerns are provided here. In addition, studies where TEPCs have been employed within landfills and pipes buried under an embankment are discussed.

2.1 Total Earth Pressure Cell

Total Earth Pressure Cell (TEPC) is a device typically used to determine the overall stress at a point within a soil mass or to evaluate the contact stress against a structure (Felio and Bauer, 1986). TEPC is also known as Earth Pressure Cell (EPC), Total Earth Stress Cell (TESC) or Total Stress Cell (TSC). Over the past years, the employment of TEPCs has been seen in many geotechnical applications specially for measuring the pressures from massive structures (Hamilton, 1960; Prakash, 1981; Daigle and Zhao, 2003 and Timmons et al., 2011). Conventionally, embedded load cells have been applied to measure the magnitude and distribution of stress within embankments and backfill materials; however, contact earth pressure cells have been used for measuring the pressure against retaining walls, culverts, piles and shallow foundations (Dave and Dasaka, 2011).

It is likely impractical to obtain an exact value of the total stress at a point within a soil medium using a TEPC, since the soil stress changes due to the presence of the TEPC in the soil (Selig, 1964; Triandafilidis, 1974; Hvorslev, 1976; Weller and Kulhawy, 1982;

Felio and Bauer, 1986). Due to difficulties in acquiring the real measurement of the soil pressure, measuring the stress at a point within a soil mass is more challenging than measuring the stress on a surface of a structural element (Felio and Bauer, 1986).

TEPCs can respond to ground water pressures or pore water pressures (u), in addition to soil pressures. The effective stress (σ') from the total stress (σ) can be separated by simultaneous measurement of pore water pressure using a piezometer (GEOKON, 2007). Terzaghi (1925) defines the principal of effective stress as:

$$\sigma' = \sigma - u \qquad (1)$$

2.1.1 Design Objective, Structure and Operation of TEPC

A TEPC is a device intended to measure the magnitude of the normal stress in the soil and should be designed in such a way that minimizes potential impact on the stress distribution (Labuz and Theroux, 2005). In construction of a stress-sensing instrument, it is tremendously difficult to take all the factors such as soil type, stress history profile, shear and normal stresses, boundary conditions, drainage conditions, and the other environmental factors influencing rheology of the soil into account. As a result, the stress measured by a TEPC at a certain point within a soil mass is likely different from the real stress existing at that point without the presence of the TEPC (Dave and Dasaka, 2011). TEPC needs to be tested and calibrated before installation to ensure its functionality.

As recommended by Taylor (1945), Monfore (1950), Loh (1954), Askegaard (1963), and Tory and Sparrow (1967), the ratio of TEPC's height to its diameter, known

as aspect ratio, should be as small as possible, since a TEPC with a high thickness alters the soil stress more than a thin TEPC. The minimum aspect ratio of 1 to 20 is typically suggested. Most TEPCs are cylindrical in shape, although rectangular TEPCs are also available.

A hydraulic type of a TEPC, shown in Figure 2-1, is simple in structure and consists of two circular or rectangular plates welded together around the periphery with a small intervening cavity filled with a hydraulic fluid, and a pressure transducer attached to the intervening cavity. A diaphragm type of a TEPC is a structural member deflecting under applied load. The deflection of the diaphragm is measured using a strain gauge and the strain gauge is calibrated with the applied pressure (Labuz and Theroux, 2005).

In hydraulic TEPCs, the amount of internal pressure in the cavity is equivalent to the pressure acting on the plates (Labuz and Theroux, 2005). Fluid used inside the intervening cavity should be as incompressible as possible. The pressure of the fluid increases due to the applied pressure tending to squeeze the two plates together. If the thickness of the plates is relatively small with respect to their lateral extent, the soil pressure at the centre of the cell is balanced with the internal fluid pressure. This is due to the negligibility of the supporting effect of the welded periphery at the centre of the plate. The balance between the soil stress and the pressure fluid will exist only if the TEPC is stiff so that the deflection of the plate is minimal. The pressure transducer should be stiff enough in order to minimize the volume change during the pressure increase (GEOKON, 2007).

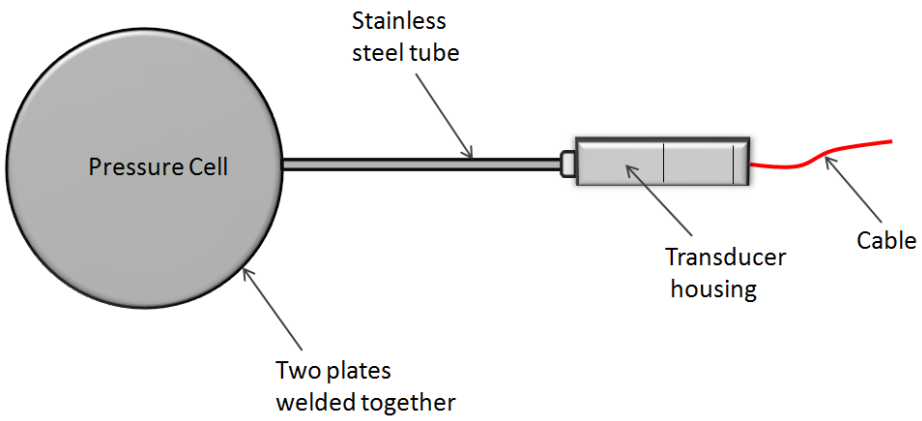

Figure 2-1: A hydraulic TEPC with circular plates

2.1.2 TEPC Calibration

To obtain an exact value of the total stress at a point within a soil, correction factors are needed to be consistently applied to the values obtained from a test. Calibrating a TEPC requires establishment of a correlation between the applied pressure and the obtained output from the TEPC. The sensitivity of the TEPC is the calibration factor applied to the output of the pressure transducer to convert the unit of the TEPC electrical output from voltage $[vdc]$ to stress $[kPa]$. The TEPC output in fact is derived from the normal stress acting on its surface (Dave and Dasaka, 2011).

Each TEPC from a manufacturer is calibrated at room temperature such that the TEPC is inserted between fluid-filled pressure bodies and then is pressurized (Dave and Dasaka, 2011). Fluid-filled pressure bodies are large enough to provide uniform pressures. A pressure tank with electric feed-troughs is suitable to conduct fluid calibration. Air, water or oil is used as the fluid inside the pressure tank. The sensitive

side of the TEPC placed on the bottom of the pressure vessel allows the pressurized fluid within the cell to be applied over the entire area of the TEPC. The aim of the calibration under fluid condition is to check the reaction of the instrument to the applied pressure, and the ability to reset to zero after unloading (Dave and Dasaka, 2011). Fluid pressure calibration is one of the standard approaches to obtain the calibration factor.

Fluid calibration can be conducted by applying fluid pressure via centrifuge technique or pressurized fluid. Fluid calibration employing centrifuge technique experiences meniscus formation that causes non-uniform pressure application. Calibrating the TEPC with pressurized fluid, specially using the air pressure, is the most successful and popular approach in geotechnical investigations from 1987 till recent years (Dave and Dasaka, 2011). Although fluid calibrating approach is economical, the results are not very satisfactory for a TEPC aimed to be placed in soil as the fluid doesn't act in the same manner as the soil; therefore it is best to calibrate the TEPC in the soil in which the TEPC will be placed (Felio and Bauer, 1986).

As suggested by Askegaard (1995), TEPCs should be calibrated under different conditions in order to obtain a good estimation of the data accuracy when the TEPCs are installed in a soil with unknown loading background. Calibration of a TEPC under the soil condition typically involves the soil and the TEPC positioned within a large diameter triaxial cell or oedometer. Calibration under soil condition is aimed to check the hysteretic behavior due to loading and unloading, variation of coefficient of calibration with soil type, soil condition, and stress history (Dave and Dasaka, 2011). Redshaw (1954), Pang (1986) and more recently Ramirez et al. (2010) calibrated a TEPC using a

soil layer overlain by an external load applied using oil pressure. Centrifuge technique was used to calibrate a TEPC overlain by a sand layer. This method of calibration was performed by Pang (1986), Take (1997) and Chen and Randolph (2006). From 1993 to late 2005, some investigators conducted successful experiments using the modified set up of a triaxial or modified Rowe cell in order to calibrate a TEPC (Dave and Dasaka, 2011). It should be noted that outside the laboratory setting, normal contact stress between TEPC and soil may not necessarily follow a uniform distribution. In addition, an arching phenomenon -explained in section 2.2- might occur as the TEPC deflects (Labuz and Theroux, 2005).

Since the results obtained from TEPC may vary under fluid and soil calibration conditions, it is necessary to calibrate the TEPC before installation to obtain the most accurate field measurements. TEPC placement should be done with considerations and must be calibrated and tested in the same manner as it is going to be installed in the field (Labuz and Theroux, 2005). Direct contact with large rocks should be avoided during TEPC installation as plates could be extensively deformed, and all chunks greater than 10 mm should be removed prior to installation (GEOKON, 2007).

2.1.3 Important Factors in TEPC Calibration

Broad laboratory experiments were conducted to determine the influencing factors on the performance of TEPCs. Felio and Bauer (1986) embedded twenty identical TEPCs of type SOLINST on a bridge abutment and conducted 51 tests. The employed TEPCs were calibrated at $21°C$ in the laboratory by the manufacturer. During hot and cold weather,

significant temperature change was sensed by thermocouples of the TEPCs that were in touch with the sand backfill and were located at the back-face of the abutment.

First, Felio and Bauer (1986) calibrated TEPCs for different temperatures under no load conditions to estimate the dependency of the pre-stress on temperature. The TEPCs were inserted in a water bath and temperature changed from -4°C to 45°C. Variation of the pre-stress (regarding the reference pre-stress) versus temperature was plotted. From the plotted curves for different temperatures, the relationships between actual TEPC pre-stress at temperature T (P_T), pre-stress at calibration temperature in the laboratory i.e. room temperature (P_{cal}), and temperature difference from calibration temperature (dT) were obtained. When the pre-stress of the TEPC was greater or less than $20kPa$, the actual TEPC pre-stress at temperature T could be derived from the following formulas:

$$\mathrm{P_T} = \mathrm{P_{cal}}(1 + 3.64 \times 10^{-3}\mathrm{dT}) \qquad \text{When TEPC pre-stress} \geq 20\ kPa \qquad (3)$$

$$\mathrm{P_T} = \mathrm{P_{cal}}(1 + 1.24 \times 10^{-2}\mathrm{dT}) \qquad \text{When TEPC pre-stress} \leq 20\ kPa \qquad (4)$$

At temperatures of 1 °C and 21°C, the TEPCs were calibrated against applied hydrostatic pressures. Based on the calibration results, the temperature variation did not affect the slope of the calibration curve, although it caused a shift of the TEPC pre-stress. The obtained calibration curves were parallel to one another (Felio and Bauer, 1986).

TEPCs were placed flush with concrete side of the bridge abutment in order to determine the effect of contact material on performance of the TEPCs. Some SOLINST TEPCs were installed at the base to find out the contact stresses between the abutment

footing and the granular pad and some TEPCs were situated on the vertical abutment wall to measure the lateral pressure due to the compacted sand backfill.

In order to calibrate the TEPCs against different types of contact materials, a calibration chamber that consisted of a steel tank with a cover plate and a concrete base was used. The TEPCs flush with the surface of the base were calibrated against four types of materials, including granular pad material, sand backfill, uniform silicas, and kaolin powder. A highly polished stainless steel sheet was used along the inside walls of the tank to minimize the effect of side friction on the tank wall and any potential arching across the TEPC. The developed calibration curves from various materials were compared to the manufacturer's calibration curve and percentage deviation was determined. Calibrations were also conducted at different temperatures which resulted in quite similar curves at the same temperature for the four materials. Thus, it was concluded that soil type had little influence on the performance of the TEPC (Felio and Bauer, 1986). Figure 2-2 represents the variation of calibration curve for four different types of soil.

To determine the effect of the installation method on the TEPC response, several TEPCs of type SOLINST were placed on a sand bed within a large sand tank. As the TEPCs were being covered by the extra sand that was rained on top of the TEPC, the readings of the TEPCs were recorded with respect to the additional sand. It was determined that the results of the TEPC in the large sand tank were almost identical with the manufacturer's calibration curve as well as calibration curve obtained from the TEPC embedded flush in the base of the calibration chamber. Thus, the effect of TEPC

installation method, within a soil or on the face of the structure, can be ignored (Felio and Bauer, 1986).

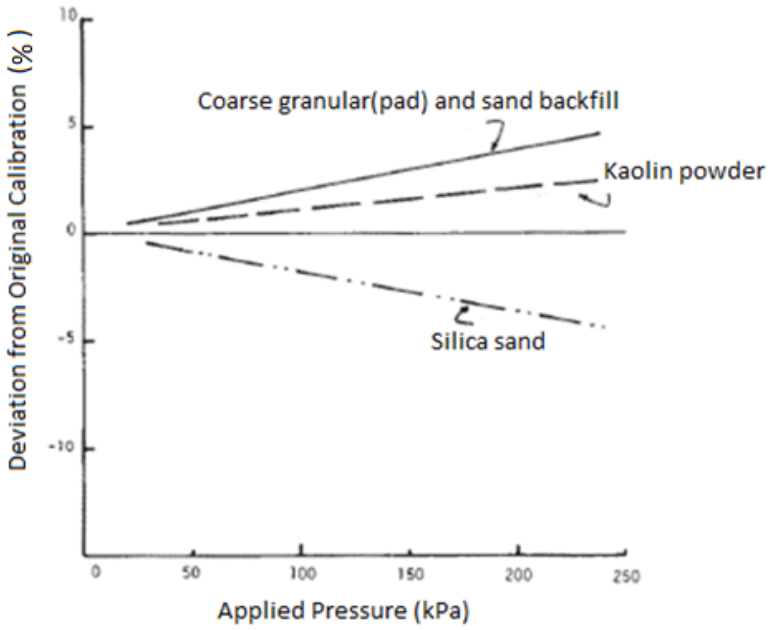

Figure 2-2: Variation of calibration with four different types of soil (Felio and Bauer, 1986)

From the experiments, it was found that the performance of a TEPC was significantly affected by temperature changes with a predominant influence on the pre-stress of the TEPC. Type of the soil that TEPC was in contact with and placement method (TEPC within the soil mass versus in contact with a structure) were also found to have impact on the TEPC response, but in a lesser magnitude (Felio and Bauer, 1986).

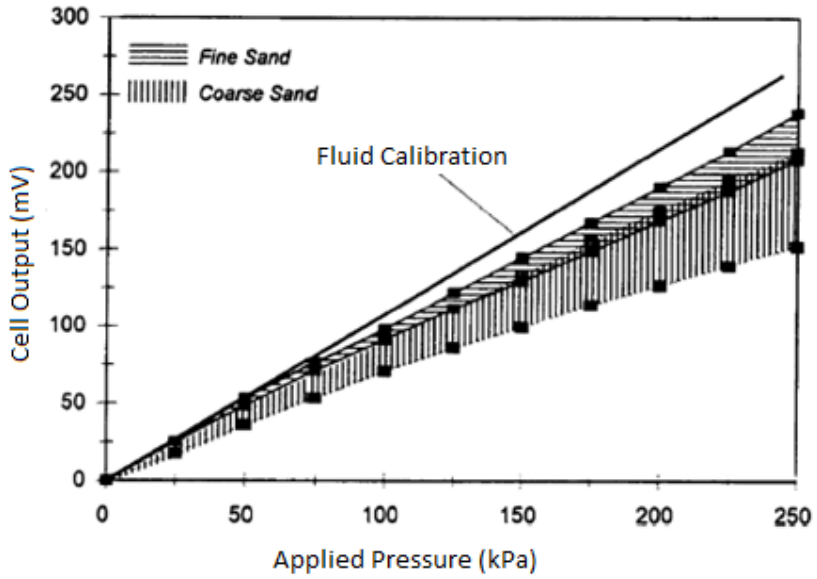

Figure 2-3: Effect of grain size on calibration relationship (Clayton and Bica, 1993)

Soil particle size may have a significant impact on calibration output. Clayton and Bica (1993) observed a major effect of particle size, while Labuz and Theroux (2005) did not notice a significant impact. Figure 2-3 represents the meaningful effect of grain size on calibration relationship based on Clayton and Bica's studies in 1993. In addition to particle size, soil density could have a notable effect on calibration curves. Stiffness of the soils with the same relative densities might differ greatly. Also, effect of sandy soil layer thickness on calibration result has been investigated by Dave and Dasaka (2011b). The general conclusion obtained from the results showed that larger sand bed thickness results in a lower stress output.

2.2 Hard and Soft Inclusion Concepts

Performance of TEPCs has been discussed in several studies (Tory and Sparrow, 1967; Askegaard, 1963; Loh, 1954; Monfore, 1950; Taylor, 1945 and Kogler and Scheidig, 1927) with similar perspectives. A typical approach considers TEPC as an inclusion within an elastic medium (e.g. soil). In this way, applied stresses on the cell would depend on the elastic moduli (Young's moduli) of the inclusion and the surrounding bedding material, as well as the shape of the inclusion. Preferably, the TEPC ought to be as stiff as the bedding material with the same compressibility which practically is very difficult to achieve (GEOKON, 2007).

Young's modulus, frequently denoted by E, measures resistance of a material to elastic deformation under applied load. Young's modulus, with a unit of pressure, is the ratio of the stress acting on a substance along an axis to the generated strain. Shape of a stiff material with a high Young's modulus changes only slightly when subjected to an elastic load. On the other hand, a material having a low Young's modulus is a flexible substance with considerable changes in shape under an elastic load (IUPAC, 1997).

In ideal scenarios that the moduli of the TEPC and surrounding bedding material are equal, the applied stress is equally distributed on the TEPC and the surrounding material. For the cases that the modulus of the TEPC is greater than the modulus of the surrounding medium (the cell is stiffer and less compressible than the surrounding medium), the stress will be mainly concentrated on the TEPC. TEPC with a larger modulus than the surrounding medium senses larger stress than the real normal stress

applied in the vicinity of the TEPC. More stress sensation than the free-field stress, known as passive arching phenomenon or hard inclusion, results in recording elevated stresses by TEPCs (Dave and Dasaka, 2011; Labuz and Theroux, 2005 and GEOKON, 2007). Figure 2-4 represents stress distribution profile of a stiff TEPC in contact with a weak bedding material. A great contrast in stiffness of the TEPC and the surrounding medium is shown in Figure 2-5. Stress is more concentrated at centre of the TEPC, leading to a much higher stress sensation than the mean stress. Therefore, de-stressed regions around the rim of the TEPC are formed.

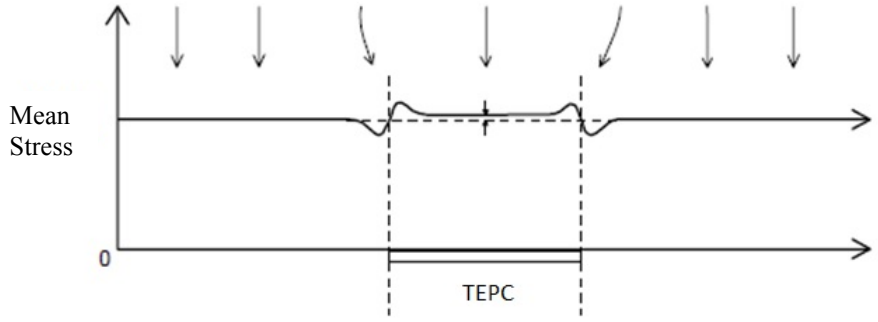

Figure 2-4: Stress distribution on a stiff TEPC within a less stiff medium (GEOKON, 2007)

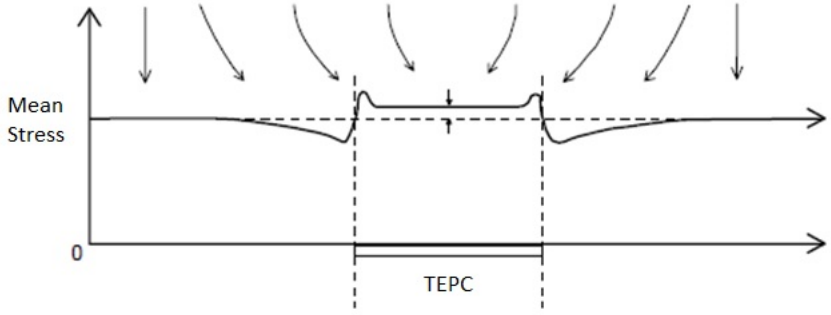

Figure 2-5: Great contrast in stiffness of the TEPC and the surrounding medium (GEOKON, 2007)

When TEPC is less stiff than the bedding material, the normal stress exerted on the TEPC's face is reduced by the shear stress which leads to smaller stress sensation than the free-field stress, shown in Figure 2-6. If the stress on the TEPC is smaller than the actual loading, the phenomenon is known as active arching or soft inclusion (Terzaghi, 1943). In this case, the stress values are under-estimated because stresses in the bedding material are likely to bridge around the TEPC (Dave and Dasaka, 2011; Labuz and Theroux, 2005; GEOKON, 2007).

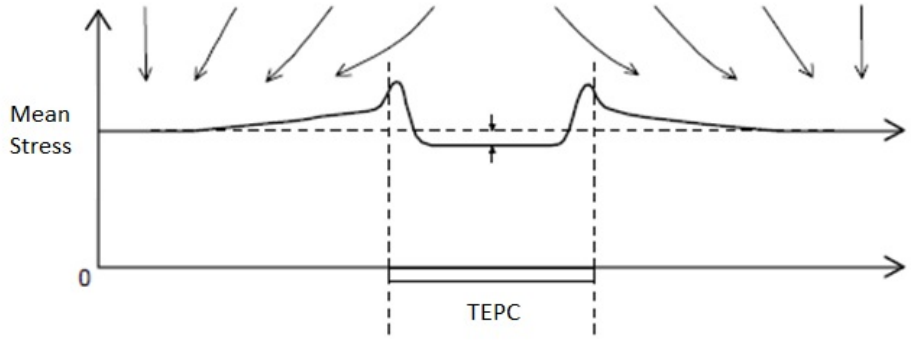

Figure 2-6: Stress distribution on a less stiff TEPC than surrounding medium (GEOKON, 2007)

To avoid arching phenomenon, the TEPC must behave similar to its surrounding media in terms of stiffness. The best results are achieved when the differential deformation between the TEPC and its bedding material is minimum (Labuz and Theroux, 2005).

2.3 Bioreactor Landfill

A bioreactor landfill is defined by the United States Environmental Protection Agency (U.S. EPA, 2000) as "a landfill operated to transform and more quickly stabilize the

readily and moderately decomposable organic constituents of the waste by proposed control to enhance microbiological processes. Stabilization means that the environmental performance measurement parameters remain at steady level along the process implementation". A bioreactor landfill tends to control, monitor and optimize the process of waste stabilization whereas a conventional landfill is aimed to store the waste (Reinhart et al., 2001; Townsend et al., 2008).

2.3.1 Fundamental Advantages

The bioreactor landfill is designed to promote microbiological processes to increase the degradation rate in order to stabilize the waste. In fact, the theory behind bioreactor landfills is opposite to that of conventional landfills which minimize the moisture that can enter the landfill, i.e. tightly sealing the waste from the environment (Karthikeyan and Joseph, 2007). Although fast stabilization and air space recovery due to rapid settlement during operating period are among the objectives of a bioreactor landfill, there are other potential benefits associated with it. Some of the advantages of a bioreactor landfill over a conventional landfill are listed below:

- Maximizing landfill gas generation used for energy recovery,
- Improving leachate treatment and storage via leachate recirculation,
- Decreasing post-closure care, maintenance and risk,
- Reducing negative environmental impacts, i.e. contaminating lifespan of the landfill,

- Reducing costs associated with capital and operating costs (Townsend et al., 2008; Pacey et al., 2000).

Bioreactor landfills focus on bringing the inert state of a landfill forward in a much shorter period of time (Karthikeyan and Joseph, 2007). The bioreactor landfill stabilizes waste typically within five to ten years in comparison to a conventional landfill that typically takes thirty to fifty years or more. Thus, bioreactor landfills recover more airspace which allows additional waste to be placed in the prescribed landfill volume. Due to the stabilization of waste, density of waste mass increases and about 15 to 30 percent of the landfill space is recovered (Townsend et al., 2008).

Bioreactor landfills promote the rate of gas production under controlled conditions (Karthikeyan and Joseph, 2007). Methane gas generation rates are about 200-250% greater than the rates in conventional landfills. Due to the large amount of gas produced as a result of microbiological processes, the viability of a gas-to-energy option is enhanced (Benson et al., 2007; Townsend et al., 2008).

The bioreactor landfill controls and optimizes the biodegradation process through addition of liquid amendments, or leachate recirculation. Besides rainwater infiltration, additional sources of moisture for bioreactor landfills can include sewage sludge and effluent, septic tank sludge, animal manure and old MSW rich in inoculant. Through leachate recirculation, inoculant is distributed by liquid movement. The local deficiency of nutrients is minimized while the contact between insoluble substrates, soluble nutrients and the microorganism is enhanced. Potential toxins are diluted, heat is transmitted and in

turn, microbial activities are improved (Karthikeyan and Joseph, 2007; Warith et al. 2005). Increase in the liquid content in turn increases the rate of waste decomposition to enhance stabilization. Leachate recirculation can not only promote waste stabilization and settlement, also improves leachate quality as well as landfill gas production (Karthikeyan and Joseph, 2007; Reinhart et al., 2001). Leachate is slowly filtered while passing through the waste, thus recirculation of the leachate through waste provides treatment during bioreactor landfill operation (Townsend et al., 2008). Consequently, considerable costs associated with leachate treatment and storage can be saved. Due to the increase in the decomposition rate, post-closure monitoring as well as overall landfill operation cost is decreased (Warith et al. 2005).

2.3.2 Fundamental Concerns

Despite several advantages that bioreactor landfills offer, improper design and operation of these landfills can cause detrimental effects. The common concerns of are as follow (Karthikeyan and Joseph, 2007; Townsend et al., 2008):

- Leachate seeps: Seeps that are verified by wet spots and attract insects, occur usually on the side slopes and at the base of the landfills. It is typically easier for the moisture to migrate sideways since the waste is compacted in layers. This makes the waste more permeable laterally than vertically.
- Landfill slope instability: Due to excess moisture in the bioreactor landfill, the pore water and in turn the total weight of the waste mass are increased and the

shear strength of the waste is decreased. Landfill failures can cause catastrophic results including serious environmental damages, property loss and life loss.

- Odour: Excess production of gas with its nuisance odour needs to be controlled to prevent health and environmental problems.
- High temperature, explosion and fire: Increase in temperature as a result of waste degradation can lead to fire which is mainly concerned in aerobic bioreactor landfills. Therefore, temperature should be monitored at depth in the landfill and other various locations. Besides the rise of temperature in aerobic bioreactor landfills, mixture of methane gas and air has potential flammability. The range of 5% to 14% is estimated for flammability of methane with air. The flammability percentage decreases when nitrogen and other diluent gases are produced.
- Greater greenhouse gas emissions: Increased greenhouse gas emissions during the filling and/or operational phases of the bioreactor landfill require effective collection of the landfill gas during operating conditions.

2.3.3 Types of Bioreactor Landfill Design

Bioreactor landfills can be operated either under aerobic, anaerobic and hybrid (combination of anaerobic and aerobic systems) conditions. Adding moisture to waste is an intrinsic practice to all these three systems (WM., 2004).

- Aerobic bioreactor operates through injecting air or oxygen into the waste as well as leachate recirculation to optimize the conditions for aerobes. Although the process requires about two years for complete biodegradation, the cost of

implementation is high (WM., 2004). Figure 2-7 shows an aerobic bioreactor landfill operation.

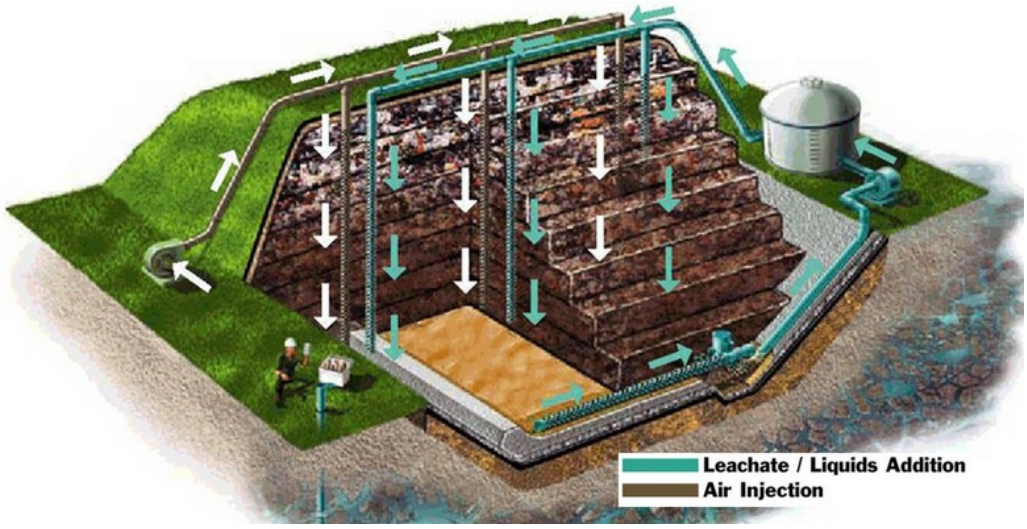

Figure 2-7: Aerobic bioreactor (WM., 2004)

- Anaerobic bioreactor landfill incorporates leachate recirculation to promote generation of methane gas while the oxygen infiltration to the system is limited. In this bioreactor, waste stabilization will be completed within six to seven years (WM., 2004; Karthikeyan and Joseph, 2007). As shown in Figure 2-8, gas collection pipes are used to withdraw the produced landfill gas to be converted to energy and vertical leachate recirculation pipes are used to spread out moisture to the waste. In addition to leachate recirculation, there are further governing abiotic factors which provide control and process optimization for anaerobic bioreactor landfills. Addition of buffering materials, bio-solids and nutrient supplementation as well as temperature, particle size, and waste lift design and control are among these factors (Warith et al. 2005).

- Hybrid bioreactor landfill is a combination of both aerobic and anaerobic bioreactor landfills. The top waste lift is aerated for thirty to sixty days before being covered by the next waste lift. Afterwards, the system goes under anaerobic condition. Figure 2-9 shows a common hybrid bioreactor landfill with the path of leachate, gas collection, and air injection.

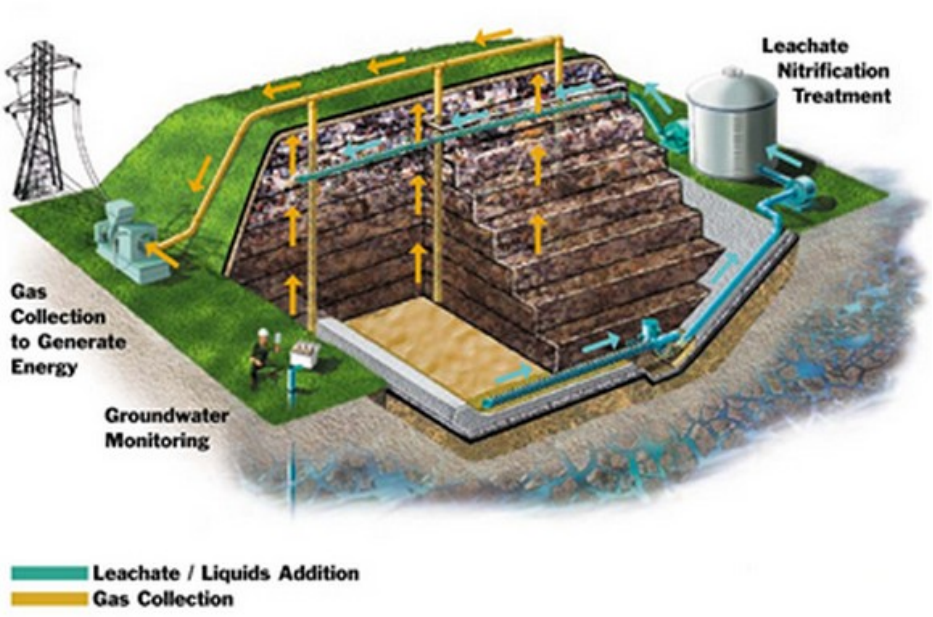

Figure 2-8: Anaerobic bioreactor landfill (WM., 2004)

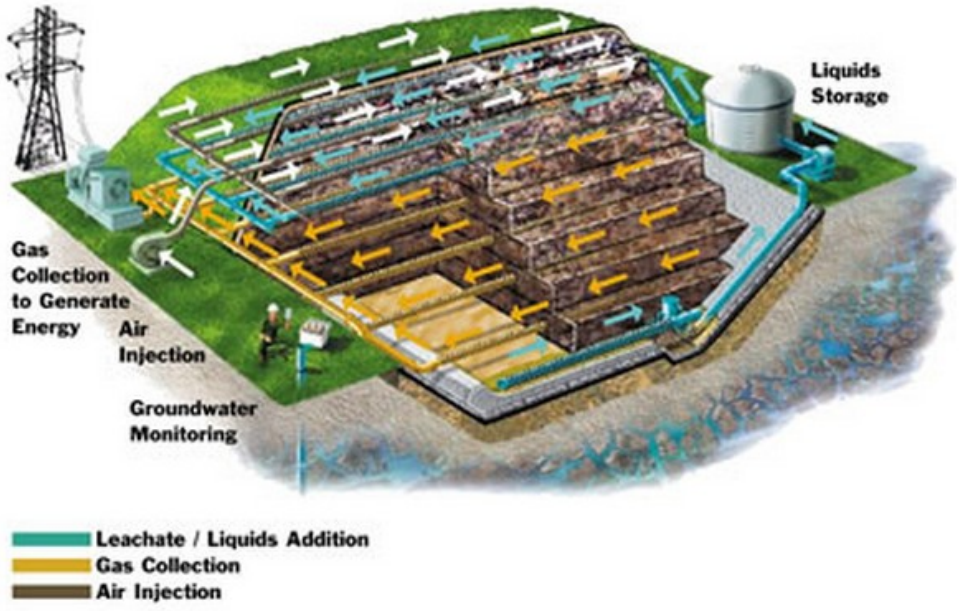

Figure 2-9: Aerobic-anaerobic bioreactor landfill (WM., 2004)

According to Warith et al. (2005), the moisture control through leachate recirculation (under aerobic or anaerobic condition) has been known as the most successful and practical method for enhancing the waste biodegradation rate and in turn stabilization and settlement. But, it should be stated that it is difficult to control and ensure uniform distribution of recirculated leachate throughout the waste in the landfill.

2.4 TEPC in Landfill

Several studies have employed TEPCs in landfill environments to determine the overburden pressure derived from the overlying waste and soil (Vingerhoeds, 2011; Timmons et al., 2011). A TEPC is typically used to measure the stress within a soil or to evaluate the contact stress against a structure (Felio and Bauer, 1986). Obtained stress value could be underestimated or overestimated corresponding to stress bridging around

the TEPC or stress concentration on the TEPC. The results obtained during a full-scale landfill study at Sainte-Sophie in Quebec are examples of overestimated stress measurements compared with the expected overburden pressure (Vingerhoeds, 2011). On the other hand, the obtained results from a study at the New River Regional Landfill in Florida are underestimated stress measurements (Timmons et al., 2011).

2.4.1 Bioreactor Demonstration, the New River Regional Landfill, Union County, Florida

Florida full-scale bioreactor project was carried out by the Hinkley Center for Solid and Hazardous Waste Management, and participation of the University of Florida, and the University of Central Florida. The objective of the project was to design, construct, operate and monitor a full-scale bioreactor landfill in such a way that allows a fair and complete evaluation of this technology as a long term solid waste management method in Florida. In this project, research was conducted at several landfill sites, including the New River Regional Landfill (NRRL). The NRRL in Union County was the first site selected by FDEP to demonstrate the full-scale bioreactor landfill, to study and compare the both aerobic and anaerobic solid waste decomposition processes. The NRRL managed approximately 800 tons per day of waste coming from North Florida Counties for seven years, from 2001 to 2008. The landfill was equipped with a leachate recirculation system, air injection system, gas collection system, and segregated leachate collection system. Some instruments were also installed in-situ in the landfill such as pressure transducers for measuring leachate head on the liner, moisture sensors, thermocouples, vibrating wire

piezometers for measuring pore water pressure, and TEPCs (Townsend et al., 2008; Reinhart et al., 2002).

In-situ measurements of overburden pressure using TEPCs were provided by Timmons (2004). Twenty three TEPCs were horizontally placed in the sand drainage layer of the landfill Cell 3 for measuring the overburden pressure resulting from compacted waste in the landfill. The layout of the Cell 3 in NRRL is shown in Figure 2-10. The TEPC model with an accuracy of approximately 0.30kPa was chosen for this research. It was a commercially available hydraulic TEPC constructed of two circular plates welded together and the liquid between the circular plates was de-aired hydraulic oil. The installed TEPCs were monitored for 3,110 days to measure the overburden pressure as well as temperature. The overburden pressure at a point is the product of the depth of the material and its unit weight.

To obtain the landfill volume for indirect unit weight estimation and to measure the height of waste deposited on top of the TEPCs, periodic topographic surveys of the landfill surface were conducted. Topographic survey data were gathered employing a Z-model dual-frequency real-time kinematic (RTK) global position system (GPS). The unit weight of the combined waste and cover soil was considered in overburden pressure calculation. The landfill volume was assumed to be occupied by 15% cover soil with a unit weight of 17kN/m^3. The overburden pressure output along with the topographic survey data were used to determine the unit weight of the landfilled waste (Timmons et al., 2011).

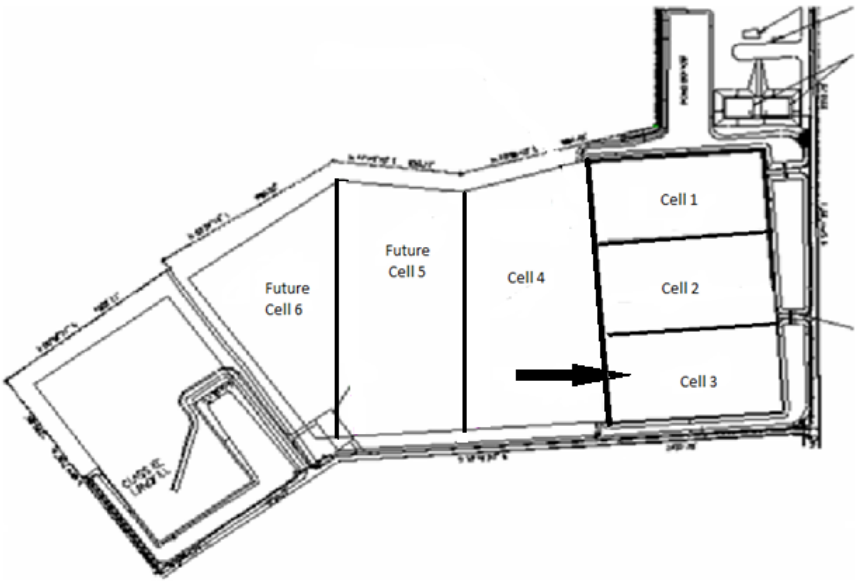

Figure 2-10: Layout of NRRL, Cell 3 (Reinhart et al., 2002)

Tracking temperature around the TEPC over the study period revealed that before waste placement, the temperature changed on a daily and seasonal basis relative to ambient temperature. After waste placement, the exhibition of the extreme daily variability vanished and the temperature gradually increased.

The results of the TEPC indicated that by applying overburden pressure from cover soil and waste placement, the TEPC responded positively with respect to the placement of waste lifts as an indication of increased load. Over the period of study, 16 TEPCs remained operative among a total of 23 TEPCs. Four sensors failed due to lightning, and couple malfunctioned due to damage of the connection wire between the logger and the pressure cell. The overburden pressures obtained from the TEPCs were compared to the theoretically calculated pressures using the waste depth and unit weight. The installed TEPC near the toe of the landfill measured the overburden pressures to be greater than

the calculated values, while the TEPCs installed further away from the toe, toward the center of the landfill, recorded smaller pressure values than the theoretical ones. Figure 2-11 shows overburden pressure, depth of waste deposited, and temperature change over the entire study period (i.e. 3,110 days) obtained by a TEPC (Timmons et al., 2011).

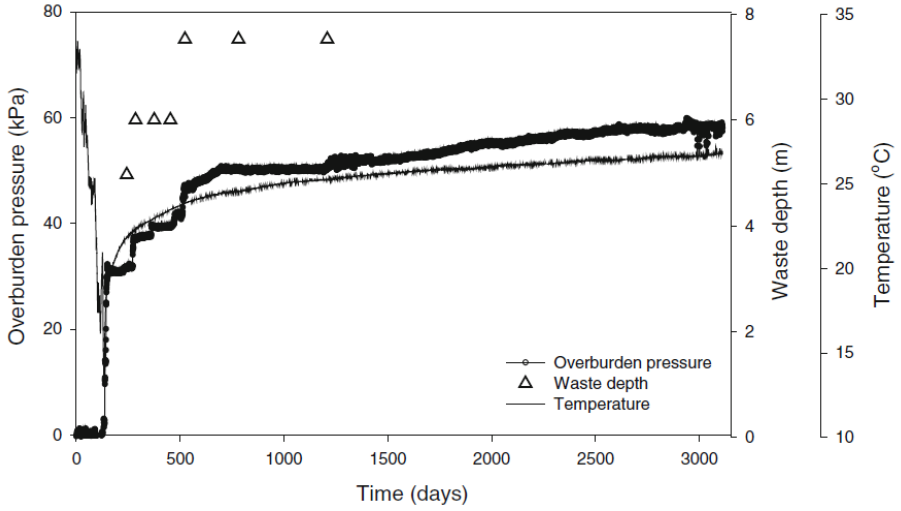

Figure 2-11: Sample data of overburden pressure, depth of waste, and temperature change during entire period of study (Timmons et al., 2011).

The average values sensed by the TEPCs placed in the sand drainage layer were underestimated as the average ratio of measured overburden pressure to predicted values was obtained to be 0.60. This indicated that the TEPCs measurements, on average, were 40% less than the expected overburden pressures. It was proposed that the reason for this underestimation was due to arching of the load around the TEPCs resulting from uneven distribution of forces due to heterogeneous nature of the waste and cover soil (Timmons et al., 2011). It is believed that drainage layer provided a support to the TEPC and led to bridging of the load around the TEPC.

2.4.2 Full-Scale Landfill, Sainte-Sophie Quebec, Canada

Waste Management of Canada (WM), Ontario Centres of Excellence (OCE), Natural Sciences and Engineering Research Council (NSERC), Carleton University, and three other engineering consulting firms initiated a research program with a goal to optimize the operation of landfills in northern climates. Sainte-Sophie Quebec, Canada has a landfill cell, known as zone 4, which is designed and operated to enhance waste stabilization without leachate recycle. Some researchers (e.g. Vingerhoeds, 2011) have referred to this landfill as a bioreactor landfill. However, as the definition of a bioreactor landfill has evolved, more and more definitions and researchers associate leachate recycle as a critical or required component of a bioreactor landfill. As a result, zone 4 at Sainte-Sophie is referred to as a landfill.

The landfill was equipped with 12 instrument bundles comprised of different sensors. Instrument bundles consisted of a 61cm by 61cm by 2.5cm thick steel plate on which different sensors, including a TEPC, a settlement system, an oxygen sensor, moisture and electrical conductivity sensor, and a piezometer, are mounted as shown in Figure 2-12 (Vingerhoeds, 2011). The instrument bundles and the collection pipes have been placed in the landfill cell as the landfill was actively filled with waste. The landfill houses four levels of horizontally-placed biogas collection pipes.

The instrument bundles were covered with sand before being covered by waste. The first two bundles were directly installed on the gravel layer of the leachate collection system on October 2009. The sensors on each bundle were wired individually to a

connection box that was placed on the steel plate. The connection box was used to connect the instrument bundles to a data acquisition system through a single data cable. The data logger recorded data every half an hour.

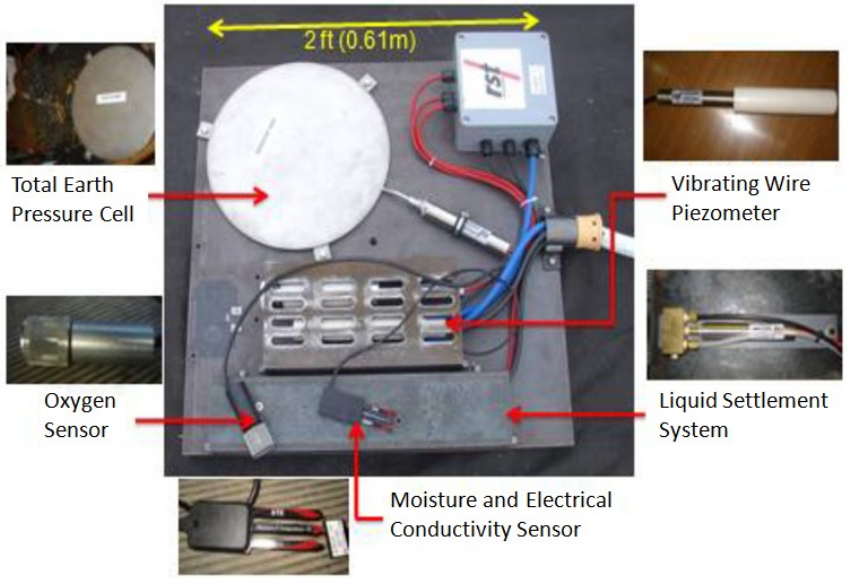

Figure 2-12: Instrument bundle installed in Sainte-Sophie landfill (Vingerhoeds, 2011)

The instrument bundles were installed in two vertical columns such that six instrument bundles were installed in each column with a slight shift in location for the two top bundles i.e. bundles 11 and 12. Bundle 11 is closer to the instrument shed and has less cover than bundle 12. The two columns were 18 m apart from each other, as shown in Figure 2-13; in such a way that column 2 was more into the landfill cell. The total depth of waste was determined based on the elevations of the instrument bundles as of April 2014, and the elevation of the top of the landfill above the instrument bundles as of June 2014 (Murray, 2014).

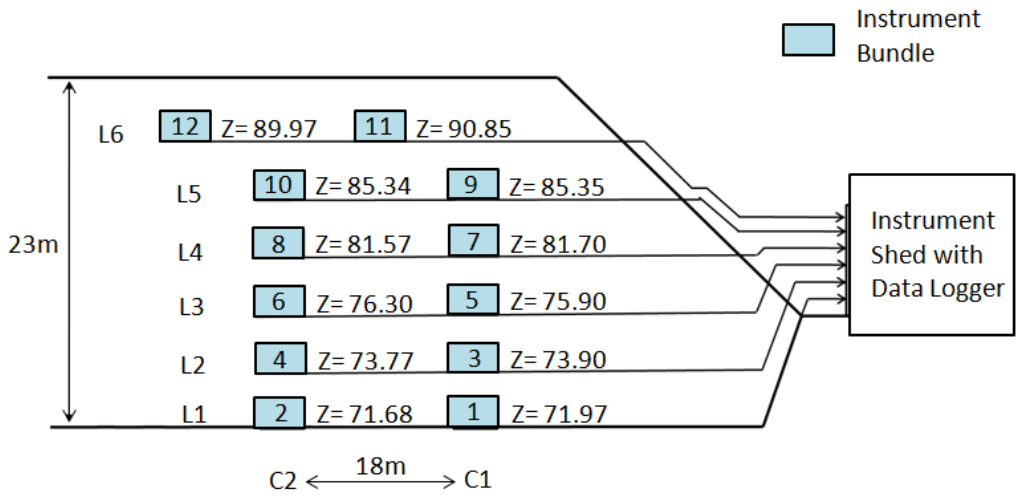

Figure 2-13: Cross section of bioreactor landfill (not to scale), showing instrument bundle placement and current elevations (Murray, 2014)

The TEPC evaluated the total overburden pressure as a result of waste placement above the instrument bundles. The amount of waste placed on top of each bundle was expected to generate a normal stress acting on the TEPC. Sharp increases in pressure were logged by the TEPCs due to waste lift placement. Increase in pressures continued over time such that the stress data collected in the field indicated higher values than the expected normal stress derived from the depth of waste above each bundle, as shown in Figure 2-14. The expected pressures were estimated based on the waste lift heights considering a constant unit weight of waste of 10kN/m^3. The unit weight of waste was obtained from quarterly surveys of the landfill site done by Waste Management personnel (Vingerhoeds, 2011). Table 2-1 presents the total depth of waste placed on top of each bundle, expected pressures due to the overlying waste, approximate pressures measured by the TEPCs, and the calculated stress ratios.

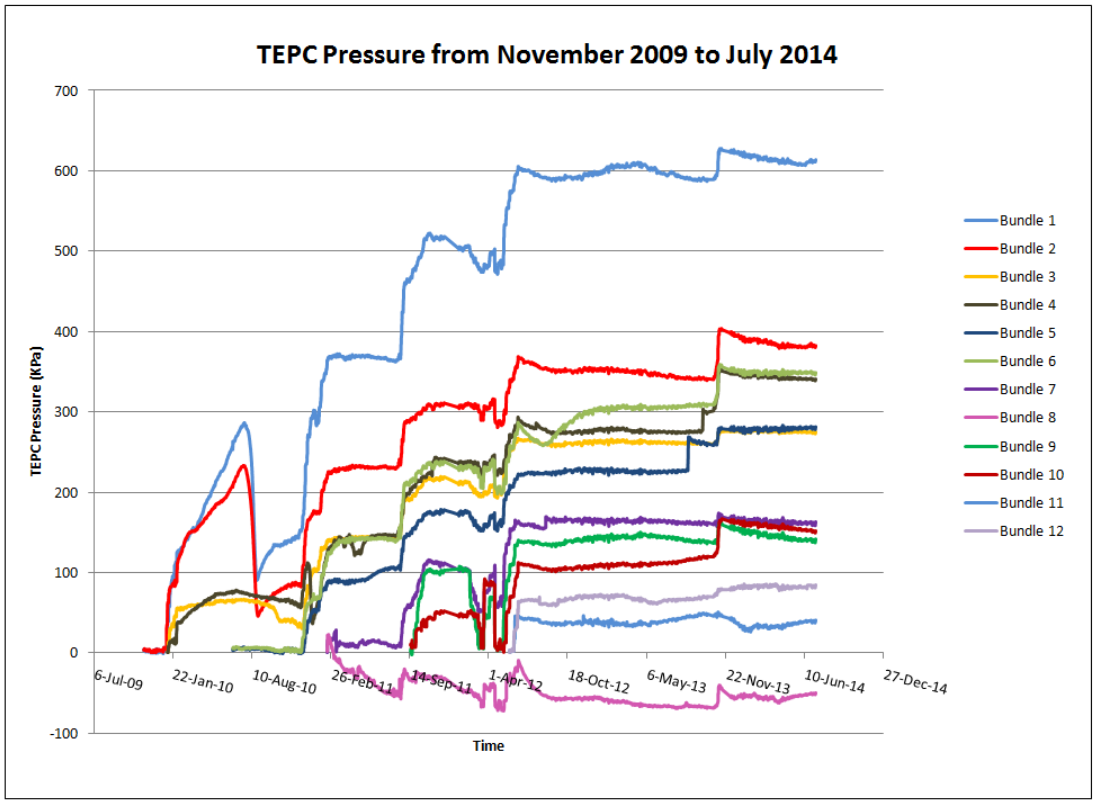

Figure 2-14: Stress measurements obtained by TEPC (Murray, 2014)

Table 2-1: The expected overburden pressures versus the pressures measured by the TEPCs

Bundle	Depth of Waste (m)	Overburden Pressure (kPa)	Approximate Pressure from Plot (kPa)	Stress Ratio
1	24.46	244.6	610	2.49
2	27.85	278.5	380	1.36
3	21.52	215.2	280	1.30
4	24.75	247.5	340	1.37
5	18.7	187	280	1.50
6	21.58	215.8	350	1.62
7	10.98	109.8	160	1.46
8	13.9	139	-	-
9	6.82	68.2	140	2.05
10	9.99	99.9	150	1.50
11	1.43	14.3	40	2.80
12	4.28	42.8	80	1.87

The stress ratio obtained for each bundle shows that the TEPC readings are 30% to 180% greater than the expected overburden pressures. Settlement and infiltration water might increase the pressure approximately 20kPa over the five years from the time of bundle installation and waste placement. Additional approximate 10kPa could be associated with the final cover. Yet, the data collected by the TEPCs significantly overestimates the overburden pressures. Research is required to understand the processes that lead to the overestimated overburden pressures.

3.0 Laboratory Experiments

Studies of TEPCs found in the literature did not provide an intimate knowledge of stress distribution within waste in landfills. At the Sainte-Sophie site, the TEPC outputs were revealed to be very different compared with the expected field pressure. Therefore, laboratory experiments were conducted to investigate the proposed hypothesis (section 1.3) causing the elevated stresses recorded by TEPCs in waste. Experimental work conducted in the lab was aimed to verify the concept of a "hard inclusion" as a result of contrasts in moduli of materials in relation to one another. Tests were performed employing a medium with high modulus of elasticity surrounded by a medium with low modulus of elasticity. The aim is to study the stress behavior of the materials with respect to the hard inclusion concept.

A low-weighted material with a low modulus of elasticity was required as a bedding material to create a high contrast in moduli. Woodchips were selected for this purpose. *Fibre Top Mulch Woodchips*, shown in Figure 3-1, provided by *Greely Sand and Gravel supplier of landscape and construction products* were chosen as the bedding material. Fibre Top Mulch Woodchips had a low modulus of elasticity and were relatively uniform in size. The woodchips were buried under snow and needed to be dried before being used in the laboratory experiments. The woodchips were used to fill a steel cell box with approximate dimensions of 2.71m x 1.47m x 1.01m without any compaction as shown in Figure 3-2.

Figure 3-1: Fibre Top Mulch Woodchips

Figure 3-2: Woodchips filled up the cell box

A TEPC with approximate diameter of 31.7cm was used in the experiments to measure the vertical stress. Initially, the TEPC was tested as an inclusion within the strong steel cell box to investigate the stress concentration on the TEPC itself. The TEPC

was positioned at the base and at the middle of the steel cell box filled with woodchips, respectively presented in Figures 3-3 and 3-4.

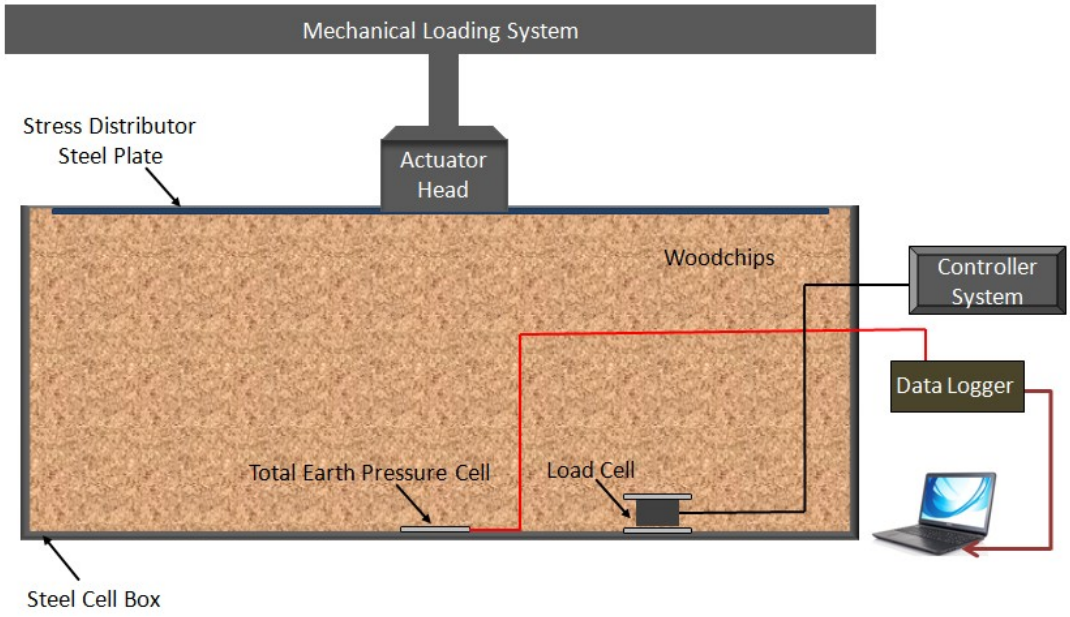

Figure 3-3: TEPC placement at the base of the cell box (not to scale)

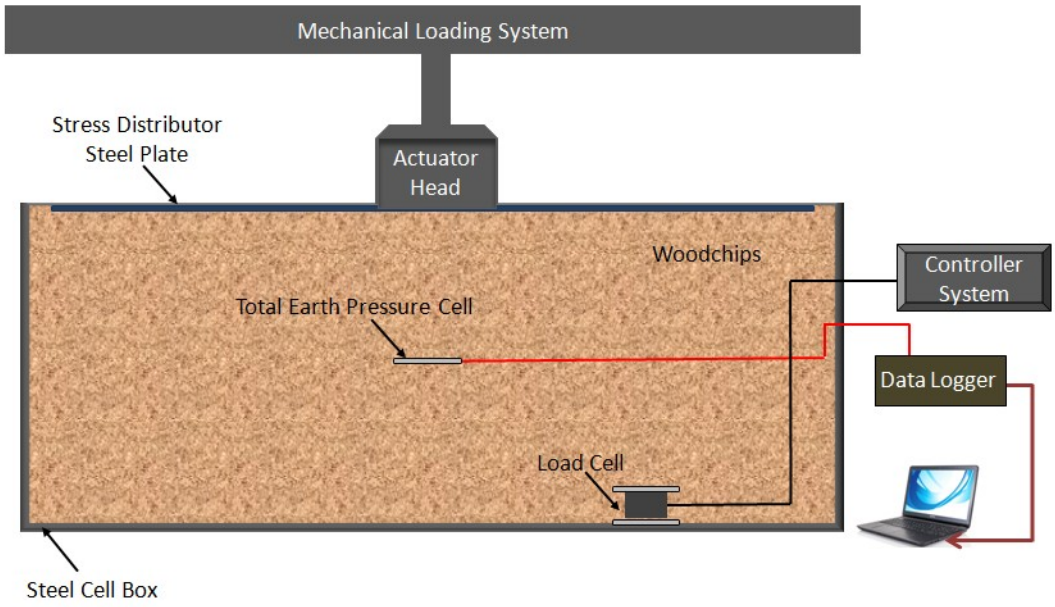

Figure 3-4: TEPC placement at the middle of the cell box (not to scale)

The objective of placing the TEPC at the base versus mid-depth in the woodchips was to demonstrate the increased stresses generated due to the concept of a hard inclusion. It is assumed that the TEPC placed at the base of the box will record the vertical stress that will be uniformly distributed over the base of the box. In comparison, it is assumed that the TEPC placed at mid-depth will act as a hard inclusion, given its higher stiffness, and therefore record higher stresses than those recorded by the TEPC at the base of the box.

TEPCs mounted on steel plates were further considered in the tests to increase contrasts of the moduli of elasticity of the TEPC and the woodchips while investigating the stress distribution. Tests were performed employing two steel plates positioned within the bedding material. Two square shaped steel plates with different sizes were individually used in the tests to investigate the effect of sizing. The first steel plate size was approximately 31.7cm x 31.7cm x 1.27cm and the second one was a larger steel plate with approximate dimensions of 59.7cm x 59.7cm x 1.27cm. The TEPC mounted on the steel plate was used to measure the applied stresses on the steel plate. Schematics of the TEPC with steel plates within the cell box are illustrated in Figure 3-5.

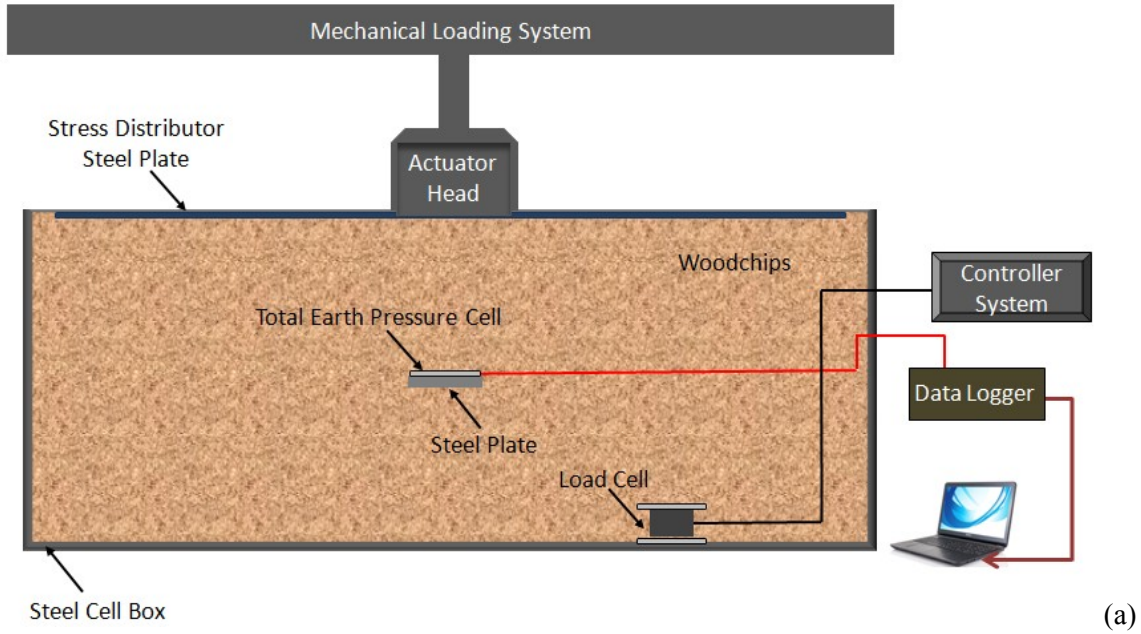

(a)

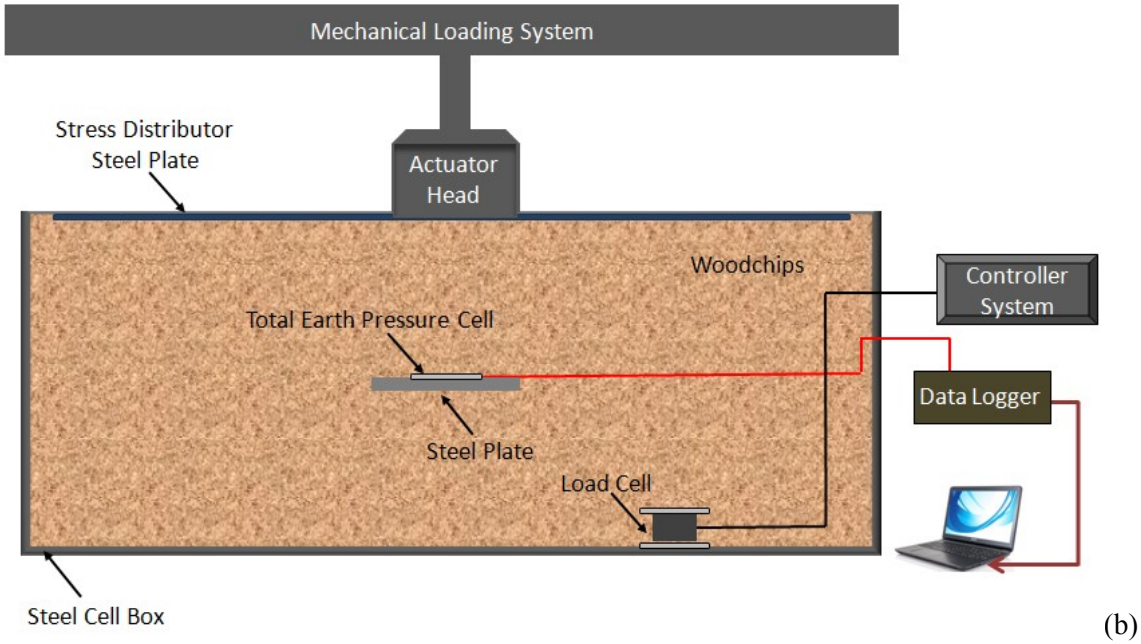

(b)

Figure 3-5: TEPC with steel plate testing (a) steel plate with approximate length of TEPC's diameter (b) steel plate with approximate length of double TEPC's diameter (not to scale)

Gas collection and leachate recirculation pipes surrounded in gravel in landfills may also experience elevated stresses due to the concept of the hard inclusion. To

demonstrate this, laboratory experiments were conducted to investigate the stress concentration on pipes. Experiments were carried out to determine stress distribution profile of the pipes positioned within the steel cell box filled with woodchips. Similar to the TEPC tests, one pipe was placed at the base of the box such that it would be exposed to the uniform overburden stress over the base of the box and the second pipe placed at mid-depth acting as a hard inclusion. Pressure measurement films were used to monitor the stress distribution on the pipes. Schematic of pipe testing is illustrated in Figure 3-6. Details of the experimental set-up are provided in Section 3.3 after a discussion outlining the sensors and devices used in the experiments.

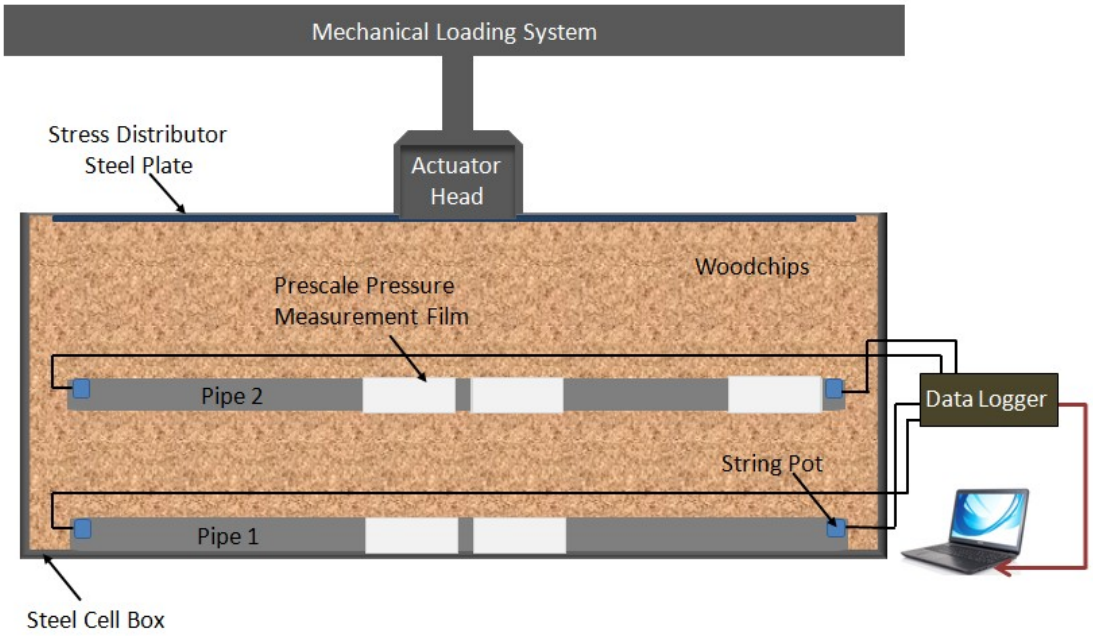

Figure 3-6: Pipe testing (not to scale)

3.1 Apparatus

The key equipment employed in laboratory experiments included the following:

- TEPC
- Load cell
- String potentiometers
- Prescale pressure measurement film
- Strong steel cell box, dimensions 2.71m x 1.47m x 1.01m
- Two standard HDPE pipes, 6inch diameter and 2m length
- Steel plates, approximate dimensions of 31.7cm x 31.7cm x 1.27cm and 59cm x 59cm x 1.27cm
- Woodchips, required for the volume of steel cell box , approximately 4 m^3
- Dead-load weights
    - Steel plate #1 (102kg)
    - Steel plate #2 (98kg)
    - Skewer steel plate (462kg)
    - Steel beam (116kg)
- Mechanical loading system (actuator)
- Data Acquisition System, required for TEPC and string pots
    - Flexi-Mux multiplexer
    - CR1000 FlexDAQ Datalogger
    - Loggernet Computer Program
    - PC200W Computer Program
- Controller system (Readout box), required for load cell
    - MTS 458.20 MicroConsole
- Laptop, to collect data from data acquisition system
- Vernier Caliper
- Shovels and rakes
- Steel tamper
- Power source
- Scissors
- Scale

3.2 Description of Devices

In this section, the main devices used in laboratory experiments are described. Additional instrument specifications are provided in Appendix A.

3.2.1 Total Earth Pressure Cell

The TEPC used in the experiments was designed by RST Instruments. The TEPC, shown in Figure 3-7, consisted of two circular stainless steel plates welded together forming an annular space filled with de-aired glycol. A stainless steel tube connected the cell to a transducer such that a closed hydraulic system was made. Stress applied on the sensitive side of the cell was measured by the vibrating wire pressure transducer as the result of pressurizing the glycol. Any changes caused by the applied stresses on the surface of the cell are converted to signals that can be read using a data logger.

The TEPC was calibrated to the 9053 B-units of readings for the vibrating wire readout at initial temperature and barometric pressure readings of 23.4°C and 1020.8 millibars, respectively, during calibration at the manufacturer. The TEPC was calibrated within the range of 0 to 500kPa and linearity full-scale error was obtained to be 0.35% (RST Total Earth Pressure Cell Calibration Record, 2008).

Using the program pre-installed in the data logger, the output of the vibrating wire readout generated in B-units was converted to a pressure reading in kPa. The recorded TEPC pressure in kPa was corrected for barometric pressures and initial zero readings, as

explained in Appendix B in detail. Following equation was used to convert the pressures to kPa (RST Total Earth Pressure Cell Calibration Record, 2008):

$$\text{Linear recorded TEPC pressure (kPa)} = (9053 - \text{Vibrating wire readout}) \times 0.15672 \frac{\text{kPa}}{\text{B} - \text{unit}}$$

Figure 3-7: TEPC

3.2.2 Load Cell

The employed load cell (Figure 3-8) designed by *MTS Systems Corporation* was an axial force transducer that provided an electrical signal with proportional magnitude to the force being measured. The load cell was calibrated at temperature of 73°F before shipping within the range of -2 KIP to 2KIP. Full-scale error was obtained to be less than 0.035 (MTS Force Transducer Calibration Record, 1993).

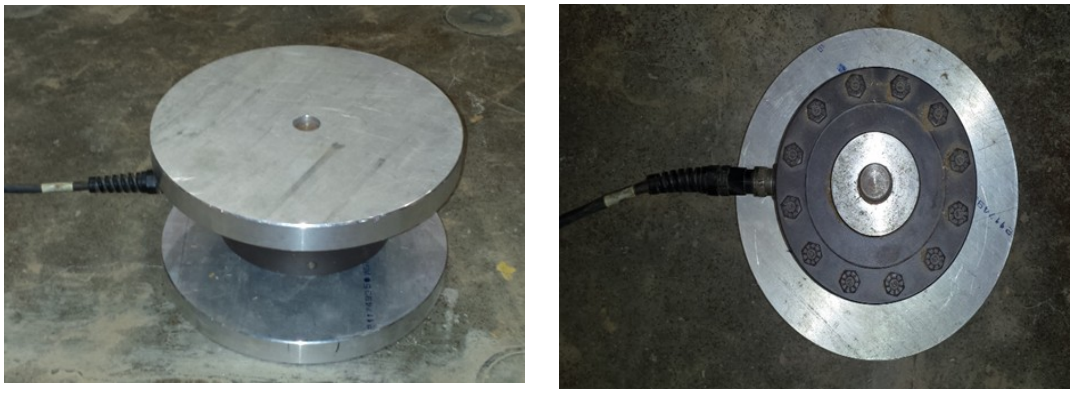

Figure 3-8: Load cell

3.2.3 Prescale Pressure Measurement Film

The Prescale Pressure Measurement Film (PPMF) designed by *Fujifilm Holdings Corporation* was used to measure the stress concentration on the pipe. The PPMF, shown in Figure 3-9, was an Extreme Low Pressure (4LW) two- sheet type film composed of two polyester bases. The top polyester base was coated with a micro-encapsulated color forming layer known as A-film and the bottom polyester base was coated with a layer of the color-developing product known as C-film. A-film is a translucent white color and C-film is whitish before applying any pressure (Prescale Pressure Measurement Film Instruction Manual, 2014).

The PPMF works such that the micro-capsules are broken as the pressure is applied and the color-forming material responds to the color-developing material to create pink color with different densities. The pink color density varies according to the amount of pressure applied in such a way that light red color indicates a low applied pressure and deep pink color corresponds to a high applied pressure (Prescale Pressure Measurement Film Instruction Manual, 2014).

Pressure charts and Prescale standard color sample are available to determine the pressure values measured by PPMF. The pressure values can be obtained by choosing a pressure curve from the standard pressure chart considering temperature, humidity and pressure condition (Prescale Pressure Measurement Film Instruction Manual, 2014).

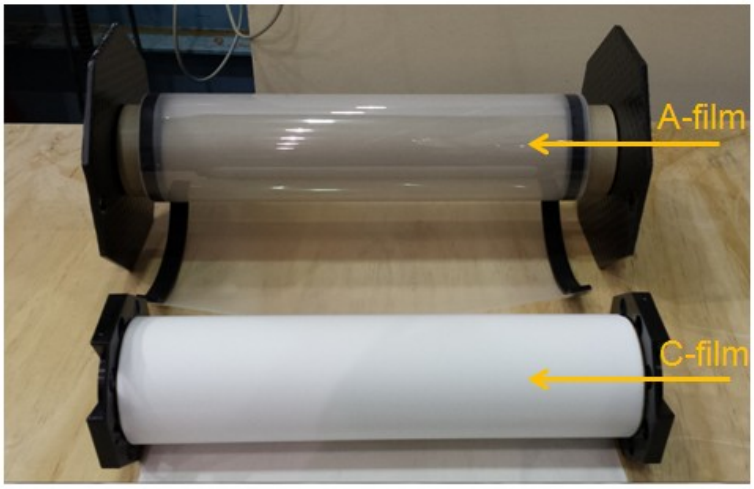

Figure 3-9: PPMF

3.2.4 String Potentiometer

Position sensors of type Celesco SP1-25 string pots designed by *Measurement Specialties* were employed in the pipe testing (Celesco SP1 Instruction Manual, 2014). These compact string pots with voltage divider outputs were capable of providing measurement ranges up to 635mm (25inch). The string pots shown in Figure 3-10, were used to determine the linear displacement changes in pipe diameter. The SP1 string pot was supplied 5V from a regulated stable source. The varying output voltage was measured with the CR1000 data logger and visualized on the PC200W software.

Figure 3-10: String pot

3.2.5 Data Acquisition System

The Data Acquisition System, shown in Figure 3-11, included Campbell FlexDAQ Data logger Model CR1000 and RST Instruments Flexi-Mux multiplexe (Campbell Manual, 2006; RST Flexi-Mux Manual, 2004). The system encased in a weatherproof enclosure was used to record TEPC's outputs over time and the collected data was retrieved using Loggernet software. The Data Acquisition System was also used to record the outputs of the string pots that were retrieved using PC200W software.

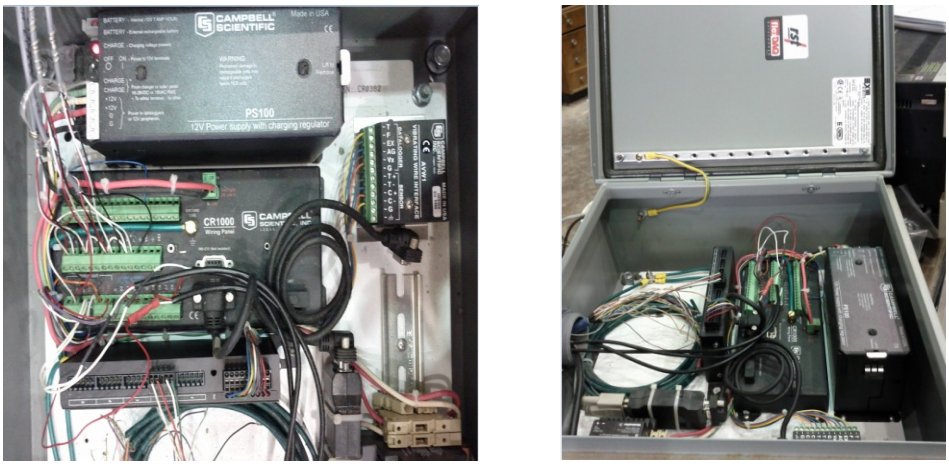

Figure 3-11: Data Acquisition System

3.2.6 Test System

The test system (controller system), configured with a 458.10 MicroConsole and its associated controllers including 458.12 DC and 458.14 AC controllers, was designed by MTS Systems Corporation (MTS MicroConsole Manual, 1986). The test system, shown in Figure 3-12, was used to control a hydraulic actuator during loading and unloading phases of the tests. The actuator consisted of a linear variable differential transformer (LVDT) and a load cell. The actuator LVDT outputs were managed by the AC controller while load cell outputs were controlled by DC controller. The same test system was also used to monitor the outputs of the load cell placed at the base of the steel cell box.

Figure 3-12: Controller system

3.3 Experimental Set-up

The conducted experiments with the test procedure are explained in detail below. All the tests were carried out in a steel cell box, with dimension of 2.71m x 1.47m x 1.01m.

3.3.1 Initial TEPC Testing

- **TEPC at the Base of Steel Cell Box (Initial Base TEPC Testing)**

1. Load cell was placed at a distance of about 50cm from the edges of the box, at the base of the cell box.
2. TEPC was placed at the base of the cell box, as shown in Figure 3-13, at a distance of 50cm away from the load cell to compare the outputs of the TEPC.
3. TEPC electrical lead was connected to the Data Acquisition System and load cell electrical lead was connected to the test system.
4. A no-load zero reading was recorded for the TEPC and the load cell.

5. The cell box was filled up manually with woodchips with initial compaction using a steel tamper. Woodchips were placed in 10 lifts compacted layer by layer as shown in Figures 3-14 through 3-16.
6. Top layer of woodchips was spread over the length of the cell box.
7. Two steel plate dead-loads serving as a load distribution system were spanned on top of the woodchips to uniformly distribute the applied stresses using the actuator. A skewer steel plate and a steel beam were then placed on top of the steel plate dead-loads. Total approximate dead-loads of 7.6kN were placed on the top layer of woodchips as presented in Figures 3-17 through 3-19. Dead-loads included:
    - Steel plates
        - Steel plate #1 (102kg)
        - Steel plate #2 (98kg)
    - Skewer steel plate (462kg)
    - Steel beam (116kg)

8. A hydraulic jack system (actuator) arranged near the steel cell box was used to apply vertical loads as shown in Figure 3-20. The applied loads were incremented from 0kN to 10kN, 20kN, 30kN, 40kN, 50kN, 60kN, 70kN, 75kN, 80kN, 90kN, 100kN, 110kN, 120kN, 130kN, 140kN and 150kN by the actuator.
9. Pressure measured by the load cell and the TEPC were recorded for each loading stage.
10. Displacement data were recorded by the actuator LVDT for loading stages.
11. The applied loads were decrementally averted back to 0kN.
12. Pressure and displacement data were recorded for unloading stages.
13. Required corrections were made for the recorded data.
14. Total height of compacted woodchips inside the bin was measured. The final woodchips height at the end of the experiment is provided in Appendix C.

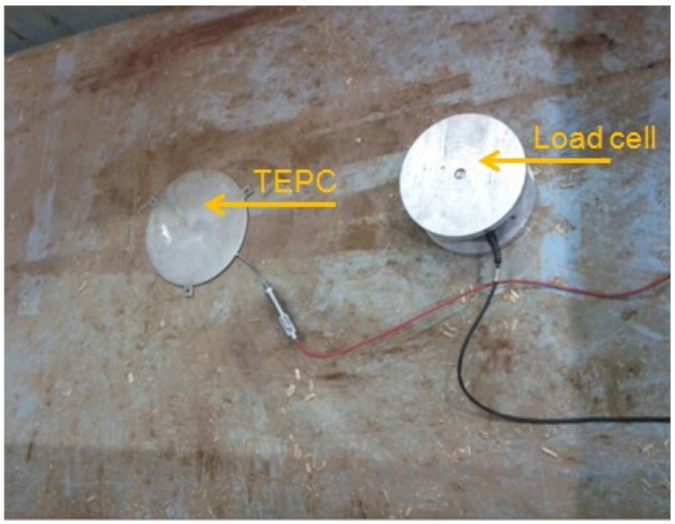

Figure 3-13: Placement of TEPC and load cell at the base of the cell box.

Figure 3-14: First woodchips lift with initial compaction

Figure 3-15: Placement of additional lifts of woodchips within the cell box

Figure 3-16: Placement of final lift of woodchips within the cell box

Figure 3-17: Placement of steel plate dead load #1 (102kg)

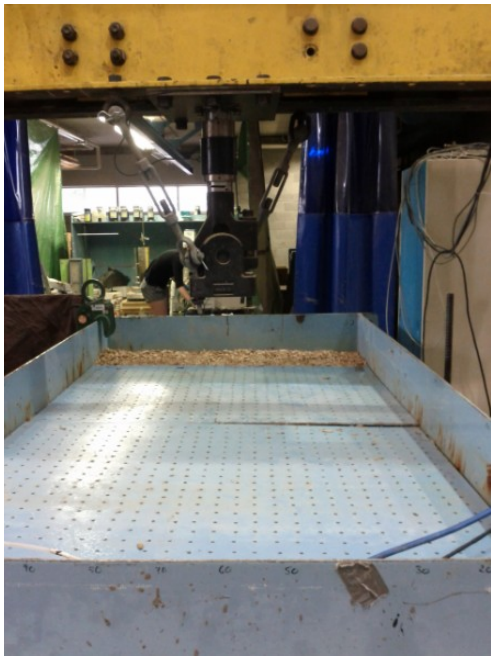

Figure 3-18: Placement of steel plate dead load #2 (98kg)

Figure 3-19: Placement of skewer steel plate and steel beam

Figure 3-20: Load applied via actuator

- **TEPC Placed over Woodchips at the Middle of Steel Cell Box (Initial Middle TEPC Testing)**

1) The load cell was placed at the base of the cell box at its previous location.
2) The wire attached to the load cell was fed out of the cell box and attached to the test system.
3) The load cell was covered by woodchips that were placed in different lifts with initial compaction using the steel tamper.
4) At middle height of compacted woodchips measured at the end of previous test, approximately 0.40m from the base of the box, the TEPC was placed on the woodchips layer that was completely leveled as presented in Figure 3-21. The TEPC was pressed in place to ensure a uniform contact.

Figure 3-21: Placement of TEPC at middle height of woodchips

5) The TEPC cable was led out of the cell box and attached to the data logger.
6) Additional woodchips lifts were placed on top of the TEPC with initial compaction. Each lift height was approximately 10cm.
7) Steps 6 through 14 in Initial Base TEPC Testing were followed.

3.3.2 TEPC Placed over Steel Plate at the Middle of Steel Cell Box (Steel Plate Testing)

The conducted experiment procedure was similar to the Initial Middle TEPC Testing. After placement of the load cell at the base of the cell box and deposit of woodchips with compaction up to the middle height of total woodchips, the steel plate was positioned at the centre of the cell box on the compacted woodchips layer. The TEPC was placed on top of the steel plate and the TEPC cable was led out of the box and attached to the data logger.

The steel plate testing was conducted using two different sizes of steel plate. One steel plate had the same approximate length and width as the TEPC's diameter. The other selected steel plate was increased in size such that it had the same approximate length and width of double the TEPC's diameter. Figure 3-22 and 3-23 show the TEPC on the two steel plates.

After placement of the combined steel plate and TEPC within the woodchips, additional woodchips were added to the cell box and compacted in 10cm lifts. Steps 6 through 14 in TEPC Testing were repeated.

Figure 3-22: Smaller steel plate and TEPC within the woodchips

Figure 3-23: Larger steel plate and TEPC within the woodchips

3.3.2.1 Steel Plate Testing with Silicon at the Middle of Steel Cell Box

In the previous tests, the TEPC was just placed on top of the steel plate. To ensure that the TEPC did not shift or slide off the plate, the TEPC was attached to the steel plate using silicon. Small steel plate testing was re-conducted employing silicon between the TEPC and the steel plate as presented in Figure 3-24 and 3-25. Unexpectedly, the performance of the TEPC was determined to be significantly affected by the use of the silicon.

Figure 3-24: Use of silicon

Figure 3-25: Silicon glued the TEPC to the small steel plate

3.3.3 Pipe Testing at the Bottom and Middle of Steel Cell Box

The objective of pipe testing was to evaluate stress concentration on pipes typically used in landfills and measure vertical and horizontal changes in interior diameter of the pipes. In this experiment, two identical 2m long standard High Density Polyethylene (HDPE) pipes were used. The pipes were type schedule 80 perforated pipes with measured outside diameter of approximately 16.5cm and wall thickness of about 1cm. The pipes were subjected to loading while one pipe (pipe #1) was placed at the base of the cell box and the other pipe (pipe #2) was positioned at the middle of the woodchips height. The instrumentation of the pipes and the setup procedure are explained in detail below.

- **Step 1: String Pot Installation**

Celesco string pots were installed inside the pipes to measure the interior diameter changes of the pipes. One string pot per measurement location was required by making a

tiny hole in the pipe at that location to bolt the string pot to the pipe. To measure vertical and horizontal changes to the diameter at the middle of the pipe, two string pots were required to be installed at that location. Due to string pot installation difficulties inside the pipe, bolts were used around the periphery of the pipe at the middle of the longitudinal length to place eyelets inside the pipe for string pot installation. High strength, coated, non-stretch string was fastened to the top-side of the pipe, halfway down the length. The string was then strung straight down through the pipe to the bottom-side and routed through one eyelet, thus making a vertical line across the diameter of the pipe and continuing the line 90 degrees down the length of the pipe to the opening on one end as shown in Figure 3-26 and 3-27. This end of the string was attached to the string pot mounted near the outer edge of the pipe as presented in Figure 3-28. The string was fastened in a way that the string pot was already stretched out a few centimeters to allow movement during testing without the string pot bottoming out. One string pot was placed at one end of the pipe to measure vertical diameter changes and the other string pot was placed at the other end of the pipe to measure horizontal diameter changes. In total, two string pots were placed inside each of the pipes to measure the vertical and horizontal diameter changes at the middle length of the pipe.

Before hooking up the string pots in the pipes, they were individually calibrated with a Vernier caliper to determine the calibration factor and convert the output (mV) to a displacement (mm).

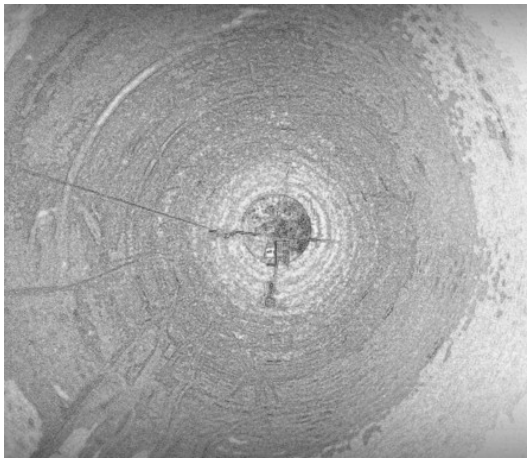

Figure 3-26: String fastened into the pipe for string pot setup

Figure 3-27: String routed through eyelet

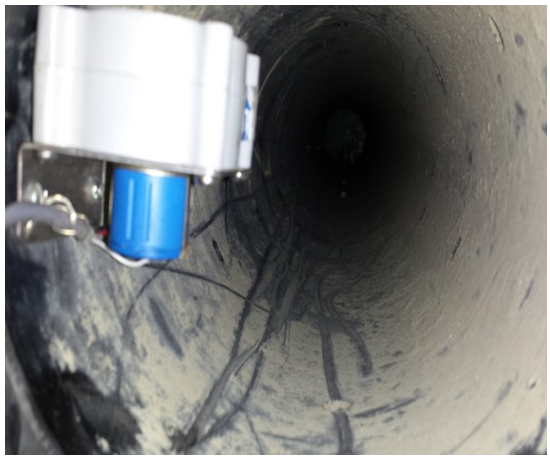

Figure 3-28: String pot positioned inside the pipe at near the edge

- **Step 2: PPMF Preparation**

The PPMF consisted of A-film and C-film that were delivered within separate dedicated cases with octagonal flanges. The films were unwound with the inner side of the roll facing up by rotating the flanges. Each film was cut in five pieces with approximate

length of 21inch. Extra attention was paid to avoid bending or touching the color-forming material layer. Once the films were cut to the required size, they were placed together such that the coated sides (color-forming material side of the A-film and the color-developing material of the C-film) faced towards each other. The films were wrapped around the HDPE pipes at their centers where pressure concentration was aimed to be investigated. Stress concentration around the end of pipe #2 was also inspected by employing a piece of pressure film around one corner end.

- **Step 3: Pipe #1 Preparation and Placement**

Due to the existence of the bolts on the outside of the pipes for eyelet installation inside the pipes, it was impossible to place the pipe at the base while avoiding the pipe sitting on the bolts. Therefore, a layer of sand with approximate thickness of 1cm was poured on the base of the cell box to provide bedding for pipe #1. The sand bedding was placed throughout the length of the cell box in the middle and manually compacted with shovel. The instrumented pipe #1 with the string pots was then placed on top of the sand layer as shown in Figure 3-29. Once the pipe was placed at its desired location, the pressure films were wrapped around the pipe centre as shown in Figure 3-30. The wires of the string pots were fed out of the cell box and attached to the Data Acquisition System.

Figure 3-29: Placement of pipe #1 on a layer of sand

Figure 3-30: Locations at which pressure films were wrapped around pipe #1

- **Step 4: Filling Half the Cell Box**

The cell box was filled in 10cm lifts of woodchips to the approximate height of 40cm from the base. Each lift of woodchips was manually compacted with the steel tamper similar to the TEPC tests. During the woodchips deposition, extra care was taken not to directly stand on the area where pressure films were used around the pipe. Figure 3-31 shows the deposition of woodchips in the cell box.

Figure 3-31: First woodchips lift deposition on top of pipe #1

- **Step 5: Pipe #2 Preparation and Placement**

Pipe #2 that was already instrumented with string pots was placed on top of the woodchips. Pressure films were wrapped around pipe #2 at its centre and one end to evaluate the stress concentration at these locations as shown in Figure 3-32.

Figure 3-32: Locations at which pressure films were wrapped around pipe #2 positioned at a woodchips layer

- **Step 6: Load Application**

After placement of pipe #2 inside the box, additional woodchips lifts were deposited in the cell box with manual compaction. Once the box was filled with woodchips, steel plates #1 and #2 were spanned on top layer of woodchips to distribute the stress. Other steel dead loads similar to previous tests were placed on top of the steel plates.

An actuator capable of applying a maximum load of approximately 225kN was used to apply load on the cell box system. The applied loads via the actuator were incremented by 10kN from 0kN to 220kN and then increased to 225kN, the maximum applied load. The incremented loads were removed in stages as applied.

- **Step 7: PPMF and Displacement Data Results**

After unloading and removing the dead loads from inside of the cell box, the woodchips were shovelled out and the buried pipes were taken out from the woodchips to investigate the pressure film results. The A-film was peeled off from the C-film in order to detect color density on the C-film. The C-film was placed on white sheets of paper to visually check the pressure distribution. The color density was observed from the polyester base side in the light.

The horizontal and vertical changes in diameter of both pipes were monitored using PC200W program installed on the laptop. The diameter changes were measured for each loading and unloading stage.

3.4 Complementary Tests

Woodchips and HDPE pipe were tested to determine their material properties. The modulus of elasticity of the woodchips was obtained in-situ during the aforementioned experiments. The modulus of the pipe and shear strength parameters of the woodchips that were determined after the TEPC and pipe testing are explained in Appendix D.

- **Shear Strength Parameters of Woodchips**

A direct shear test was used to determine the shear strength parameters of the woodchips. For this purpose, a direct shear box with approximate dimensions of 63.5mm x 63.5mm was utilised to determine cohesion and internal friction angle of the woodchips for normal confining stresses of 40kPa, 60kPa and 80kPa.

- **Modulus of Elasticity of HDPE Pipe**

A cross section of the HDPE pipe with initial outside diameter of 16.5cm and approximate length of 10cm was selected in order to determine modulus of elasticity of the pipe. The cross section of the pipe was placed inside the Instron 5582 Universal Testing Machine as shown in Figure 3-33. The pipe was tested under a pressure of 60kPa and the vertical displacements were measured using a computer software program. A total displacement of approximate 0.45mm was recorded for a maximum pressure of 60kPa. The modulus of the pipe was determined from the slope of the plot line of the stress versus strain.

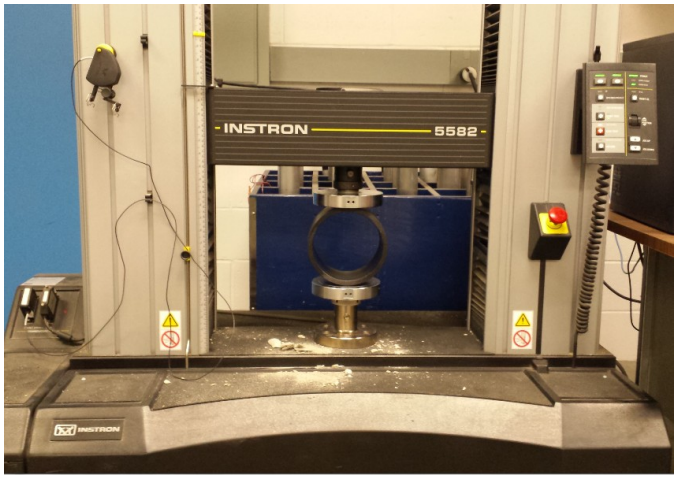

Figure 3-33: Instron 5582 Universal Testing Machine with positioned pipe

4.0 Experimental Results

The results obtained from the laboratory experiments involving initially testing of the TEPC at the base and the middle of the cell box, testing two different steel plate sizes on which the TEPC was mounted, and investigating two HDPE pipes placed in the same cell box are illustrated in this chapter. The final height of the woodchips inside the box at the end of each experiment obtained based on the vertical displacement of the woodchips recorded by the LVDT is provided in Appendix C.

4.1 TEPC Results

Outputs of the TEPC placed within the cell box were recorded in B-unites and converted to pressure in kPa. The maximum applied load via the actuator reached 150kN during the loading phase. This amount of load was applied over the approximate 4 square meter area of the cell box used in the experiments, producing a maximum applied pressure of approximately 38kPa. The results obtained during each test in terms of measured pressure by the TEPC have been plotted versus the total applied pressure. The total applied pressure included pressure applied by the actuator, the dead loads and the weight of woodchips.

4.1.1 Initial TEPC Testing Results

When the TEPC was placed at the base of the cell box and 150kN of load was applied over the steel plates spanned on top of the woodchips, the measured pressure by the TEPC was obtained to be 29kPa. This value is significantly lower than the expected value

of approximately 40kPa. The difference between the maximum applied pressure and the recorded pressure by the TEPC placed at the base of the box may be attributed to either the frictional forces at the box boundary and/or an improper calibration curve of the TEPC. The manufacturer's calibration curve was used since Carleton University does not have a proper liquid pressure vessel to re-calibrate the TEPC. The TEPC tested was the TEPC contained in the initial prototype bundle tested in 2008/2009. The calibration curve may have been altered since then. As a result, it was assumed that the TEPC calibration curve was incorrect and that the TEPC was exposed to approximately 40kPa when placed at the base of the box. Therefore, the stresses recorded by the subsequent tests were compared to the reference stress recorded at the base; increases in measured stress reflected stresses greater than 40kPa and decreases in measured stress reflected stresses less than 40kPa. To facilitate this comparison, the slopes of the total applied pressures versus the measured pressures by the TEPC were compared.

For the experiment with the TEPC at the base, the total applied pressures versus the measured pressures by the TEPC are plotted in Figure 4-1. The plot line of the pressures was obtained to have a slope of approximate 0.71. When the TEPC was placed at the middle of the woodchips height under the 150kN of applied load, the measured pressure by the TEPC was found to be approximately 37kPa (Figure 4-2). From the equation of the line plotted for the applied pressures versus the measured pressures by the TEPC at the middle of the woodchips height, a slope of approximate 0.93 was obtained.

It was found that when the TEPC was at the middle height of the woodchips, the measured pressure by the TEPC was approximately 28% greater than when it was

directly placed on a base of the cell block. In other words, moving the TEPC from the base of the cell box to the middle led to increase in stress concentration on the TEPC.

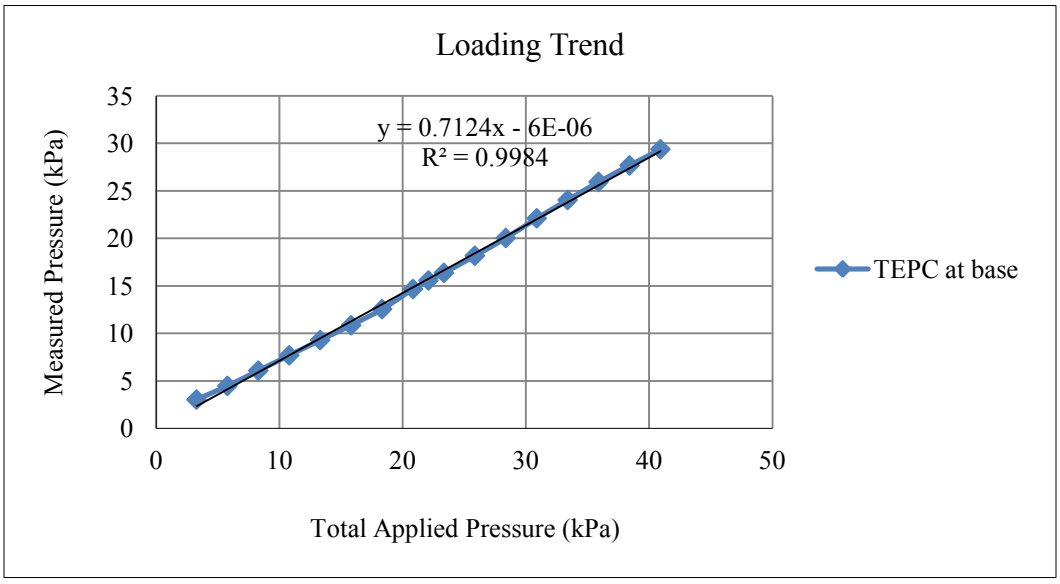

Figure 4-1: Pressure measurements by TEPC positioned at the base of the cell box

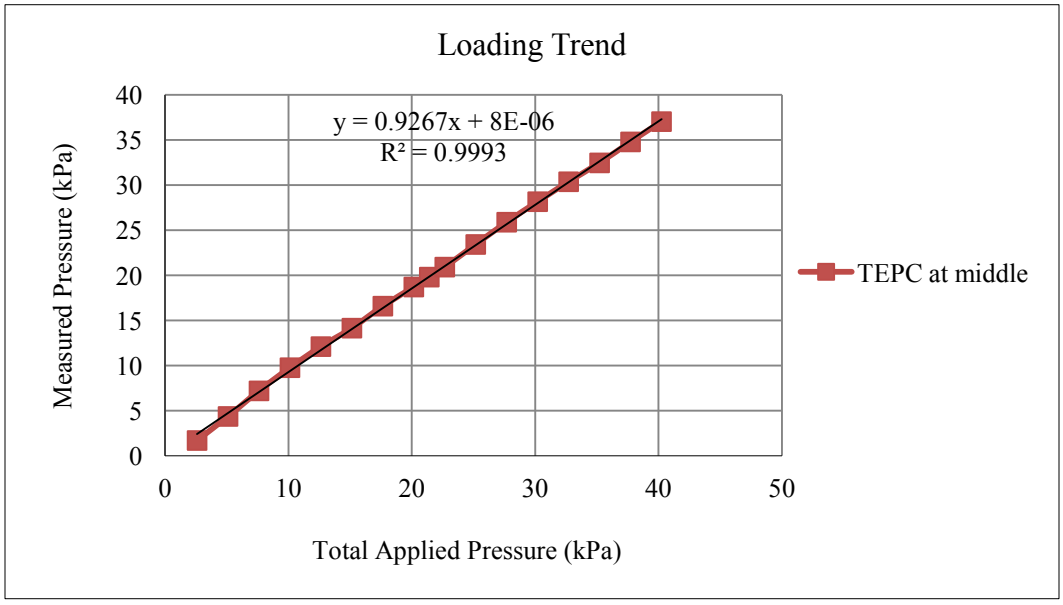

Figure 4-2: Pressure measurements by TEPC positioned at the middle of the cell box

4.1.2 Steel Plate Testing Results

Two different sizes of steel plates having the same thickness were used underneath the TEPC before installation within the middle layer of woodchips. When the smaller steel plate was used and 150kN of load was applied on the material inside the cell box, the measured pressure was about 38kPa. When the larger steel plate was used under the maximum applied load of 150kN, the pressure was measured to be approximately 35kPa. The applied pressures versus the measured pressures for both tests were plotted and the equations of the lines were obtained. The slope of the plot line with respect to the small steel plate testing was determined to be 0.93 while the slope of the plot line associated with the larger steel plate was 0.87. The results obtained from the TEPC's measurements for the TEPC mounted on the small steel plate and the larger steel plate during loading phases are shown in Figures 4-3 and 4-4, respectively. Comparing the two steel plate tests, it was determined that the stress recorded by the TEPC decreased when the steel plate size increased.

When the smaller steel plate was used in the experiment, the outputs of the TEPC were close to the findings of the TEPC placed alone at the middle of the woodchips layer, with only 1kPa difference. The results obtained from the small steel plate testing could be expected to be a bit higher compared to the TEPC results alone, since placing a steel plate underneath the TEPC increases the total thickness and stiffness of the combination of the steel plate and the TEPC. Two scenarios could explain why not much difference was observed when employing the small size steel plate:

- The first scenario could be related to the difference in stiffness. The contrast of stiffness between the TEPC alone and the woodchips as the bedding material around the TEPC was significantly different initially. The added stiffness did not change this contrast significantly because the modulus of elasticity of the TEPC was much closer to the modulus of elasticity of the steel plate compared with the woodchips.
- The second scenario could be related to the support provided to the TEPC by the steel plate. The thickness of steel plate was approximately 1.3 times greater than the thickness of the TEPC. Since the steel plate underneath the TEPC is stiffer than the TEPC itself, the stress was more uniformly distributed over the TEPC preventing an increase in the pressure measurements seen without the steel plate. Therefore, stress concentration on the TEPC was lower than expected.

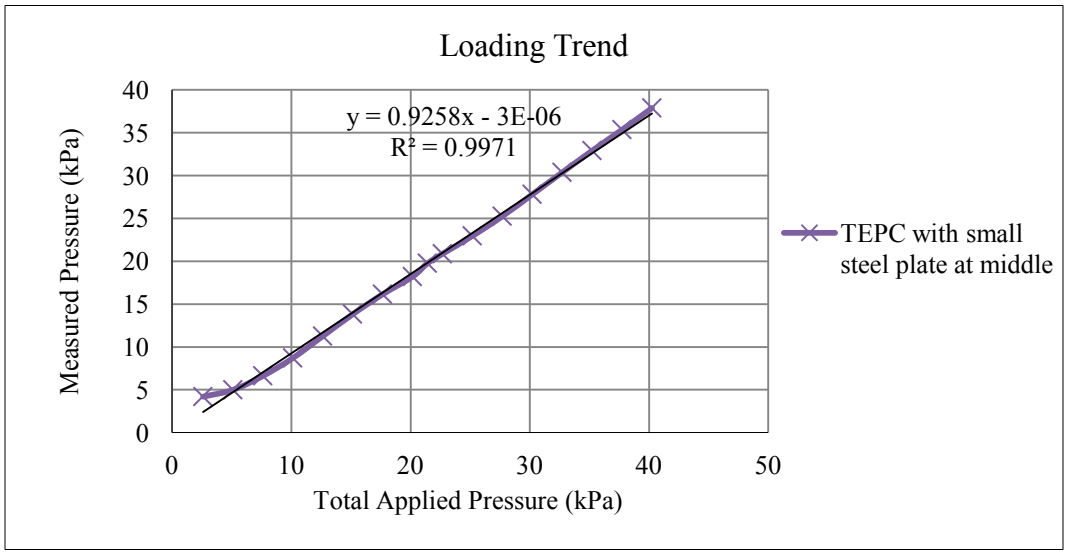

Figure 4-3: Stress concentration on TEPC mounted on the small steel plate

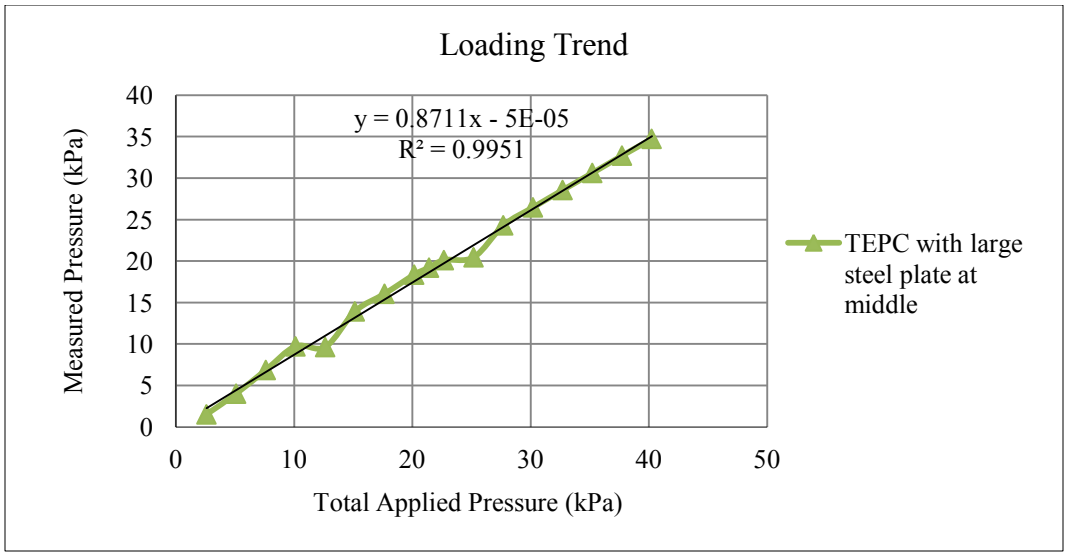

Figure 4-4: Stress concentration on TEPC mounted on the large steel plate

4.1.2.1 Pressure Measurements Repeatability

Repeatability of the small steel plate testing with loading and unloading of the same woodchips sample was investigated. Figure 4-5 shows the results of the repeated test during loading phase when the small steel plate with the TEPC was placed at the middle height of the woodchips. The plot line of the measured pressures versus the total applied pressures obtained during the repeated test fell on top of the plot line of the small steel plate test conducted in the initial test (discussed in section 4.2), as shown in Figure 4-6. This showed the repeatability on the instrumentation and the measured transferred load.

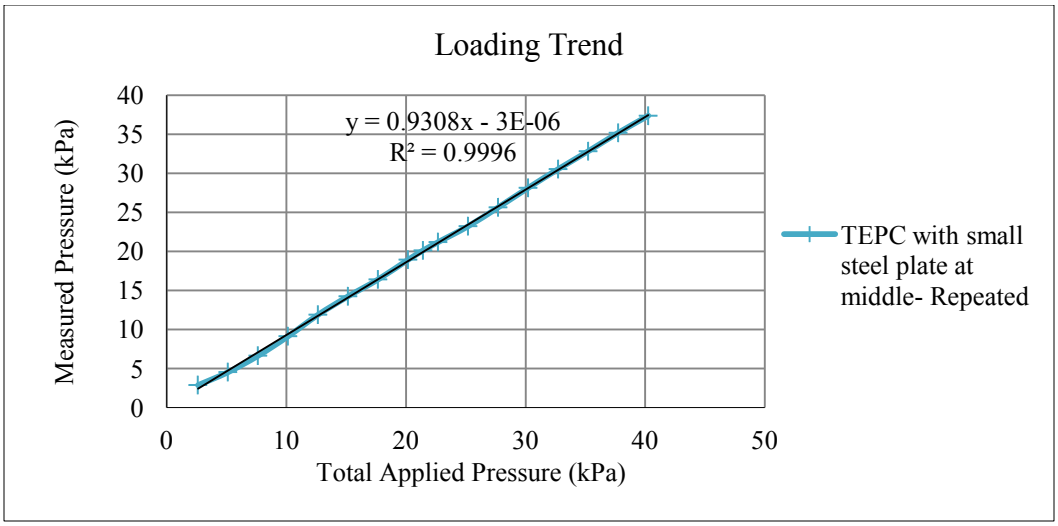

Figure 4-5: Repeatability of small steel plate testing

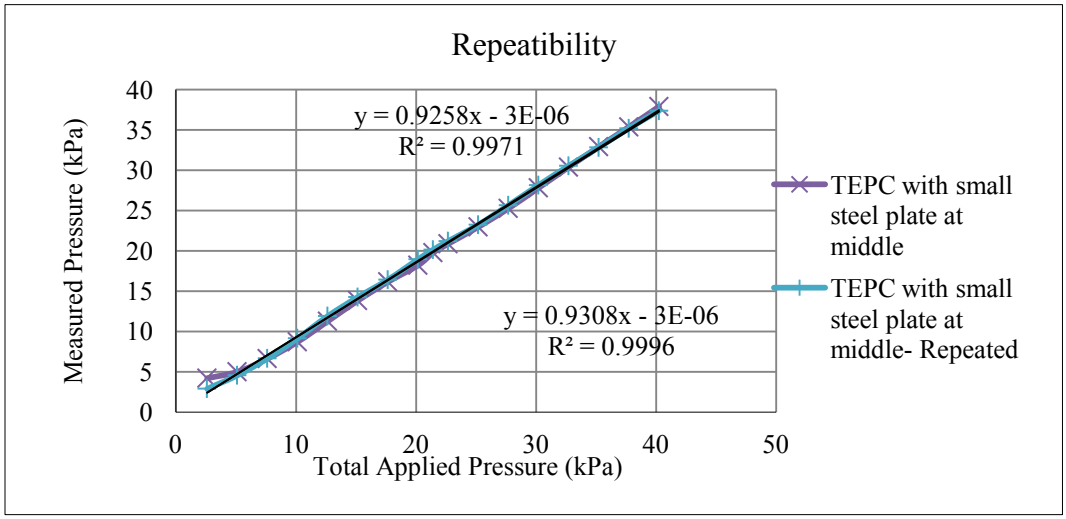

Figure 4-6: First and repeated test on the small steel plate with the TEPC

4.1.2.2 Effect of Silicon on Measurements

A thin layer of silicon was employed between the TEPC and the small steel plate. The plot of the measured pressures by the TEPC attached to the steel plate versus the applied pressures is shown in Figure 4-7. The slope of the plot line decreased from approximately 0.93 when TEPC was mounted on the steel plate without the use of silicon to 0.68 when silicon was used. The drop in the plot line is presented in Figure 4-8. Comparing the outputs of the TEPC, it was realized that silicon played a significant role on the TEPC's outputs. The TEPC did not seem to be solid anymore and acted as a softer material than the woodchips. Use of silicon showed how important it is to understand material properties around the TEPC.

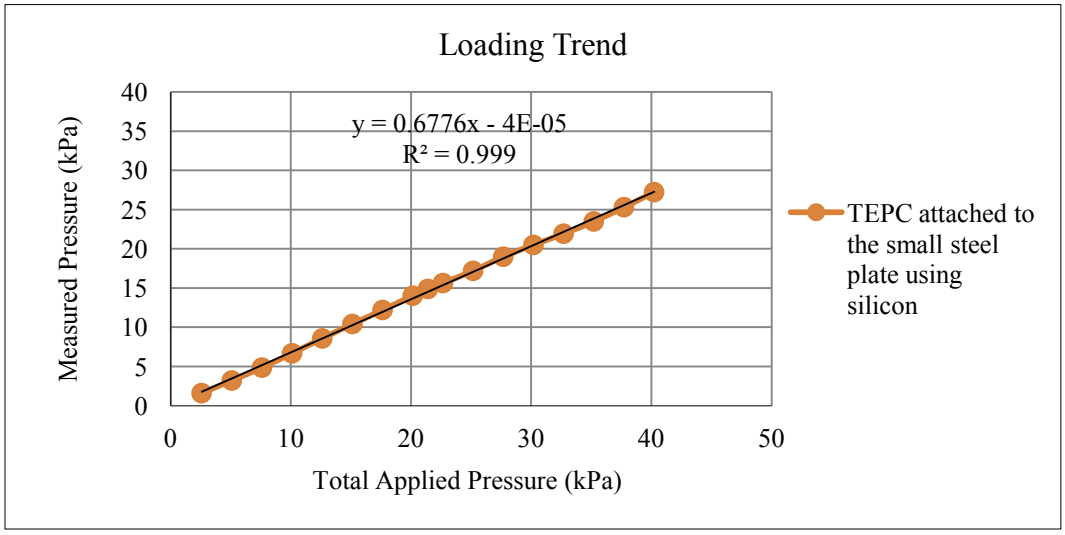

Figure 4-7: Results of TEPC attached to the small steel plate using silicon

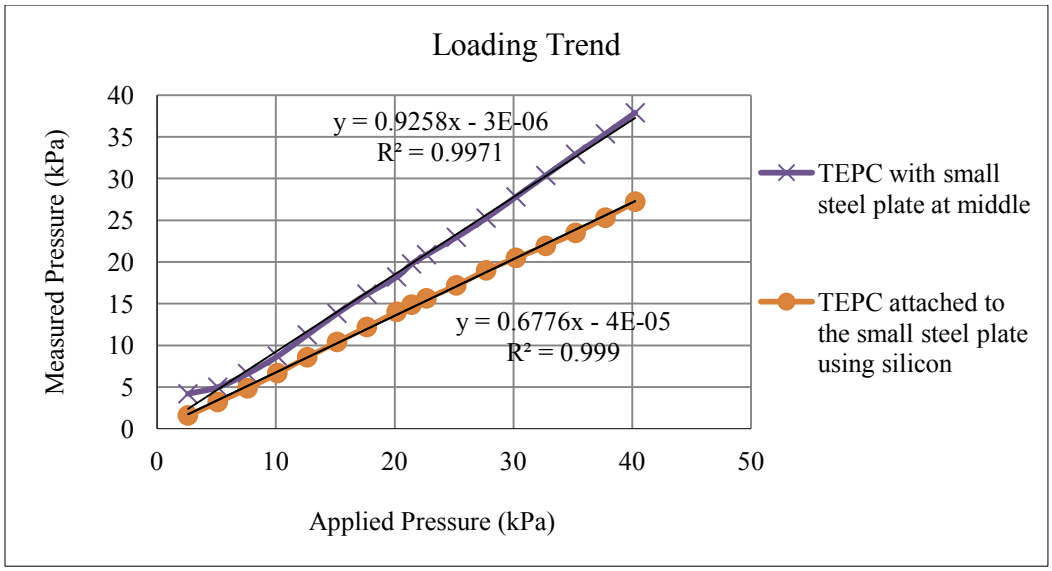

Figure 4-8: Results of TEPC on the steel plate with and without silicon

4.1.3 Summary of TEPC Results

The results obtained during each test in terms of measured pressures have been plotted versus the total applied pressure in a graph shown in Figure 4-9 for comparison purposes.

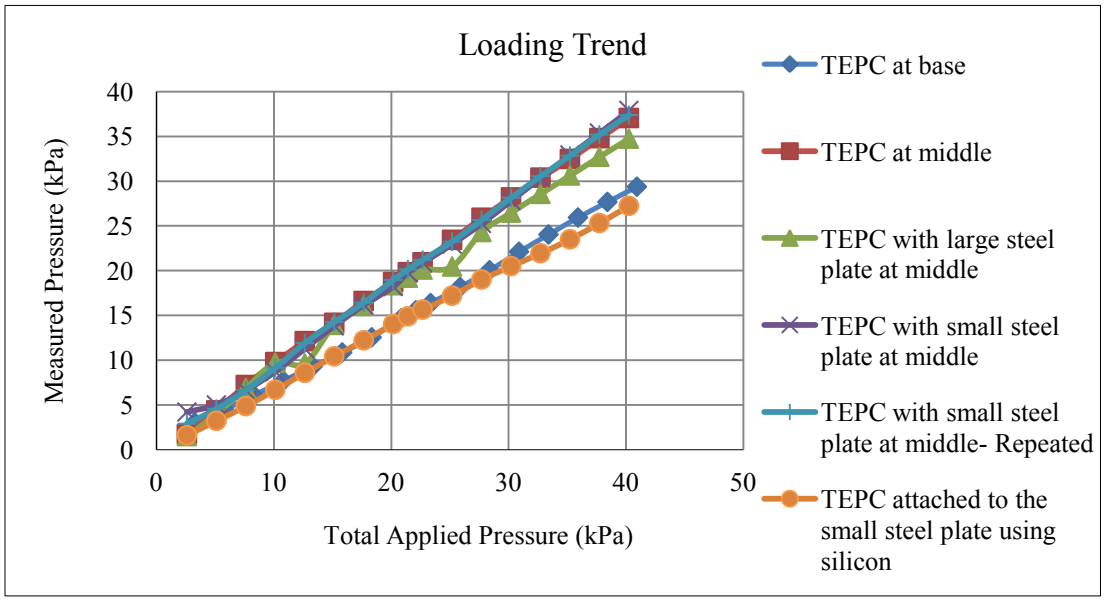

Figure 4-9: Graph of summary of TEPC results

4.2 Load Cell Results

The load cell was placed at the base of the cell box and its position remained unchanged throughout the experiments. The load cell was supposed to measure the same load during each test as the pressure at the bottom of the cell box should be the same for each test loaded to a maximum applied load of 150kN by the actuator. The data was expected to fall along one line. The load cell results, provided in Appendix E, showed erroneous data. Variability of the pressure at the base of the cell box was observed by the load cell and it did not indicate consistent data under either loading or unloading conditions. With each progressive test, woodchips may have been forced or displaced into the volume between the top plate of the load cell and the base of the box creating an upward force on the bottom of the top plate. This would in turn lead to a decreasing measured pressure trend.

4.3 Pipe Testing Results

The results obtained from the pipe testing in terms of change in diameter of the pipes and pressure distributions on PPMFs are discussed in the following sections.

4.3.1 Diameter Displacement

The outputs in mV obtained from the string pots during the loading phases were corrected for the zero voltage readings after installation inside the pipe within the cell box and converted to mm afterwards using the estimated correction factors discussed in Appendix F. Measured horizontal displacements of diameters of the pipes by the string pots were plotted versus the applied load. Figure 4-10 shows the horizontal changes in diameters

obtained from the string pots placed inside the pipes at the base of the cell box and in the middle of the woodchips layer. Also, Figure 4-11 presents the results of the string pots with respect to the vertical changes in diameters of the pipes versus the applied load.

Comparing the measured vertical and horizontal displacements corresponding to the changes in diameters of the pipes, it was determined that diameter changes in pipe 1 placed at the bottom of the cell box on a thin layer of sand were considerably higher than that of pipe 2 surrounded by woodchips. Based on the recorded displacements, both horizontal and vertical diameter changes of pipe 1 were almost twice the measured displacements of diameters in pipe 2. This confirmed that the bottom pipe was exposed to a greater vertical differential load and therefore, deformation of pipe 1 was higher compared with pipe 2, as expected. More deformation of the bottom pipe illustrated the impact of placing the pipe on the base of the box and on a stiffer sand layer. In comparison, the stress distribution around the middle pipe was much more uniform given that it is surrounded with woodchips and suspended within the woodchips.

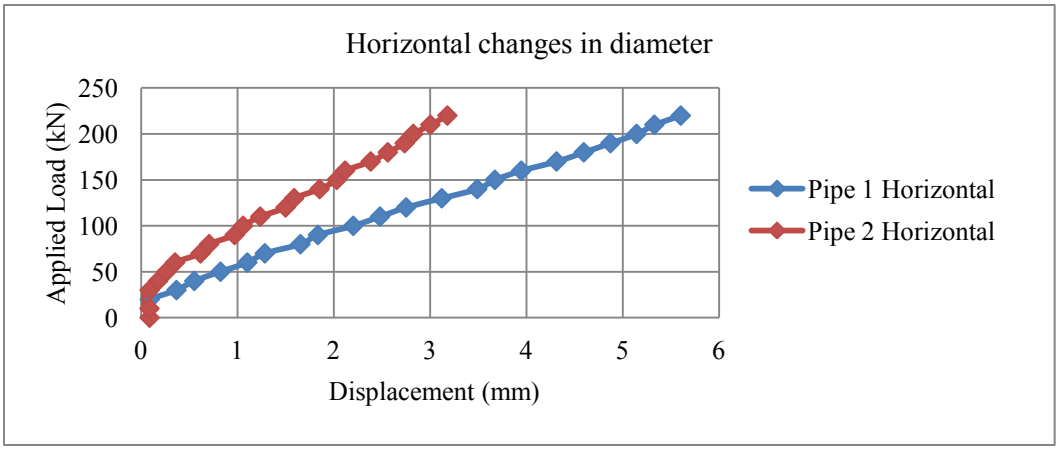

Figure 4-10: Horizontal changes in diameter of the pipes

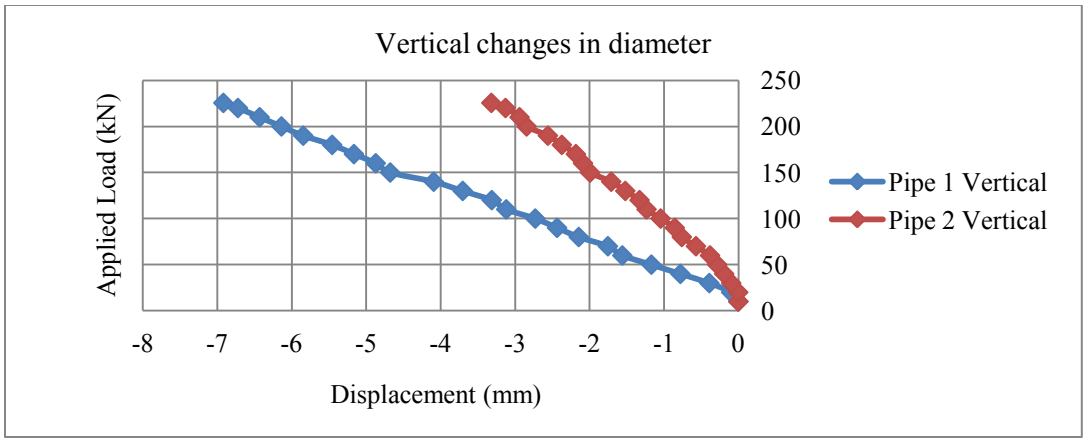

Figure 4-11: Vertical changes in diameter of the pipes

4.3.2 Pressure Distribution

As mentioned earlier, the PPMF was employed around the HDPE pipes to determine the stress concentration on the pipes. Pink color was created on the PPMF as the result of applying an approximate external load of 225kN. Figures 4-12, 4-13 and 4-14 present pressure distribution manifested on the PPMF at top, bottom and side of the pipes, respectively, due to the applied pressure.

It was observed at first glance that more area of the pressure film wrapped around pipe 2 was covered by the pink color. The pink color density, in terms of lightness and darkness, varied with respect to the amount of pressure applied. After unfolding the PPMFs from the pipes, the images of the colored pressures were analysed to extract pressure distribution information.

Figure 4-12: Top sides of PPMFs on pipe 1 and pipe 2

Figure 4-13: Bottom sides of PPMFs on pipe 1 and pipe 2

Figure 4-14: Sides of PPMFs on pipe 1 and pipe 2

It should be recalled that pipe 1 was positioned on a layer of sand to avoid having the bolts previously installed around outer side of the pipe in direct contact with the base of the steel box. Considering Figure 4-13, the bottom side of the pressure film showed two parallel horizontal lines forming a region all across, but darker along the lines. This led to the assumption that the bolts extending out from pipe 1 may have come in contact with the base of the steel cell box. It seemed that the pipe was resting along the horizontal lines considering them to be darker. It was indeed expected to see a darker region all across the bottom of pipe 1.

The pressure values sensed by the PPMF were quantified using the available pressure charts and Prescale standard color sample provided in Appendix G. For this purpose, the PPMF sheets were first scanned to color images. Using Adobe Photoshop software, the scanned images of PPMF placed on top section of the pipes were cut into

separate images for processing purposes. Same size images of the cut sections were considered to evaluate the pressure on the PPMF shown by pink colors with different densities.

The manual for PPMF advises on a method to roughly determine the pressure values. Knowing the approximate humidity of the lab environment, a region was selected using Figure G-1 (Appendix G). Then from the Figure G-2, the corresponding graph was used for image processing. The graph shows a relation between pink color densities of PPMF (0 to 1) versus amount of pressure (0 to 0.2MPa).

The relative humidity of lab environment in August 2014 was determined to be above 80 percent (Environment Canada, 2014) with temperature of +25°C. This corresponds to region 'A' in Figure G-1 and graph A in Figure G-2.

A Matlab code was developed to read the images and calculate pressure values on top of the pipes. Four samples of PPMF images for pipe 1 and pipe 2 are shown in Figure 4-15. It was identified that the resolution of images is proportional to the calculated pressure. If the image is scanned with higher resolution, calculated pressure would be higher. Using the same image resolution, the ratio of the pressure on top of the pipe 2 to that on top of pipe 1 was calculated. It was found that the average pressure on pipe 2 was about 30% higher than that of pipe 1.

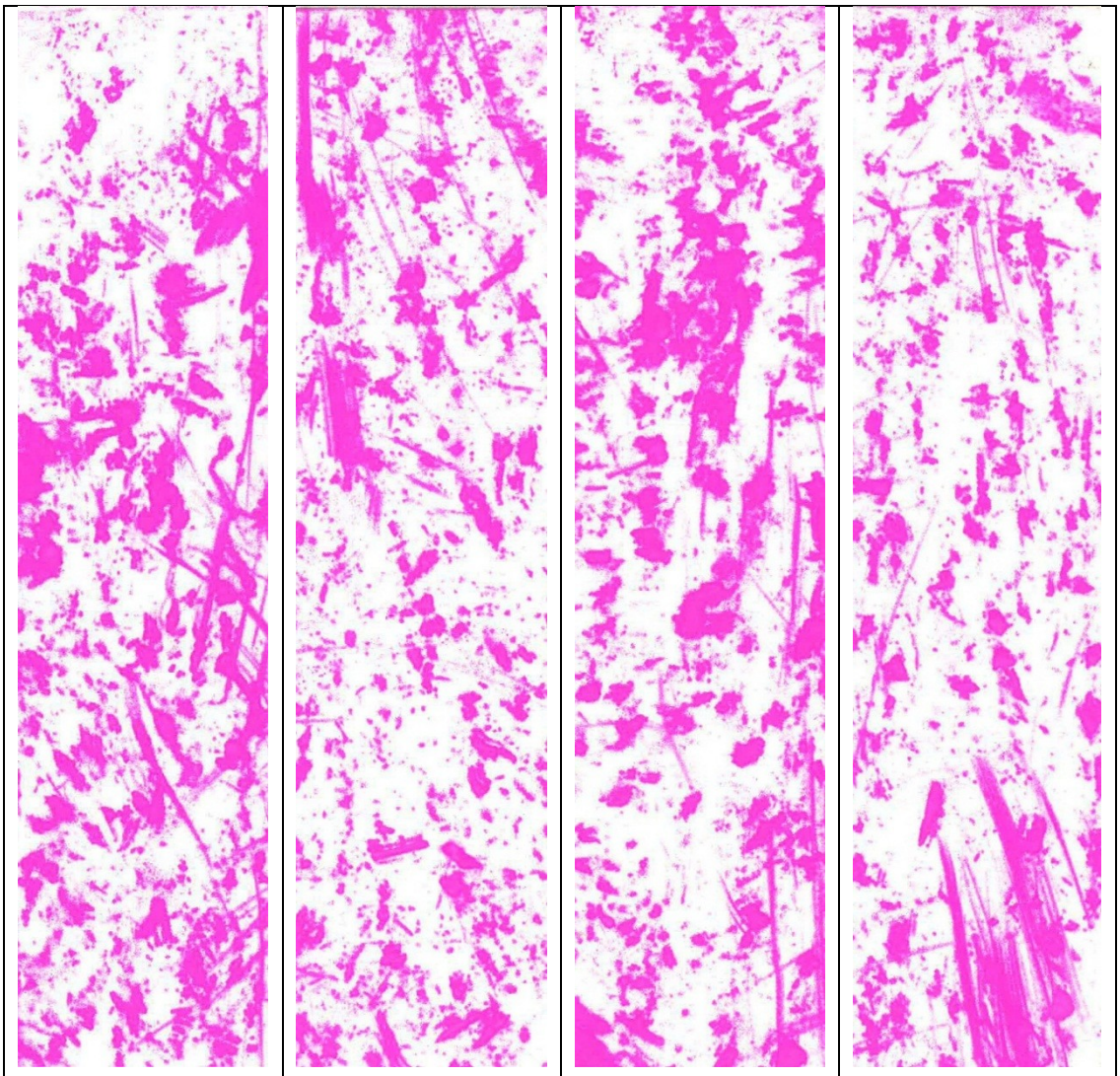

Pipe 2 (middle left)	Pipe 1 (middle left)	Pipe 2 (middle right)	Pipe 1 (middle right)

Figure 4-15: Sample of PPMF sheets for pipe 1 and pipe 2

5.0 Numerical Simulations and Discussion

This chapter presents the numerical simulation results for the conducted laboratory experiments, including a steel plate test and a pipe test using a finite element CAD software product. The numerical simulations were based on a two dimensional finite element analysis. The performed laboratory experiments were limited in terms of number of parameters being used such as material type and size. Thus, as part of this research, simulations were also conducted while varying a few parameters to investigate stress distribution behaviour for different material stiffnesses and sizes. Sigma/W, which is one of the eight products of the GeoStudio suite, has been employed to simulate the trend of stress distribution, analysing the concept of a hard inclusion.

5.1 Evaluation of Material Properties

To model the concept of a hard inclusion, solid waste, sand, shredded tire and woodchips were selected as the model materials. These materials are different in their properties such as unit weight, Young's modulus, Poisson ratio and cohesion. To simulate the behavior of these materials as close as possible to their actual mechanical behavior, appropriate material model and parameters are required for the software. A material model describes the relationship between stress and strain.

The mechanical behavior of the solid waste, sand, shredded tire and woodchips were simulated using an elastic-plastic material model with stresses directly related to the strains up to the yield point. The elastic-plastic model in Sigma/W describes a perfectly-

plastic relationship beyond the yield point with completely horizontal stress-strain curve. The material properties used in simulations includes parameters such as modulus of elasticity (kPa) and Poisson's ratio for elasticity, cohesion (kPa) and friction angle (^{o}) for plasticity, and unit weight (kN/m^3) and dilation angle (^{o}). The parameters used in this study, presented in Table 5-1, were selected based on conducted test results and previous authors' works.

Modulus of elasticity of solid waste containing a variable range of waste materials depends on waste component size and composition, waste compaction, and degradation. For this reason, modulus of elasticity of solid waste was considered to have an assumed value of 1000kPa as data regarding the range of its elastic modulus is sparse. The assumed modulus of solid waste was chosen to be higher than the modulus of woodchips and lower than the modulus of shredded tire. The cohesion and friction angle of the solid waste was estimated by Singh (2008) to be in the range of 11kPa - 22kPa and 29^o - 34^o, respectively. The averages of these values were considered in simulations. The value of Poisson's ratio was taken from a study by Matasovic and Kavazanjian (1998). A typical unit weight of 10 kN/m^3 for municipal solid waste was considered.

Table 5-1: Properties of materials used in simulation

Medium	Material Properties				
	Young's Modulus, (kPa)	Cohesion, (kPa)	Unit Weight (kN/m^3)	Poisson's Ratio	Friction Angle (^{o})
Sand	24,000	0	19	0.30	28
Shredded tire	1,010	0	8.1	0.33	37
Solid waste	1,000	17	10	0.29	32
Woodchip	527	0	1.7	0.35	24

The modulus of elasticity of the sand was determined based on Ryall et al. (2000). Cohesion, unit weight, friction angle and Poisson's ratio were selected according to S&ME (2010). The young's modulus for the shredded tire was selected as an average value according to U.S. Department of Transportation Federal Highway Administration (2012) .The cohesion and friction angle of the shredded tire were selected from the results of a study conducted on mechanical properties of the shredded tire by Yang et al. (2002). Unit weight values for shredded tire were averaged from results of tests conducted by Moo-Young et al. (2003). In addition, Poisson's ratio of shredded tire was taken from a simulation on retaining walls performed by Huggins and Ravichandran (2011).

Modulus of elasticity of the woodchips was determined during the experimental work of this study to be in the range of 526kPa and 995kPa for the different tests. The modulus of elasticity of the woodchips used in the simulation, 527kPa, was selected from the stress-strain curve obtained during the experiment which tested the TEPC at the mid-depth of the woodchip. The woodchips subjected to a higher compaction load was assumed to have a modulus of elasticity of 950kPa. This value was selected such that it was less than the maximum obtained modulus, i.e. 995kPa, and less than the assumed modulus of solid waste. The cohesion and friction angle were also determined from a direct shear test conducted for three confining stresses. The unit weight of the woodchips was considered to be 1.7kN/m^3 obtained from weighting the woodchips inside the cell box. Poisson's ratio of the woodchips was taken from Hossain and Inoue (2004) who determined Poisson's ratio of recycled woodchips as part of their work.

The linear elastic material model was used to simulate structural behaviour of the steel plate having very high strength properties compared to sand, shredded tire, woodchips and solid waste. In the linear elastic model, stresses are directly related to the strains with proportionality constants. The linear elastic model involved total stress parameters of modulus of elasticity (kPa), Poisson's ratio and unit weight (kN/m^3). Table 5-2 presents the material properties selected for the steel plate. The modelled steel plate was assumed as 'mild steel' with a modulus of elasticity provided by a group of engineers in MatWeb (2014) which was also used by Fleming et al. (2011). The Poisson's ratio of the steel plate was used from the information provided by Engineers Edge (2014). The mass of the steel plate was weighted to be approximately 10kg. The unit weight of the steel plate was calculated having the volume and the mass as presented in Appendix H.

Table 5-2: Properties of steel plate

Medium	Material Properties		
	Young's Modulus, (kPa)	Poisson's Ratio	Unit Weight (kN/m^3)
Steel plate	2E+08	0.30	77

The pipe considered in simulation had an outer diameter of 16.5 cm, inner diameter of 14.5cm and a wall thickness of 1cm. The pipe was simulated as a circular opening within the bedding material. The pipe lining was designed as a structural beam having properties of a HDPE pipe. Properties such as Young's modulus (kPa), cross-sectional area and moment of inertia, shown in Table 5-3, defined the lining. The modulus of elasticity of the pipe was determined from a stress-strain curve obtained in this study. The

moment of inertia of the pipe was calculated using the following formula for pipe and tubing:

$$I = 0.0491(D^4 - d^4)$$

Where, D is the outside diameter of the pipe and d is the inside diameter of the pipe.

Table 5-3: Properties of HDPE pipe

Medium	Material Properties		
	Young's Modulus, (kPa)	Cross-Sectional Area (m^2)	Moment of Inertia (m^4)
HDPE pipe	24,671	0.021	1.5E-05

5.2 Boundary Conditions and Mesh Generation

Different types of boundary conditions were applied in the simulations. The vertical side boundaries and the bottom boundary of the domain were bounded to constrain the displacement. Zero movement in the x and y directions was prescribed for the bottom boundary. In Sigma/W this type of boundary appears as two triangles/head of arrows perpendicular to the fixed direction, shown in Figure 5-1. The left and right sides of the domain were specified as zero displacement in the x direction while allowing vertical movement along both sides i.e. roller conditions at the vertical sides. Fixed horizontal displacements appear as a series of triangles/head of arrows, pointing in the direction of fixed movement, as shown in Figure 5-2.

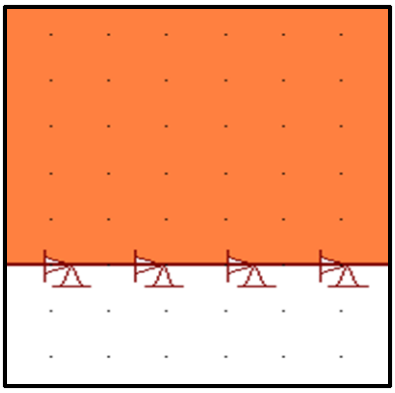

Figure 5-1: Fixed horizontal and vertical displacements

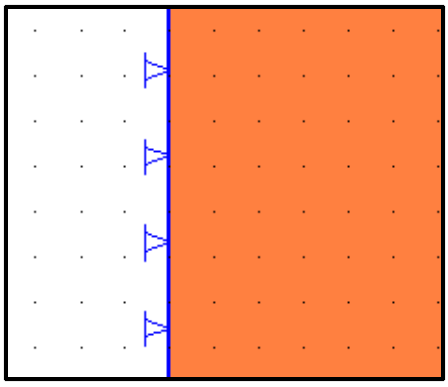

Figure 5-2: Fixed horizontal displacement

Another boundary condition used in the simulations was a normal stress applied on top boundary to simulate the applied load. Simulated normal stress was a negative constant value in the y-direction. In simulations containing the steel plate, -40kPa of normal stress was applied as a surface pressure, whereas -60kPa of normal stress was assigned in pipe simulation.

Once the boundary conditions and model parameters were set and applied to the domain, the finite element mesh was generated. Since Sigma/W was not providing a completely automatic mesh generation, compatible mesh element type and size had to be defined for each region seperately. Finite element mesh pattern of rectangular grid of quads and global element size of 0.50m were selected. Regions were discretized into smaller elements during the generation of the mesh considering the ratio of default global element size varying bewteen 0.050m and 0.012m, as required**.**

5.3 Laboratory Test Simulation

Simulations of the performed laboratory tests were conducted to support the results obtained from the experiments. A 2D computational domain was simulated for the width of the steel cell box and the total height of the woodchips. Therefore, the domain size was set to have a width of 1.47m and a depth of 0.81m. Details of the simulation in terms of material properties, boundary conditions and mesh generation were discussed in sections 5.1 and 5.2.

5.3.1 Steel Plate Testing Simulation within Woodchips

The TEPC and steel plate were simulated as a single steel plate with uniform properties located at the middle height of the domain. The represented steel plate in yellow (Figure 5-3) was considered to have a same length as the actual steel plate and TEPC used in the lab. The considered steel plate was simulated with a width of 31.7cm and thickness of 2.27cm. Woodchips were selected as the main material around the steel plate within the domain.

The geometry of the domain comprised of different regions of 10cm thickness above and below the steel plate; similar to the packing technique used to place the woodchips in laboratory cell box. A benefit of having different regions within the computational domain was that the material properties could be easily altered as required, without being worried about losing the main configuration. It was assumed that the modulus of elasticity increased with higher compaction load resulting from the cumulative manual compaction of each successive layers of woodchips and from

standing on the woodchips during deposition/plate installation. These regions included approximately 40cm down from the steel plate to the base. The region right on top of the steel plate (10cm above the steel plate) was also assumed to have a slightly higher modulus of elasticity due to greater manual compaction of the woodchips during experiment to ensure that TEPC did not slide off the plate. A vertical pressure of 40kPa was applied on the top boundary of the domain.

Figure 5-3 illustrates the fully defined geometry of the steel plate in the mid-depth of the woodchips. Stress distribution on the steel plate and surrounding woodchips as a result of the applied pressure was investigated.

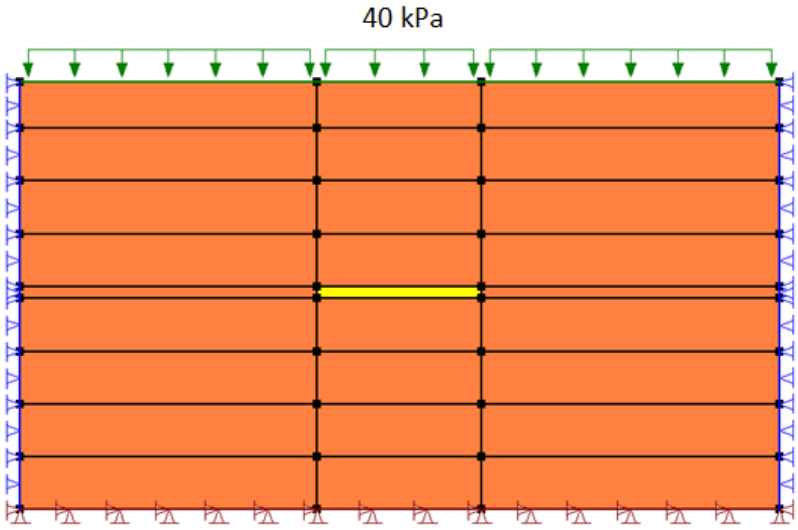

Figure 5-3: Defined geometry of steel plate in the middle of woodchips

A horizontal profile was selected covering the steel plate and woodchips on both sides. The vertical total stress along horizontal axis was plotted for all nodes. The stress concentration at each node on the steel plate was simulated to be greater compared with

the stress distribution on the surrounding woodchips, as presented in Figure 5-4. The average stress concentration on the steel plate was approximately 48kPa, and the average stress measured on the woodchips was approximately 37kPa. The average stress on the steel plate was determined to be 30% higher than the average stress on the woodchips. Higher stress concentration on the steel plate followed the results obtained from the experiment. The findings of the simulation confirm that the stress on the stiffer steel plate at mid-depth in the woodchips was greater than the stress on surrounding woodchips supporting the concept of a hard inclusion.

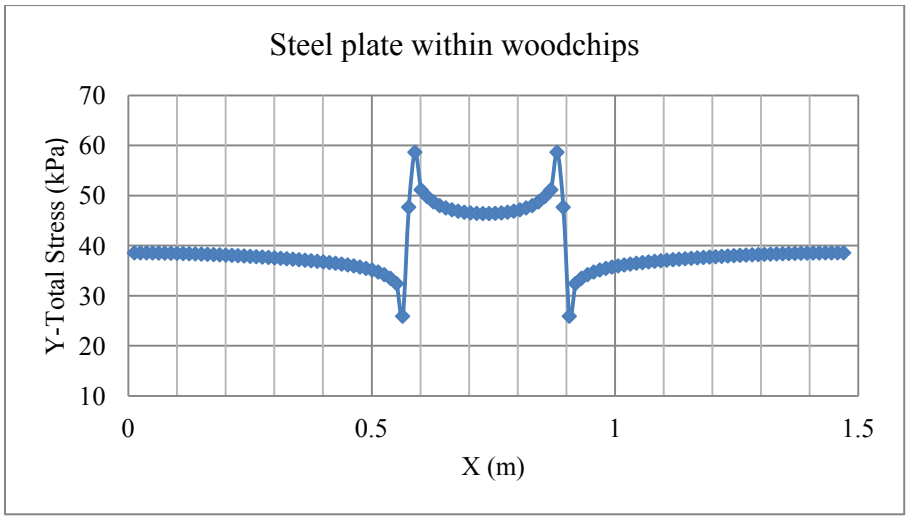

Figure 5-4: Stress distribution profile on the steel plate and surrounding woodchips

5.3.2 Pipe Testing Simulation within Woodchips

The HDPE pipe with diameter of 16.5cm used in the experiment was simulated within the domain containing woodchips as shown in Figure 5-5. The pipe was replaced by the steel plate such that the centre of the pipe was located at the middle of the cell box width.

A distributed pressure of 60kPa was applied to the top boundary of the domain. For the conducted simulation, a horizontal profile passing through the top of the pipe was considered to check for the pressure values. The vertical total stress versus horizontal axis plotted for all nodes is shown in Figure 5-6. The results of the simulation showed that the average stress on top of the pipe was approximately 71kPa and the average stress within the body of the woodchips was 55kPa. Calculating for the stress ratio, a value of 1.30 was obtained.

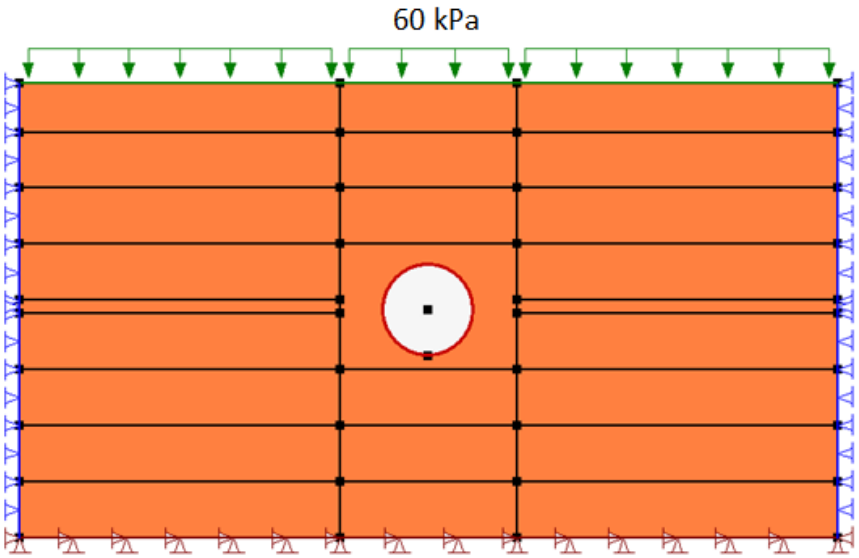

Figure 5-5: Defined geometry of the HDPE pipe within woodchips

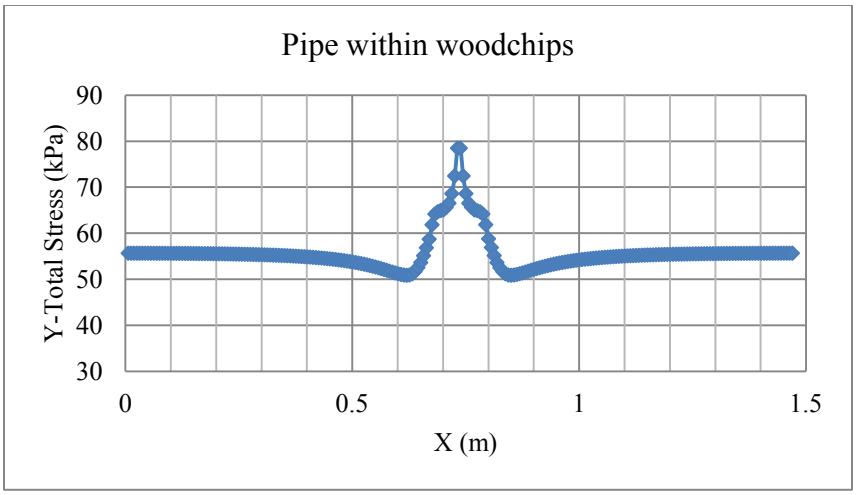

Figure 5-6: Stress distribution profile on the pipe and surrounding woodchips

5.4 Parameter Analysis using Steel Plate

Simulations were executed while varying a number of parameters to investigate the concept of a hard inclusion for two or more different materials. The effect of parameters in terms of material size and material type was examined. A 40kPa pressure was considered as the surface pressure applied to the top of the domain.

5.4.1 Material Size Effect

The impact of the size of the hard inclusions was investigated using Sigma/W software. Different sizes of steel plates were considered in the developed model to evaluate stress distribution over the steel plates and surrounding woodchips. Considering the steel plate used in experiment simulation as steel plate size A, simulations were conducted by designing steel plates having either the same length or the same thickness as steel plate size A. Table 5-4 shows the steel plate sizes when the length of the steel plate was

changed. Table 5-5 presents the steel plate sizes when the thickness of the steel plate was changing.

Table 5-4: Length of steel plates for a constant thickness of 2.27cm

Steel Plate Type	Steel Plate Length (cm)	Steel Plate Thickness (cm)	Description
A	31.7	2.27	Real experiment
B	21.7	2.27	Decrease in steel length
C	51.7	2.27	Increase in steel length

Table 5-5: Thickness of steel plates for a constant length of 31.7cm

Steel Plate Type	Steel Plate Length (cm)	Steel Plate Thickness (cm)	Description
A	31.7	2.27	Real experiment
D	31.7	1.27	Decrease in steel thickness
E	31.7	3.27	Increase in steel thickness

5.4.2 Material Type Effect

The effect of material type was investigated in the framework of a parameter analysis with the Sigma/W software. Conceptual illustration of stress distribution trend was achieved for different types of materials with different stiffnesses. Solid waste, sand, shredded tire and woodchip were defined as materials in the simulations. The steel plate A was utilised in the simulations employing different materials categorized in Table 5-6.

Table 5-6: Conducted simulations for different materials

Case No.	Intermediate Medium around Steel Plate			Main Medium	
	Sand	Shredded tire	Woodchips	Solid Waste	Woodchips
1	✓				✓
2	✓			✓	
3		✓		✓	
4			✓	✓	
5				✓	

Sand as an intermediate medium around the steel plate A was considered within the domain filled up with woodchips. Sand medium was considered to have a height of 10cm below and above the steel plate A. Once the analysis was solved, a region that passed through the steel plate was selected horizontally throughout the domain to determine the stress distribution over the steel plate and surrounding area filled with woodchips. The average stresses on the steel plate and surrounding the steel plate were determined from which the average stress ratio was calculated. Simulation of the steel plate continued using solid waste as the main material employed within the domain. Simulations were achieved using sand, shredded tire and woodchips that covered the steel plate before being covered by solid waste. The steel plate was then assumed to be in direct contact with the solid waste without any interfering material.

5.5 Authentication Analysis for HDPE Pipe

The concept of a hard inclusion was proved by parameter analysis conducted using Sigma/W for designed steel plate. To demonstrate that the concept of a hard inclusion is applicable to horizontal collection pipes, a few simulations were run to demonstrate stress

concentration on the pipes covered by materials with a high modulus of elasticity. Sand was used for this illustration. The pipe was covered by sand within the woodchips and solid waste. For comparison purposes, the pipe was also simulated within the solid waste without the use of sand. A distributed pressure of 60kPa was applied to the top boundary of the domain.

5.6 Simulation Results

The results of the steel plate and pipe simulations are presented in this section. The analysis to determine the impact of plate size on the model results conducted using Sigma/W is summarized in Table 5-7 for different steel plate sizes.

Table 5-7: Size effect on stress concentration

1.47m x 0.81m Domain					
Steel Plate Type	Steel Length (cm)	Steel Thickness (cm)	Woodchips as Bedding Material		
			Stress on Steel Plate (kPa)	Stress within Surrounding Woodchips (kPa)	Stress Ratio
A	31.7	2.27	48.2	36.9	1.30
B	21.7	2.27	49.1	36.5	1.35
C	51.7	2.27	47.3	37.4	1.27
D	31.7	1.27	47.9	37.0	1.29
E	31.7	3.27	49.0	36.5	1.34

Tables 5-8 and 5-9 provide a summary of material type effect on stress concentration employing different types of materials with different moduli of elasticity in contact with one another.

Table 5-8: Material type effect within woodchips

1.47m x 0.81m Domain						
Steel Plate Type	Woodchips + Steel			Woodchips + Sand + Steel		
	Stress (kPa)		Stress Ratio	Stress (kPa)		Stress Ratio
	Steel Plate	Woodchips		Steel Plate	Woodchips	
A	48.2	36.9	1.30	59.2	34.0	1.74

Table 5-9: Material type effect within solid waste

1.47m x 0.81m Domain												
Steel Plate Type	Solid Waste + Steel			Solid Waste + Sand + Steel			Solid Waste + Shredded Tire + Steel			Solid Waste + Woodchips + Steel		
	Stress (kPa)		Stress Ratio	Stress (kPa)		Stress Ratio	Stress (kPa)		Stress Ratio	Stress (kPa)		Stress Ratio
	Steel Plate	Solid Waste		Steel Plate	Solid Waste		Steel Plate	Solid Waste		Steel Plate	Solid Waste	
A	45.8	42.9	1.07	58.8	37.7	1.56	46.5	42.3	1.10	40.2	44.5	0.90

Table 5-10 presents the average stress values on the pipe and surrounding medium for simulated pipe alone and covered by sand within woodchips. Table 5-11 shows the results of the simulation employing solid waste.

Table 5-10: Pipe within woodchips with and without sand medium

1.47m x 0.81m Domain						
Pipe Diameter (cm)	Woodchips + Pipe			Woodchips + Sand + Pipe		
	Stress (kPa)		Stress Ratio	Stress (kPa)		Stress Ratio
	Pipe	Woodchips		Pipe	Woodchips	
16.5	71.4	55.1	1.30	82.7	50.4	1.64

Table 5-11: Pipe within solid waste with and without sand medium

1.47m x 0.81m Domain						
Pipe Diameter (cm)	Solid Waste + Pipe			Solid Waste + Sand + Pipe		
	Stress (kPa)		Stress Ratio	Stress (kPa)		Stress Ratio
	Pipe	Solid Waste		Pipe	Solid Waste	
16.5	75.0	57.4	1.31	81.6	54.5	1.50

5.7 Analysis and Discussion

It was determined that whether decreasing the steel plate length or increasing the thickness of the steel plate resulted to an increase in the average stress on the steel plate. On the other hand, increasing the steel plate length and/or decreasing the thickness of the steel plate led to a decrease in the average stress on the steel plate. The stress ratio found from the average stress on the steel plate over the average stress off the steel plate regarding the steel plate length and thickness is illustrated in Figures 5-7 and 5-8, respectively. Increased stresses generated on the steel plate could be related to the concept of a hard inclusion such that stresses are more concentrated on the steel plate with higher modulus than the surrounding medium. Increasing the length and/or decreasing the thickness of the steel plate reduce the effect of the hard inclusion as more stresses are distributed over the surrounding medium.

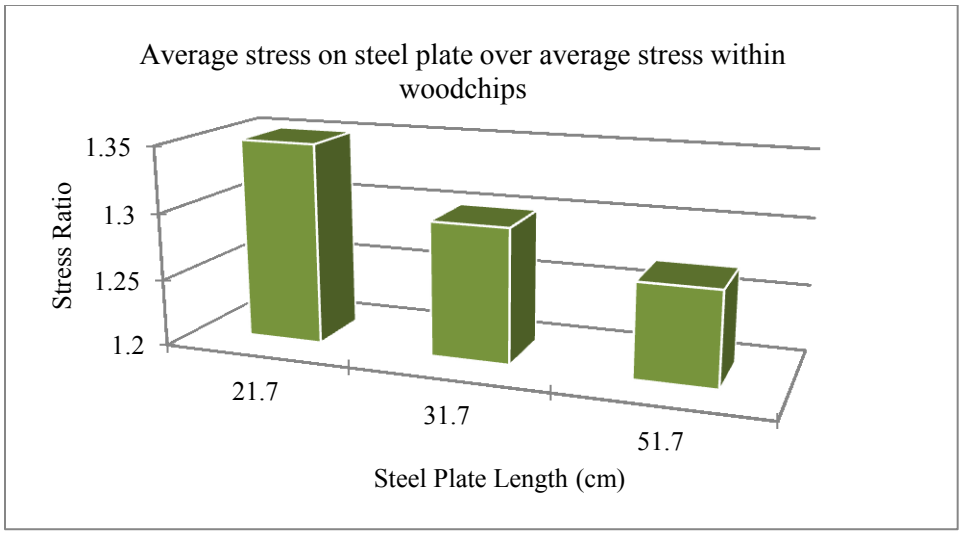

Figure 5-7: Stress ratio with respect to the change in steel plate length

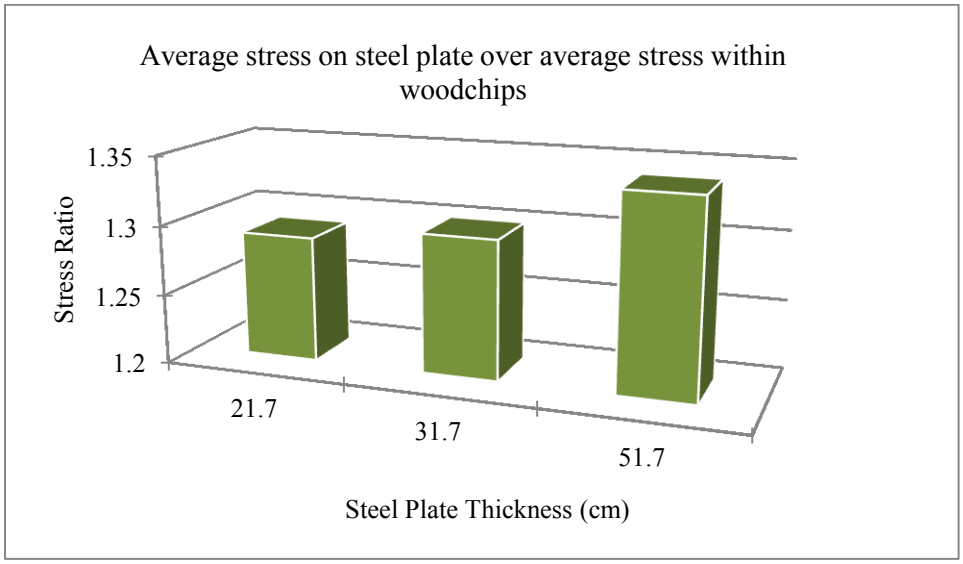

Figure 5-8: Stress ratio with respect to the change in steel plate thickness

The results from the simulations are consistent with the laboratory experimental results given that the larger steel plate used underneath the TEPC reduced the stress ratio compared to the small steel plate positioned underneath the TEPC. The observation from

the experiments and simulations are also consistent with the literature such that increasing the length of the steel plate decreased the stress ratio. The larger the length of the steel plate, the greater the plate aspect ratio becomes (length/thickness). Stress ratio is decreased with an increase of aspect ratio. Thus, the aspect ratio needs to be high enough so that its effect is negligible.

Data analysis from the modelling demonstrated that with the use of sand around the steel plate within woodchips, the stress ratio increased significantly from 1.30 to 1.74. The added sand around the steel plate decreases the aspect ratio which leads to an increase in the stress ratio. Replacing the woodchips with solid waste, without or with the sand, decreased the stress ratios as the contrast in moduli is decreased. Replacing the sand with shredded tires also decreased the stress ratio of the shredded tires have a modulus closer to that of the waste than the steel plate. Surrounding the plate with woodchips reduced the stress ratio to values less than one indicating the stresses on the plate were less than the stresses in the surrounding solid waste. Figures 5-9 and 5-10 present decrease and increase in the stress ratios calculated from the average stresses on the steel plate over the average stresses within surrounding body for the steel plate within woodchips and solid waste, respectively.

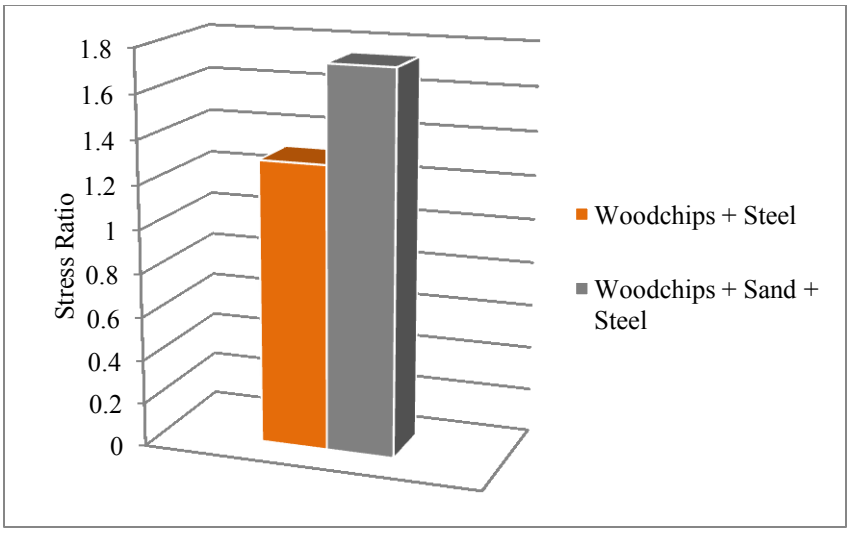

Figure 5-9: Variation of stress ratio using sand within woodchips

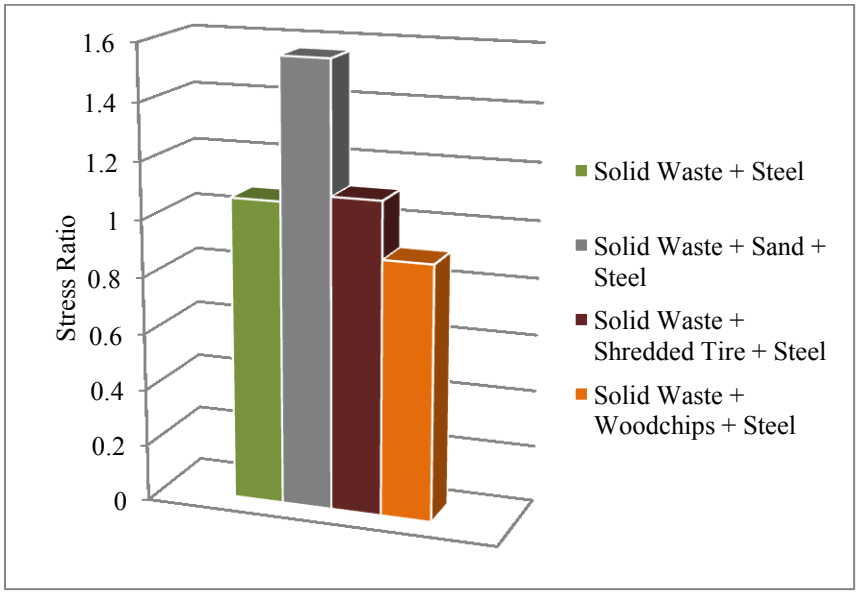

Figure 5-10: Variation of stress ratio using different materials within solid waste

Combination of the steel plate and shredded tire was less stiff than the combination of steel plate and sand. In addition, the shredded tires are similar in stiffness

to the solid waste and hence the aspect ratio is greater which led to a lower stress ratio. Having said this, employing woodchips around the steel plate further decreased stress concentration on the steel plate compared to the shredded tire. The modulus of elasticity of woodchips is almost half of that of the solid waste and hence the stresses are directed to surrounding solid waste which resulted to smaller stress sensation on the steel plate. The obtained results are less than the surrounding solid waste due to bridging around the steel plate. The result of the simulation was expected based on the literature with the concept known as a soft inclusion. Hence, the use of woodchips around the steel plate within solid waste led to more stress distribution over the solid waste and less stress concentration on the steel plate.

Simulation of the modelled pipe within the woodchips was obtained. Adding the sand around the pipe caused an increase in stress on the pipe. This can likely be attributed to the change in geometry and the decreased aspect ratio. Substituting the woodchips with solid waste material determined that average stress on the pipe simulated within the woodchips was greater than that within solid waste. Change in stress ratios is illustrated in Figures 5-11 and 5.12 for pipe within woodchips and solid waste.

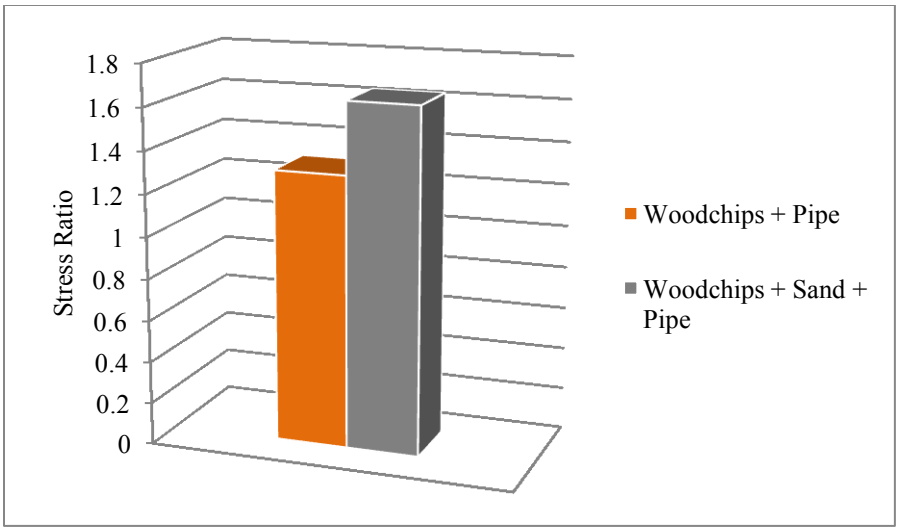

Figure 5-11 Variation of stress ratio employing woodchips

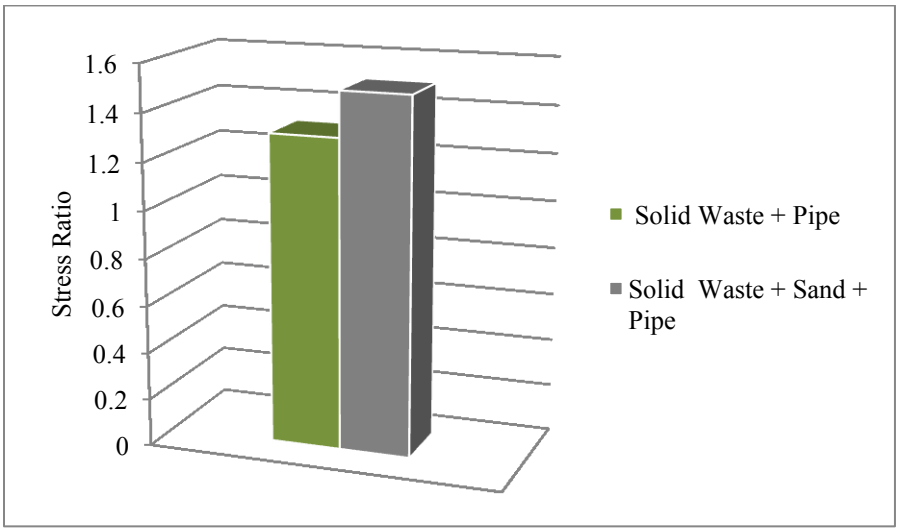

Figure 5-12: Variation of stress ratio employing solid waste

The solid waste is more stiff than the woodchips and hence, less stresses are exerted on the pipe surrounded by the solid waste. The stress on the pipe increased for the pipe buried in sand within woodchips. Same trend was observed for the simulated pipe covered by sand within solid waste. Including sand in the simulation around the pipe

increased the average stress value sensed by the pipe as a result of decrease in the aspect ratio. The solid waste and woodchips are less stiff compared to the pipe and sand. Decrease in the aspect ratio leads to a higher stress ratio. Due to the greater stiffness of the solid waste than the woodchips, the calculated stress ratio was higher for the pipe covered by sand within woodchips compared to that of pipe buried in sand within solid waste.

Based on the conducted laboratory works and simulations, it is possible that the elevated TEPC readings at Sainte-Sophie could be partially attributed to the concept of a hard inclusion. The expected over overburden pressures obtained from the depth of waste on top of each bundle versus the pressures measured by the TEPCs were presented earlier in section 2.4.2. Bundles 1 and 2 are not ideal examples of a hard inclusion as they were placed on the base of the landfill on the gravel. However, the stress ratio obtained for other bundles in the field is comparable to the conducted simulation. The results of the modelling for the steel plate surrounded by sand in solid waste indicated a stress ratio of more than 1.50. Therefore, the elevated stresses measured in the field could be partially explained by the concept of a hard inclusion, if not completely.

In the conducted laboratory experiments, no material was used as a lubricant to reduce the effect of boundary friction. Thus, the applied load may have been partially reduced by the friction force between the cell walls and the woodchips and in turn affected the measured normal force. At any point below the top boundary of the woodchips, the measured normal pressure would have been smaller than the applied pressure due to the friction force. Since the boundary conditions selected in the

simulation assume zero friction along this boundary, the wall friction forces were not simulated and the potential reduction in stress with depth was not simulated.

In this study, the behavior of solid waste was simulated using an 'elastic-plastic' model. The behaviour of solid waste could also be simulated using a 'hyperbolic non-linear elastic' model. Since stress-strain behaviour of solid waste which follows a non-linear elastic model was not particularly studied in this research, the elastic-plastic model was considered in the simulation. Xu et al. (2008) also based their design on elastic-plastic constitutive model for the solid waste.

The moduli of elasticity of the bedding materials are expected to increase over time whereas the modulus of elasticity of the pipe tends to decrease. The parameter analysis simulations implemented in this study were not based on the increase or decrease in moduli of elasticity with time.

6.0 Conclusion and Future Work

The objective of this thesis was to confirm the proposed hypothesis that the concept of a "hard inclusion" may be responsible for the elevated stresses measured by the total earth pressure cells (TEPCs) in the field, and to demonstrate that horizontal gas collection and leachate recirculation pipes surrounded by gravel may possibly sense higher stresses than the expected stresses derived from the depth of waste above the pipes. Experiments were conducted in the lab to implement the concept of a hard inclusion. The results obtained from the experimental work were coupled with the findings of numerical modelling conducted using GeoStudio finite element software.

Laboratory tests performed in the lab verified the concept of a hard inclusion as a result of contrasts in moduli of materials in relation to one another. A TEPC was placed at the base of the cell box to measure the stress applied by an actuator on top of the cell box. The TEPC was also placed at the middle of woodchips height to demonstrate the increased stresses generated due to a hard inclusion. Woodchips were employed as the main material within the cell box to create a high contrast in moduli. The experimental results indicated that the pressures acting on the TEPC at mid-depth in the box were approximately 28% greater than the expected overburden pressure recorded by the TEPC placed at the base of the box. However, it should be noted that the original calibration curve for the TEPC was assumed to be incorrect.

Experiments were continued with employing two different steel plate sizes with a same thickness to investigate the effect of sizing on the concept of a hard inclusion. The

steel plates were placed underneath the TEPC within the middle of the woodchips height. It was determined that the stress concentration on the smaller steel plate was higher compared with the larger steel plate. This result is consistent with the literature in that increasing the length of the steel led to a greater aspect ratio (length/thickness) and less stress concentration due to the concept of a hard inclusion.

Two identical HDPE pipes wrapped with Prescale Pressure Measurement Films were employed to evaluate stress concentration on pipes typically used in landfills. One pipe was placed at the base of the cell box and the other pipe was positioned at the middle depth in the woodchips to simulate the concept of a hard inclusion. Similar to the steel plate at mid-depth, the pipe at mid-depth was exposed to a greater stress, approximately 30% than the average overburden stress.

Numerical simulations were implemented to validate the performed experiments and to conduct a parameter analysis in terms of material types and sizes. The aim was to demonstrate stress distribution within materials to conceptually illustrate the concept of the hard inclusion. Parameter analysis was conducted for a steel plate within different bedding materials i.e. sand, shredded tire, woodchips and solid waste. Sand was considered to have a greater modulus of elasticity than that of solid waste. Comparing modulus of elasticity of shredded tire and woodchips relative to solid waste, shredded tire was considered to have a modulus slightly greater and woodchips to have a lower modulus compared with the solid waste. In addition to the use of different materials, the designed steel plate changed in size to analyse the developed model using different steel

plate sizes. The following conclusion can be drawn from the results of the numerical modelling:

- The numerical model was able to simulate the elevated stresses measured in the laboratory experiments on the steel plate and HDPE pipe; likewise, the model was able to demonstrate the concept of a hard inclusion and demonstrated that depending on the geometry and material properties, an increased stress ratio of up to 1.74 for steel plate and 1.64 for pipes could be simulated.
- Use of a material with a low modulus of elasticity (i.e. woodchips) as an intermediate medium around a stiff material (i.e. steel plate) placed within solid waste decreased stress concentration on the steel plate. The woodchips have a lower modulus than the steel plate and surrounding solid waste and hence acted as a soft inclusion creating a bridging effect around the steel plate.
- Use of a material with a high modulus of elasticity (i.e. sand) around the steel plate within the solid waste increased stress concentration on the steel plate. Because the contrasts in moduli of the combination of the sand and the steel plate was considerable greater than solid waste, the sand layer covering the steel plate acted to decrease the aspect ratio which in turn resulted in a greater concentration of stresses on the sand and steel plate.

The concept of a hard inclusion experienced by horizontal pipes was confirmed by simulating stress concentration on a pipe surrounded by a medium with a much lower modulus of elasticity. Adding a cover material to the pipe (i.e. sand) may in fact increase the stress depending on the aspect ratio and geometry of the sand surrounding the pipe.

It is recommended that future research consider the followings:

- In terms of experimental work, the TEPC used in the experiments should be calibrated in order to confirm the conclusions based on the assumed incorrect calibration curve for the TEPC. In addition, account for associated boundary conditions at the walls. Friction at all boundaries should be eliminated using frictionless materials, unless frictional forces at the boundaries are determined.
- In terms of the modelling, the research work should be expanded with simulating stress distribution at field scale. In addition, in order to have a more realistic understanding of stress distribution, simulations should take into account the properties of materials such as modulus of elasticity for a long term period as strength of materials changes over time.

References

Askegaard, V. (1963) Measurement of pressure in solids by means of pressure cells. Bulletin No. 17, Structural Research Laboratory, Technical University of Denmark, Copenhagen.

Askegaard, V. (1995) Applicability of normal and shear stress cells embedded in cohesionless materials. Experimental Mechanics, Vol. 35, pp. 315-321.

Benson, C.H., Barlaz, M.A., Lane, D.T., & Rawe, J.M. (2007) Practice review of five bioreactor/recirculation landfills. Waste Management, Vol. 27, No. 1, pp. 13-29.

Brachman, R.W.I., Moore, I.D., & Rowe, R.K. (2000) The design of a laboratory facility for evaluating the structural response of small diameter buried pipes. Canadian Geotechnical Journal, Vol. 37, No. 2, pp. 281-295.

Brachman, R.W.I., Moore, I.D., & Rowe, R.K. (2001) The performance of a laboratory facility for evaluating the structural response of small-diameter buried pipes. Canadian Geotechnical Journal, Vol. 38, pp. 260-275.

Bramryd, T., & Binder, M. (2001) Landfill bioreactor cells as Ecofilters for extraction of bio-energy and nutrients from solid wastes. The Environmentalist, Vol. 21, No 4, pp.297-303.

Campbell Manual (2006) - CR1000 measurement and control system overview. Revision 11/06. Campbell Scientific, Inc. Logan, UT.

Celesco SP1 Instruction Manual (2014) - SP1-25. Version: 12.0. Measurement Specialties. Available: http://www.celesco.com/_datasheets/sp1.pdf

Clayton, C.R.I., & Bica, A.V.D. (1993) The design of diaphragm-type boundary total stress cells. Géotechnique, 43(4), 523-536.

Daigle, L., & Zhao, J.Q. (2003) Assessing Temperature Effects on Earth Pressure Cells. National Research Council Canada, Research Report 131, Feb. 2003, 31 pp.

Dave, T.N., & Dasaka, S.M. (2011) A review on pressure measurement using earth pressure cell. International Journal of Earth Sciences and Engineering, Vol. 4, No. 06 SPL, pp. 1031-1034.

Dave, T.N., & Dasaka S.M. (2011, b) In-house calibration of pressure transducers and scale effects on calibration factors. Journal of Powder Technology.

Engineers EDGE, Poisson's Ratio Metals Metric Chart, last visited December 2014, [Online]. Available: http://www.engineersedge.com/materials/poissons_ratio_metals_materials_chart_13160.htm

Environment Canada, Climate, Hourly Data Report for May 23rd 2014 for Ottawa Ontario. last visited December 2014. Available: http://climate.weather.gc.ca/climateData/hourlydata_e.html

EPA (2010) U.S. Environmental Protection Agency, Landfill Gas Energy. Basics in Project Development Handbook. Available: http://www.epa.gov/lmop/documents/pdfs/pdh_chapter1.pdf

Felio, G.Y., & Bauer, G.E. (1986) Factors affecting the performance of a pneumatic earth pressure cell. Geothechnical Testing Journal ASTM, Vol. 9, No. 2, pp. 102-106.

GEOKON, Instruction Manual Model, 3500, 3510, 3515, 3600 Earth Pressure Cells, GEOKON Inc., 2007.

Hossain, M.Z. & Inoue, S. (2004) A study on mechanical properties of cementitious composites with various recycled aggregates. Proceedings of the 29th Conference on our world in concrete & structures. Singapore. Mie University, Japan. CI-Premier PTE LTD.

Huggins, E., & Ravichandran, N. (2011) Numerical study on the dynamic behavior of retaining walls backfilled with shredded tires. GeoRisk 2011 © ASCE 2011. 955-962

Hvorslev, M.J. (1976) The changeable interaction between soils and pressure cells; tests and reviews at the waterways experiment station. Technical Report S-76-7, U.S. Army Engineer Waterways Experiment Station, Soils and Pavements Laboratory, Vicksburg, MS.

ITRC (Interstate Technology & Regulatory Council). (2006) Characterization, design, construction, and monitoring of bioreactor landfills. Washington, D.C.: Interstate Technology & Regulatory Council, Alternative Landfill Technologies Team. Accessed November 2014. Available: http://www.itrcweb.org/GuidanceDocument/ALT-3.pdf

IUPAC. Compendium of Chemical Terminology, 2nd edition (2006) (the "Gold Book"). Blackwell Scientific Publications, Oxford (1997). XML on-line corrected version: http://goldbook.iupac.org. ISBN 0-9678550-9-8. doi:10.1351/goldbook.

Karthikeyan, O.P. & Joseph, K. (2007) Bioreactor landfills for sustainable solid waste management. Proceedings of National Conference on Sustainable Energy and Waste Management, Coimbatore, India, April 27 – 28, 2007.

Labuz, J.F., & Theroux, B. (2005) Laboratory calibration of earth pressure cell. Geothechnical Testing Journal ASTM, Vol. 28, No. 2, pp. 188-196.

Loh, Y.C. (1954) Internal stress gauges for cementitious materials. Proceedings of the Society for Experimental Stress Analysis, Vol. 21, No. 2, pp. 13–28.

Matasovic, N., & Kavazanjian, E. (1998) Cyclic characterization of OII landfill solid waste. Journal of Geotechnical and Geoenvironmental Engineering, ASCE, 124(3): 197-210.

MatWeb, Material Property Data, mild steel modulus (2014). Last visited October 2014. Available: http://www.matweb.com/search/QuickText.aspx

Monfore, G.E. (1950) An analysis of the stress distribution in and near stress gauges embedded in elastic soils. Structural Laboratory Report No. SP 26, U.S. Bureau of Reclamation, Denver, CO.

Moo-Young, H., Sellasie, K., Zeroka, D., & Sabnis, G. (2003) Physical and chemical properties of recycled tire shreds for use in construction. Journal of Environmental Engineering, 129 (10), 921-929. doi: 10.1061/(ASCE)0733-9372(2003)129:10(921)

MTS Force Transducer Calibration Record (1993) - 661.20E-03. MTS Systems Corporation

MTS MicroConsole Manual (1986) - Model 458.10/.20. MTS Systems Corporation. Available: http://nees.buffalo.edu/pdfs/458%20microconsole.pdf

Murray, K. (2014). Personal communication.

Ontario Ministry of Environment (1998). Landfill standards: A guideline on the regulatory and approval requirements for new or expanding landfilling sites. (Regulation 232/98). Queen's Printer for Ontario.

Pacey, J., Augenstein, D., Morck, R., Reinhart, D., & Yazdani, R. (2000) The bioreactor landfill - an innovation in solid waste management. Solid Waste Association of North America (SWANA). USA.

Pohland, F.G. (1975) Sanitary landfill stabilization with keachate recycle and residual treatment. U.S. Environmental Protection Agency, Cincinnati, Ohio, EPA-600/2-75-043.

Prakash, S. (1981) Analysis of rigid retaining walls during earthquakes. First International Conference on Recent Advances in Geotechnical Earthquake Engineering and Soil Dynamics April 26 - May 3; St. Louis, Missouri: 993-1020.

Prescale Pressure Measurement Film Instruction Manual (2014) - 4LW. Fujifilm Holdings Corporation

Reinhart, D., McCreanor, P., &Townsend, T. (2002) The bioreactor landfill: Its status and future. Waste Management and Research, 20, pp 172-186.

Reinhart, D.R., & Townsend, T.G. (1998) Landfill bioreactor design and operation. Lewis Publishers, Boca Raton, FL.

Reinhart, D.R., McCreanor, P.T., & Townsend T. (2001) The bioreactor landfill: Its Status and Future. University of Central Florida, Orlando, FL.

Reinhart, D.R., Townsend, T.G. & McCreanor, P.T. (2002) Florida bioreactor demonstration project – instrumentation. Proceedings of Waste Tech 2002, Coral Springs, FL.

RST Flexi-Mux Manual (2004) - ELM0029A. Revision 1.1. RST Instruments Ltd. Coquitlam, BC.

RST Total Earth Pressure Cell Calibration Record (2008) - Vibrating Wire Pressure Transducer. RST Instruments Ltd.

Ryall, M.J. Parke G.A.R., & Harding J.E. (2000) Manual of Bridge Engineering, Thomas Telford LTD.

S&ME (2010) Subsurface exploration: West abutment replacement Saluda Drive at Big Brushy Creek. Anderson County, SC. S&ME Project No. 1261-10-069. Report Prepared by Michael Revis, P.E. & David Swoap, P.E.

Selig, E.T. (1964) A review of stress and strain measurements in soil. Proceedings of the Symposium on Soil-Structure Interaction, University of Arizona, pp. 172–186.

Sharma, H.D. & Reddy, K.R. (2004) Geo-environmental Engineering: Site remediation, waste containment, and emerging waste management technologies. John Wiley & Sons, Inc., Hoboken, NJ.

Singh, M.K. (2008) Characterization of stress-deformation behaviour of municipal solid waste. PhD thesis. Department of Civil and Geological Engineering .University of Saskatchewan, Saskatoon, Canada

Terzaghi, K. (1925) Principles of Soil Mechanics. Engineering News-Record, 95(19-27).

Terzaghi, K. (1943) Theoretical Soil Mechanics, J. Wiley and Sons, Inc., New York, pp.66-76.

Timmons J., Cho, Y.M., Townsend, T., Berge, N., & Reinhart, D. (2011) Total Earth Pressure Cells for measuring loads in a municipal solid waste landfill. Geotechnical and Geological Engineering, pp.1-11.

Timmons, J. (2004) Total Earth Pressure Cells for measuring loads in a municipal solid waste landfill. Masters Project, University of Florida, Gainesville, FL.

Tory, A.C., & Sparrow, J.W. (1967) The influence of diaphragm flexibility on the performance of an earth pressure cell. Journal of Scientific Instruments, Vol. 44, No. 9, pp. 781–785.

Townsend, T., Kumar, D. & Ko, J. (2008) Bioreactor landfill operation: A guide for development, implementation and monitoring: version 1.0. Prepared for the Hinkley Center for Solid and Hazardous Waste Management, Gainesville, FL.

Triandafilidis, G.E. (1974) Soil-stress gauge design and evaluation. Journal of Testing and Evaluation, Vol. 2, No. 3, pp. 146–158.

U.S. Department of Transportation Federal Highway Administration (2012). User Guidelines for Waste and By-product Materials in Pavement Construction. Publication Number: FHWA-RD-97-148. Last visited October 2014. available: http://www.fhwa.dot.gov/publications/research%20/infrastructure/structures/97148/st4.cfm

Vingerhoeds, E. (2011) Instrument Installation and Preliminary Data in a Full-Scale Anaerobic Bioreactor Landfill, Sainte-Sophie, Quebec, Canada. M.A.Sc. Thesis, Ottawa, Canada.

Warith, M., Li, X., & Jin, H. (2005) Bioreactor landfills: State-of-the-art review. Emirates J. Eng.. Res., Vol. 10, No. 1, pp. 1-14.

WM (2004) The bioreactor landfill: Next generation landfill technology. Waste Management Bioreactor Program. Accessed February 2013. Available: http://www.wm.com/sustainability/pdfs/bioreactorbrochure.pdf

Weller, W.A., & Kulhawy, F.H. (1982) Factors affecting stress cell measurements in soil. Journal of the Geotechnical Engineering, ASCE, Vol. 108, No. GT12, pp. 1529–1548.

Xu, C., Xiao, Y.Y., Liao, X.Y., & Chen, T.T. (2008) Influence of waste and subgrade settlement on landfill Linier stability and integrity. Proceeding of the 4th Asian Regional Conference on Geosynthetics, pp. 564-568.

Yang, S., Lohnes, R.A., & Kjartason, B.H. (2002) Mechanical properties of shredded tires. Geotechnical Testing Journal, GTJODJ, Vol. 25, No. 1, pp. 44-52.

Appendix A - Instrument Specifications

Information of the apparatus used in the laboratory experiments is described in Tables A-1 through A-6, as shown below.

Table A-1: Specifications of Total Earth Pressure Cell

Total Earth Pressure Cell	
Description	**Specifications**
Manufacturer	RST Instruments Ltd.
Model #	LPTPC12-V-M
Transducer Type	Vibrating Wire Pressure Transducer
Range	Up to 5,000 psi
Accuracy	0.1% full-Scale
Resolution	0.025% full-Scale (minimum)
Excitation Voltage	5 V sq. Wave
Signal Output	1200-2000 Hz
Operating Temperature Range	29°C to +65°C

Table A-2: Specifications of Load Cell

Load Cell	
Description	**Specifications**
Manufacturer	MTS Systems Corporation (MTS)
Model #	661.20E-03
Transducer Type	Force Transducer
Range	Up to 22 KIP
Repeatability	0.03% full-scale
Hysteresis	0.05% full-scale
Maximum Excitation Voltage	20 Vdc
Output	2 mV per V
Operating Temperature Range	–54°C to +93°C

Table A-3: Specifications of String Pot

String Pot	
Description	**Specifications**
Manufacturer	Measurement Specialties
Model Type	Celesco SP1-25
Sensor	Plastic-hybrid precision potentiometer
Output Signal	Voltage divider (potentiometer)
User Interface Software	PC200W
Accuracy	±0.25%
Repeatability	± 0.05% full stroke
Full Stroke Range	0-25 inch (635mm)
Measuring Cable	0.019 inch diameter; nylon-coated stainless steel
Recommended Maximum Input Voltage	30 V (AC/DC)
Operating Temperature,	-18°C to 70°C

Table A-4: Specifications of Prescale Pressure Measurement Film

Prescale Pressure Measurement Film	
Description	**Specifications**
Manufacturer	FUJIFILM
Film Type	Two-sheet Type: Extreme Low Pressure (4LW)
Product Size (W x L)	0.310m x 3m
Pressure Range	0.05- 0.2 MPa
Precision	± 10% or less
Temperature Range	15°C to 30°C
Humidity Range	20% RH to 75% RH

Table A-5: Specifications of Data Acquisition System

Data Acquisition System	
Description	**Specifications**
Manufacturer	RST Instruments Ltd.
Multiplexer Model #	Flex-Mux
Datalogger Model #	FlexDAQ Datalogger CR1000
User Interface Software	Campbell Scientific LoggerNet 3.4.1
Power	12 Vdc (under load), unregulated
Operating Temperature	-40°C to +70°C
Switching Current	1 A (maximum)
Actuation Relay Time	20 ms (maximum)

Table A-6: Specifications of MicroConsole MTS Test System

MicroConsole MTS Test System	
Description	**Specifications**
Manufacturer	MTS Systems Corporation (MTS)
Model #	458.10
Operating Temperature	10°C to 50°C
Relative Humidity	0 to 85%, non condensing

Appendix B - TEPC Calibration

The TEPC used in the experiments generated vibrating wire outputs in B-units. Using the program previously installed in the data logger, the output of the vibrating wire readout generated in B-units was converted to a pressure reading in kPa using the following equation (RST Total Earth Pressure Cell Calibration Record, 2008):

$$\text{Linear } P = CF \times (L_i - L_c) + [1(P_{Bi} - P_{Bc})]$$

Where:

P = Pressure (kPa)

CF = Linear calibration factor= 0.15672 (kPa/B-unit)

L_i = Initial (at installation) reading for vibrating wire readout (B-units)

L_c = Current reading for vibrating wire readout (B-units)

P_{Bi} = Initial (at installation) barometric pressure (millibars)

P_{Bc} = Current barometric pressure (millibars)

The obtained values in B-units converted to kPa needed to be zeroed from the time of calibration. At the start of the calibration, a no load zero reading was recorded for the TEPC in B-units which was converted to kPa. The no load zero reading was the initial uncorrected pressure that was used to calculate the TEPC zeroed Pressure in kPa. Therefore,

$$P_z = P_c - P_i$$

Where:

P_z= Zeroed pressure (kPa)

P_c = Current uncorrected pressure (kPa)

P_i = Initial uncorrected pressure or no load zero reading (kPa)

The barometric pressures for Ottawa over the calibration period were obtained from Environment Canada's website in order to correct the pressure readings for barometric pressures. The corrected pressures were obtained using the following equation:

$$P_{cd} = P_z + (P_{Bi} - P_{Bc})$$

Where:

P_{cd}= Corrected pressure (kPa)

P_z = Zeroed pressure (kPa)

P_{Bi} = Initial (at start of calibration) barometric pressure (kPa)

P_{Bc} = Current barometric pressure (kPa)

Appendix C - Woodchips Height and Modulus of Elasticity

The utilised actuator in the laboratory experiments was equipped with an LVDT which represented the movement of the actuator frame. The vertical displacement of the woodchips with respect to the applied load was recorded by the LVDT. Recorded displacements of the woodchips during each test helped obtain the initial and final woodchips height at the start and the end of each experiment. The final height of the woodchips during a test was indeed the initial height of the woodchips for the test conducted after. The initial height of the woodchips was required to obtain the modulus of elasticity of the woodchips which was an important input parameter in the software. The final woodchips height at the end of each experiment is illustrated in Table C-1. The total displacement of the woodchips after the end of steel plate tests was approximately 33cm.

Table C-1: Height of woodchips in the cell box after each test

Height of cell box (m)	Height of woodchips after (m)						
	Initial compaction	TEPC at base	TEPC at middle	Large steel plate+ TEPC	Small steel plate+ TEPC	Small steel plate+ TEPC (Repeated)	Small steel plate+ TEPC (Silicon)
1.010	0.80	0.808	0.769	0.744	0.717	0.707	0.684

To find the modulus of elasticity of the woodchips inside the steel cell box, strain parameter of the woodchips during loading phases was obtained using the displacement measurements provided by the actuator sensor and the initial height of the woodchips. The modulus of elasticity of woodchips obtained from the slope of the plotted applied

pressure versus the strain was varying between 526kPa and 995kPa over the experiments. The modulus of the woodchips during loading phase is presented in Figure C-1.

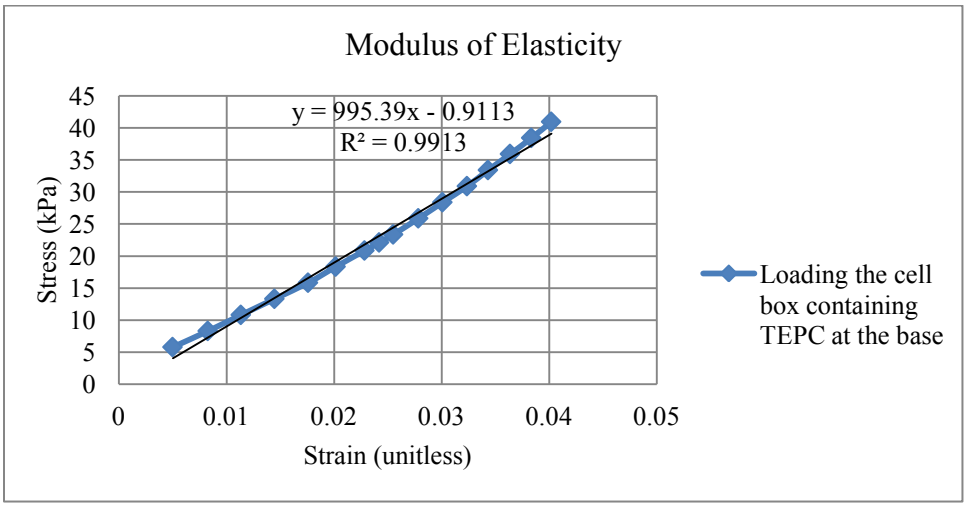

(a)

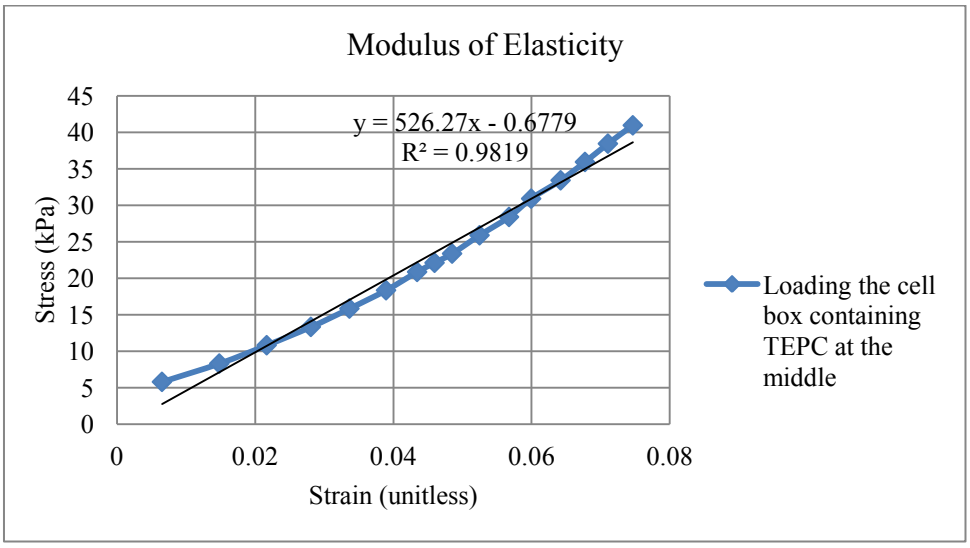

(b)

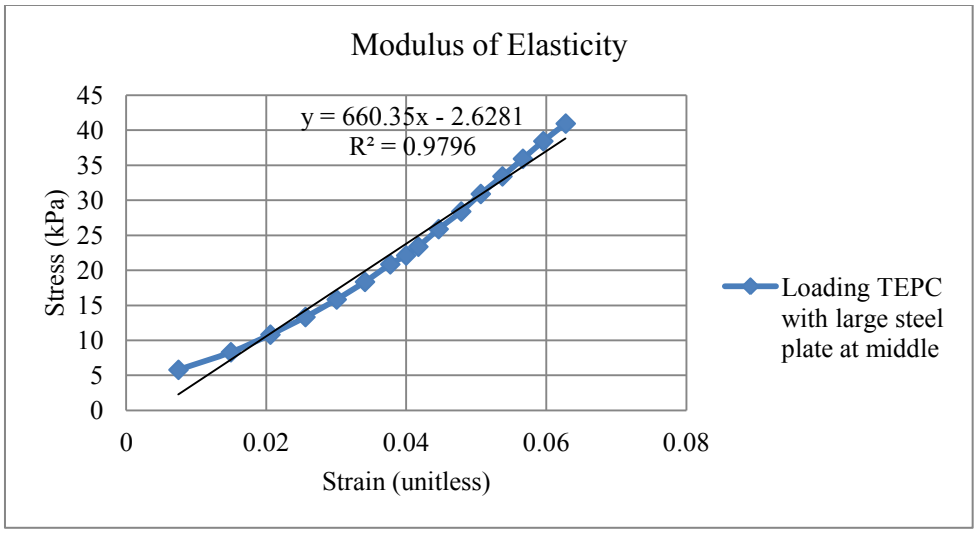
Modulus of Elasticity
y = 660.35x - 2.6281
R² = 0.9796
Stress (kPa)
Strain (unitless)
0
5
10
15
20
25
30
35
40
45
0
0.02
0.04
0.06
0.08
Loading TEPC with large steel plate at middle

(c)

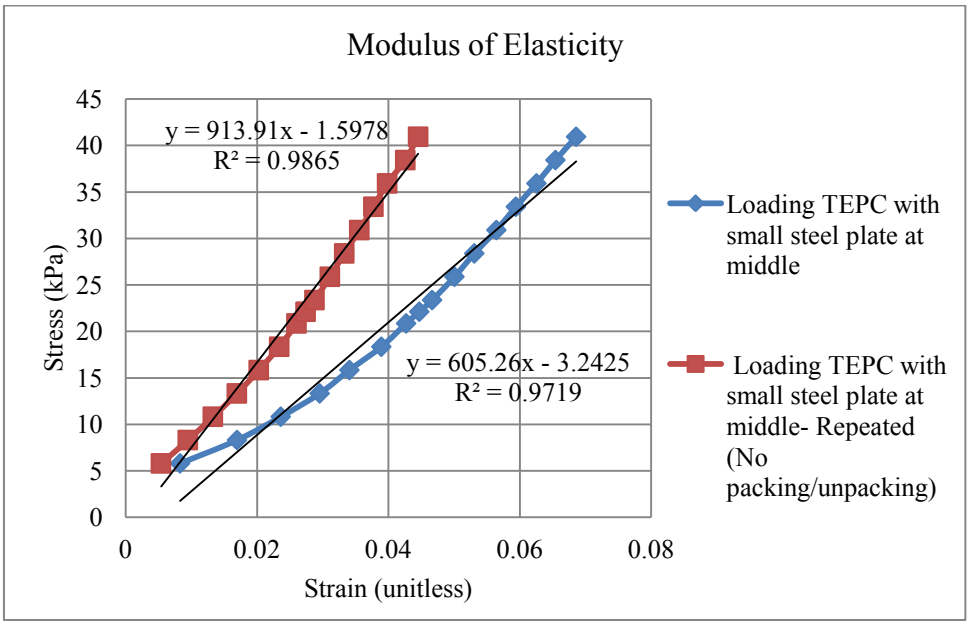
Modulus of Elasticity
y = 913.91x - 1.5978
R² = 0.9865
y = 605.26x - 3.2425
R² = 0.9719
Stress (kPa)
Strain (unitless)
0
5
10
15
20
25
30
35
40
45
0
0.02
0.04
0.06
0.08
Loading TEPC with small steel plate at middle
Loading TEPC with small steel plate at middle- Repeated (No packing/unpacking)

(d)

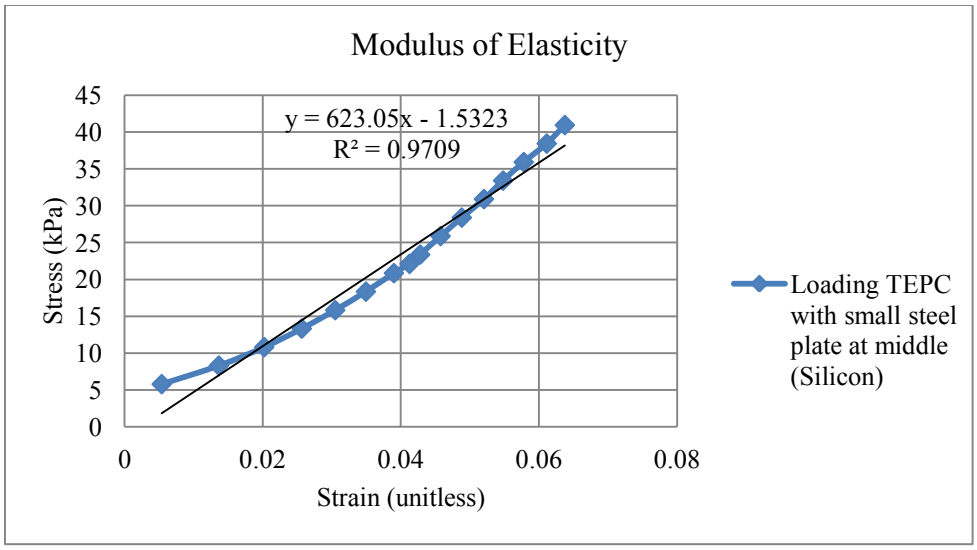

(e)

Figure C-1: Modulus of Elasticity of woodchips during the conducted experiments (a) TEPC at the base (b) TEPC at middle (c) TEPC and large steel plate (d) TEPC and small steel plate (first time and repeated) (e) TEPC and small steel plate using silicon

Not a consistent trend in the strains was observed during the experiments over time. This could be because of change in woodchips properties as woodchips were repacked and reloaded during the tests unless same woodchips sample was used (Figure C-1 (d)). With loading and compressing the woodchips, material properties of the woodchips in terms of grain size and texture are changing. During utilising the small steel plate and the TEPC, the modulus of woodchips during the first and the repeated tests was found out to be improved from 605kPa to 914kPa approximately, for the same woodchips sample. The repeated test was indeed conducted without packing and unpacking the woodchips.

Appendix D - Complementary Test Results

The shear strength parameter values of the woodchips and the modulus of the HDPE pipe are provided below.

- To determine the shear stress parameters of the woodchips, the shear stress versus the strain for the confining stresses (40kPa, 60kPa and 80kPa) was plotted from which the maximum shear stress at each confining stress was obtained. A new plot line of the maximum shear stresses versus the three normal confining stresses was then achieved. From the plot line, the frictional angle of the woodchips was estimated to be approximately 24kPa and the cohesion of the woodchips was determined to be 0kPa.
- To determine the modulus of the pipe, the plot of the applied stress versus strain was provided (Figure D-1) and the modulus of the pipe was determined from the slope of the line. The modulus of elasticity of the pipe was obtained to be approximately 24,670kPa.

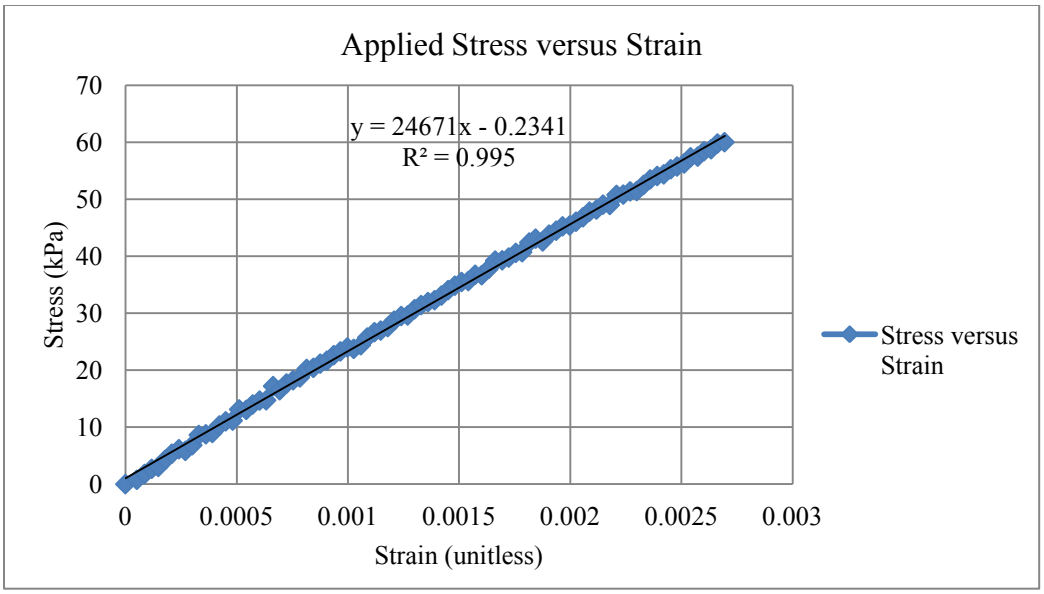

Figure D-1: Plot of stress versus strain for HDPE pipe

Appendix E – Load Cell Results

In order to understand how variable or repeatable the stress data was at the bottom of the cell box, the measured pressures obtained from the load cell for all tests were plotted versus the calculated pressures on the load cell plate for loading and unloading pressures as shown in Figures E-1 and E-2, respectively. Pressure on the load cell plate was calculated from the pressure at the base of the cell box, considering the total applied load and the area of the cell box, by the area of the load cell plate. The load cell plate had an approximate area of 0.049 square meters.

The load cell was expected to record the same load during each test as the pressure at the bottom of the cell box should be the same for each test loaded to a maximum applied load of 150kN by the actuator. The recorded loads had a decreasing trend under the same applied load of 150kN as different experiments progressed in time.

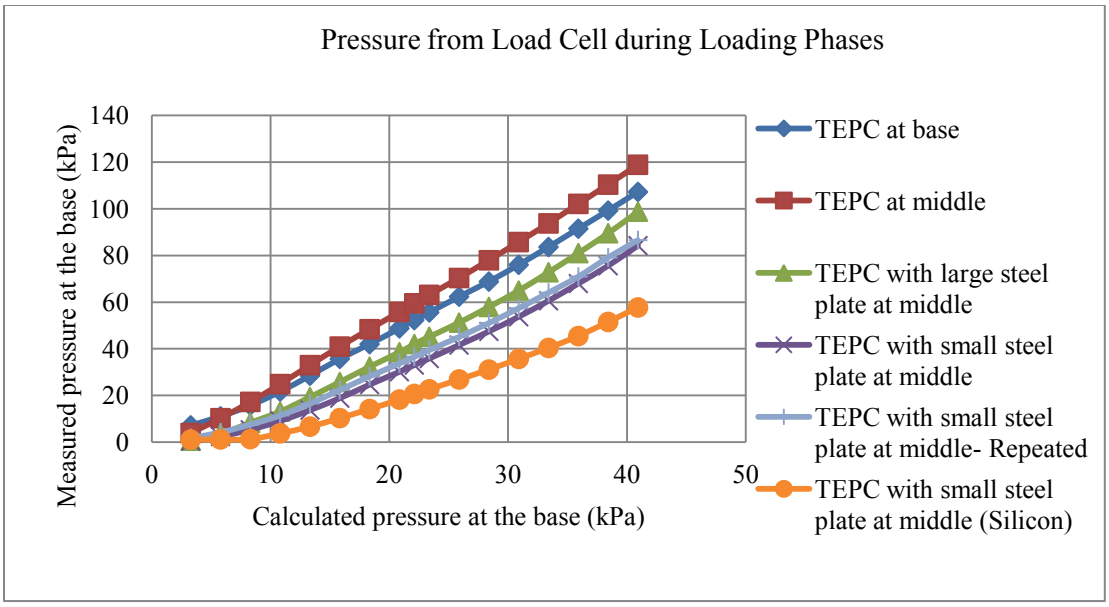

Figure E-1: Measured pressure by load cell versus calculated pressure at the base of the steel box during loading phases

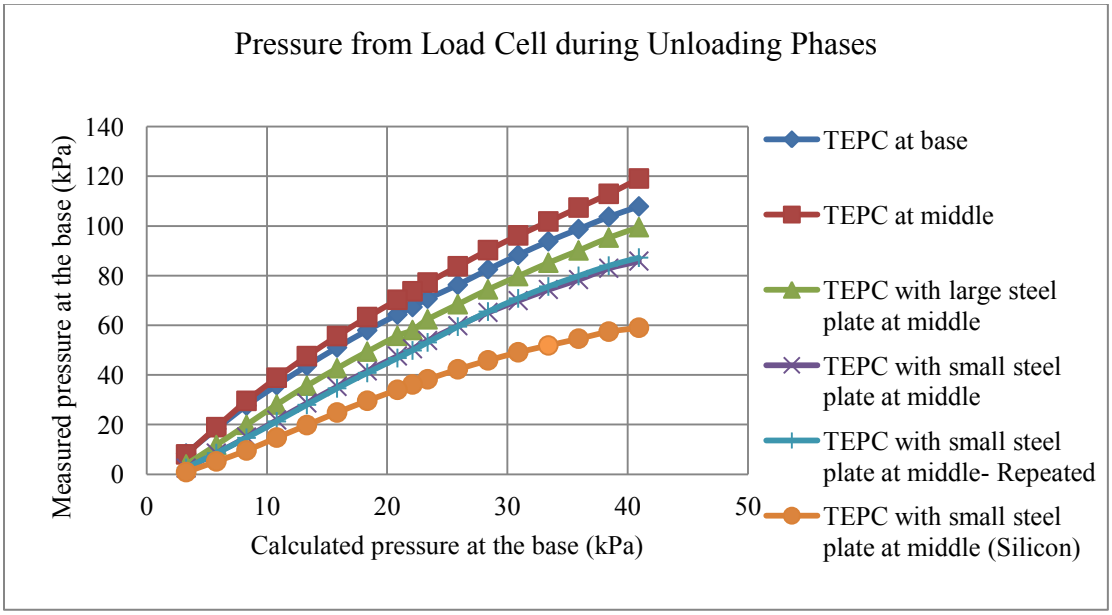

Figure E-2: Measured pressure by load cell versus calculated pressure at the base of the steel box during unloading phases

Appendix F - String Pot Calibration

String pots were calibrated before being installed inside the pipes in order to obtain a correction factor to convert the voltage output (mV) to displacement (mm). A zero value were recorded for all four string pots with voltage readings corresponding to 5mm, 10mm, 11mm and 12mm of displacement obtained using Vernier caliper. The difference in voltages of the new reading and the zero reading for each string pot was determined. The ratio of the difference in voltages over the corresponding displacement i.e. 5mm, 10mm, 11mm and 12mm was calculated as shown in Tables F-1 and F-2. Based on the results obtained from these tables, a correction factor for each string pot was estimated as shown in Table F-3.

Table F-1: String Pot Calibration

String Pot Calibration	Zero Voltage Reading (mV)	5mm			10mm		
		Reading (mV)	Difference (mV)	Ratio	Reading (mV)	Difference (mV)	Ratio
Pipe 1 Horizontal	33.6	68.55	34.95	6.99	106.18	72.58	7.26
Pipe 1 Vertical	2.69	37.63	34.94	6.99	71.24	68.55	6.86
Pipe 2 Horizontal	40.32	79.30	38.98	7.80	116.94	76.62	7.66
Pipe 2 Vertical	30.91	67.20	36.29	7.26	102.15	71.24	7.12

Table F-2: String Pot Calibration

String Pot Calibration	Zero Voltage Reading (mV)	11mm			12mm		
		Reading (mV)	Difference (mV)	Ratio	Reading (mV)	Difference (mV)	Ratio
Pipe 1 Horizontal	33.6	114.25	80.65	7.33	120.97	87.37	7.28
Pipe 1 Vertical	2.69	77.96	75.27	6.84	86.02	83.33	6.94
Pipe 2 Horizontal	40.32	123.66	83.34	7.58	131.72	91.40	7.62
Pipe 2 Vertical	30.91	109.54	78.63	7.15	115.59	84.68	7.06

Table F-3: Estimated correction factors for each string pots

String Pot	Correction Factor
Pipe 1 Horizontal	7.3
Pipe 1 Vertical	6.9
Pipe 2 Horizontal	7.6
Pipe 2 Vertical	7.1

Appendix G - Charts for PPMF

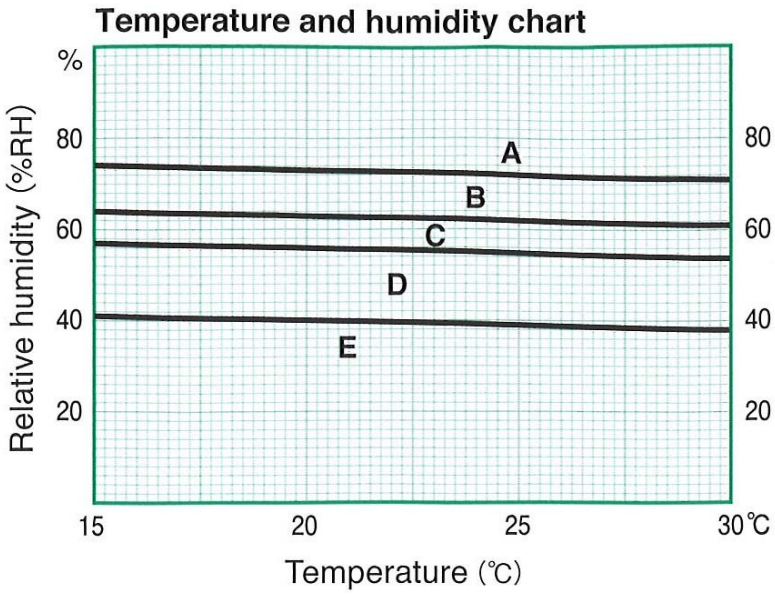

Figure G-1: Temperature and humidity chart

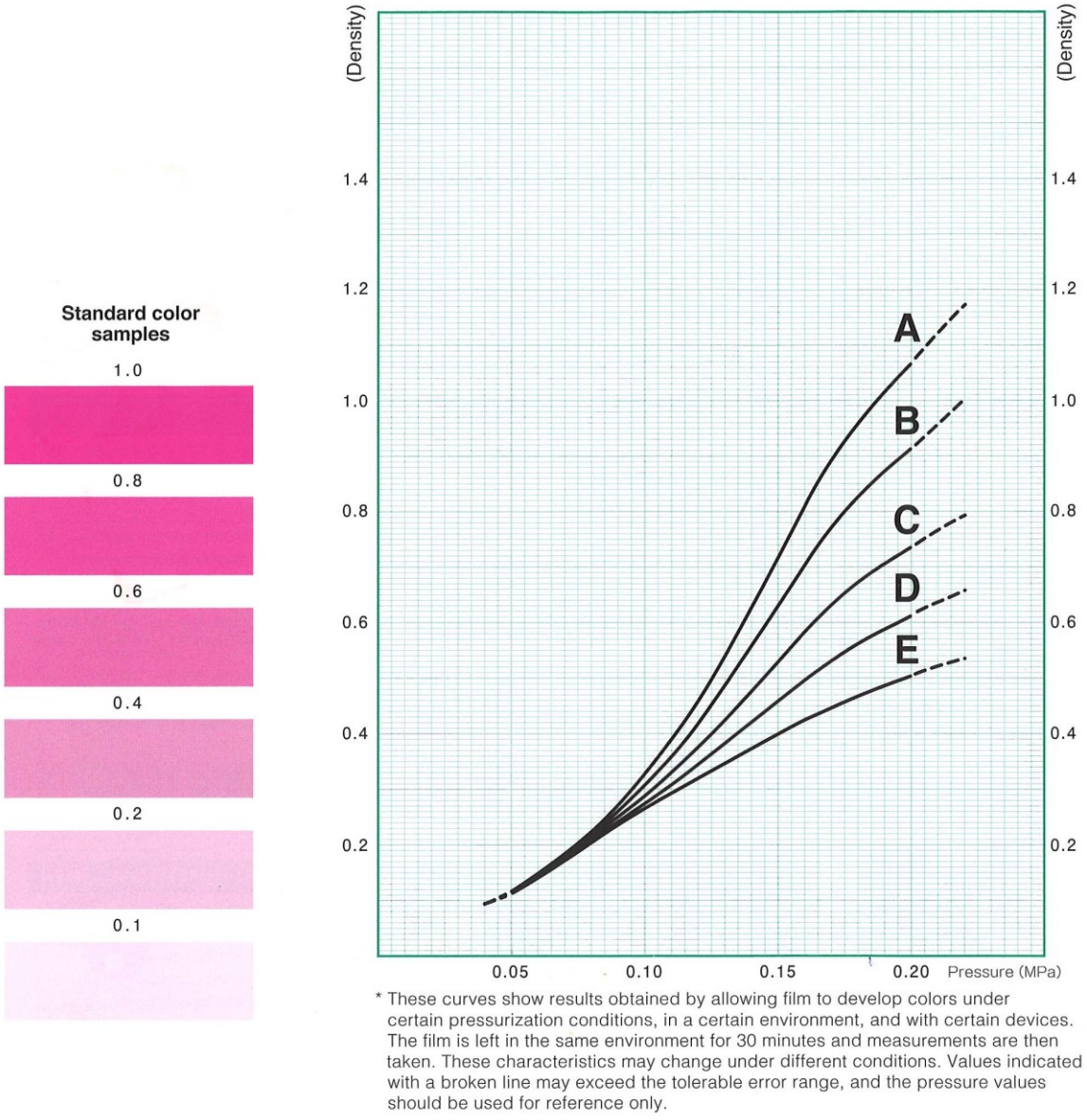

Figure G-2: Pressure chart based on color density

Appendix H - Unit Weight of Woodchips and Steel Plate

Steel plate

Mass of steel plate = 10kg

Dimensions of steel plate = 0.317m x 0.317m x 0.0127m

The density of the steel plate is calculated as:

$$Density = \frac{10kg}{0.317m \times 0.317m \times 0.0127m}$$

$$Density = 7835.7 \ \frac{kg}{m^3}$$

Therefore, the steel plate has a unit weight of:

$$Unit\ weight = 7835.7 \frac{kg}{m^3} \times 9.81 \ \frac{m}{s^2}$$

$$Unit\ weight = 76868.21 \ \frac{N}{m^3}$$

$$Unit\ weight = 76.9 \ \frac{kN}{m^3}$$

Woodchips

Empty mass of cell box =1070kg

Total mass of cell box and woodchips = 1624 kg

Mass of woodchips is calculated as:

$$Mass\ of\ woodchips = 1624kg - 1070kg$$

$$Mass\ of\ woodchips = 554kg$$

Having the mass of woodchips, the weight of woodchips is found to be:

$$Weight\ of\ woodchips = \frac{554kg\ \times 9.81\ \frac{m}{s^2}}{1000}$$

$$Weight\ of\ woodchips = 5.43\ kN$$

Height of woodchips in the cell box after initial compaction =0.8

Volume of woodchips before starting the experiments= 2.71m x 1.47m x 0.8m

Therefore, the unit weight of the woodchips was calculated to be:

$$Unit\ weight = \frac{5.43kN}{2.71m \times 1.47m \times 0.8m}$$

$$Unit\ weight = 1.70\ \frac{kN}{m^3}$$